NASA TECHNICAL TRANSLATION NASA TT F-15,064

INFRARED SPECTRA OF THE RADIATION OF THE EARTH INTO OUTER SPACE

Yu.G. Andrianov, I.I. Karavayev,
Yu.P. Safronov, V.I. Tulupov

(NASA-TT-F-15064) INFRARED SPECTRA OF THE RADIATION OF THE EARTH INTO OUTER SPACE (Linguistic Systems, Inc., Cambridge, Mass.) ~~123~~ 122 p HC $9.25 N74-19422
CSCL 03B G3/29 Unclas 32661

Translation of: "Infrakrasnyye Spektry Izlucheniya Zemli v Kosmos," Moscow, "Sovetskoye Radio" Press, 1973, 112 pages.

APR 1974 RECEIVED NASA STI FACILITY INPUT BRANCH

NATIONAL AERONAUTICS AND SPACE ADMINISTRATION
WASHINGTON, D.C. 20546 MARCH 1974

STANDARD TITLE PAGE

1. Report No.	2. Government Accession No.	3. Recipient's Catalog No.
NASA TT F-15,064		

4. Title and Subtitle	5. Report Date
INFRARED SPECTRA OF THE RADIATION OF THE EARTH INTO OUTER SPACE	March 1974
	6. Performing Organization Code

7. Author(s)	8. Performing Organization Report No.
Yu. G. Andrianov, I. I. Karavayev, Yu. P. Safronov, V. I. Tulupov	10. Work Unit No.

9. Performing Organization Name and Address	11. Contract or Grant No.
LINGUISTIC SYSTEMS, INC. 116 AUSTIN STREET CAMBRIDGE, MASSACHUSETTS 02139	NASW-2482
	13. Type of Report & Period Covered TRANSLATION
12. Sponsoring Agency Name and Address NATIONAL AERONAUTICS AND SPACE ADMINISTRATION WASHINGTON, D.C. 20546	14. Sponsoring Agency Code

15. Supplementary Notes

Translation of "Infrakrasnyye Spektry Izlucheniya Zemli v Kosmos", Moscow, "Sovetskoye Radio" Press, 1973, 112 pages.

16. Abstract The book is devoted to the description of the results of measurements of the intensity of infrared radiation of the Earth into outer space, obtained with the use of a spectral apparatus, mounted on board artificial Earth satellites. Some basic propositions of the theory of the radiation of the Earth are presented and a survey of substantial articles on this question is given. The procedure and results of statistical processing of measurements of infrared spectra of the radiation of the Earth in the range of wave lengths from 7 to 26 microns are described. Statistical characteristics and histograms of laws of the distribution of intensities of radiation at various wave lengths are given. Correlation dependences between intensities of radiation in various ranges of wave lengths and histograms of two-dimensional laws of the distribution of these magnitudes are considered. Results of measurements are compared with data obtained by American scientists.

The book is intended for engineers and specialist-geophysicists, who work on applied problems of cosmic optical electronics, and likewise for a wide range of readers interested in questions of the infrared radiation of the Earth.

17. Key Words (Selected by Author(s))	18. Distribution Statement
	UNCLASSIFIED - UNLIMITED

19. Security Classif. (of this report)	20. Security Classif. (of this page)	21. No. of Pages	22. Price
UNCLASSIFIED	UNCLASSIFIED	123	

TABLE OF CONTENTS

NASA TT F-15,064

INFRARED SPECTRA OF THE RADIATION OF THE EARTH INTO OUTER SPACE

Yu.G. Andrianov, I.I. Karavayev
Yu.P. Safronov, V.I. Tulupov

INTRODUCTION

Investigation of the characteristics of radiation of the Earth that depart in the infrared region of the spectrum is necessary for the solution of many applied problems of meteorology and geophysics, and likewise in the development of optical electronic equipment intended to be mounted on flying craft, in particular on orbiting space objects. /3*

Accurate determination of characteristics of departing cosmic radiation is impossible without its global measurements, that began to be conducted only in recent times with the help of artificial Earth satellites, equipped with the appropriate equipment.

A fairly large number of works, both by domestic and by foreign authors, are devoted to the experimental study of departing infrared radiation of the Earth on the basis of measurements from artificial Earth satellites. However, in spite of this, information on the colorimetric and spectral distribution of thermal radiation is quite scanty; therefore, at the present time it is difficult to determine the energy contribution of each spectral range in the overall energy of departing radiation. This, in turn, makes it impossible to compile a sufficiently complete and accurate energy thermal balance of the Earth both as a whole for the planet, and for separate parts of its surface taking account of seasonal and diurnal variations.

The book is a source of initial information, necessary both for specialists in geophysics and for designers-developers of optical electronic equipment. The factual base of the book is the results of measurements from several scientific research satellites of the "Kosmos" series in 1964 and 1965.

In the first chapter basic propositions of the theory of the radiation of Earth are discussed, and likewise a survey

---

*Numbers in the right-hand margin indicate pagination in the foreign text.

is presented of earlier published experimental and theoretical works, devoted to the investigation of the intrinsic radiation of the Earth. The second chapter contains a description of an apparatus, used in the measurement from an artificial Earth satellite of the intensity of the departing infrared radiation of the Earth, of the procedure of its calibration and recording of information. Samples of traces and the results of their decoding are presented. An estimate is given of the accuracy of the measurements conducted. In the third chapter a description is presented of the procedure and results of the statistical processing of data obtained in measurements. Here also a comparison is made of these results with data of other authors. The fourth and final chapter describes statistical characteristics of the combined distribution of intensities of radiation for various pairs of parts of the spectral range. Correlation matrices are presented, that characterize the correlation connection between intensities of radiation in various parts of the spectrum. The results of statistical processing of experimental data are presented in the appendix in the form of graphs and tables.

The book is one of the first works devoted to the experimental investigation of the spectral composition of the radiation of the Earth departing into outer space; and, therefore, makes no claim to full coverage of all questions of the given problem.

In conclusion, the authors consider it their duty to mention the exceptionally large role and the services of the untimely deceased Professor Aleksandr Ignat'yevich Lebedinskiy in the scientific supervision and organization of the theoretical and experimental investigations, the results of which lay in the bases of the present book.

The authors express deep appreciation to associate member of the Academy of Sciences of the USSR K.Ya. Kondrat'yev, and to candidates of engineering sciences Ye.A. Kashcheyev and V.V. Kozelkin, who took upon themselves the labor of reviewing the book.

CHAPTER ONE

/5

INTRINSIC THERMAL RADIATION OF THE EARTH

1.1 A Brief Account of the Thermal Radiation of the Earth.

Planet Earth obtains the basic share of its energy from the Sun. This energy enters Earth in the form of electromagnetic radiation, the maximum of the energy of which occurs in the visible region of the spectrum. The solar radiation that reaches the Earth is reflected in part into outer space, in part absorbed by the Earth's surface and atmosphere.

The Earth-atmosphere system radiates energy into outer space, that is equivalent to the energy absorbed. However for separate parts of this system absorbed and radiated energies can have different values. Although the values of energies absorbed and radiated by the Earth-atmosphere system are very close to one another, the spectral distributions of absorbed and radiated radiation differ very substantially. This can be seen from Fig. 1.1, in which are presented normalized /6 curves of the spectral distributions of the intensity of radiation of bodies with a temperature of 6000°K, that corresponds to solar radiation, and with a temperature of 250°K, that corresponds to the radiation of the Earth-atmosphere system. These two curves are sharply divided into two spectral ranges -- shorter and longer than 4 microns. Solar radiation obtained by the Earth is usually called short wave, and intrinsic thermal radiation of the Earth-atmosphere system is called long wave departing radiation. An overwhelming part of the energy of long wave departing radiation occurs in the range of wave lengths from 4 to 40 microns.

The difference between the magnitudes of absorbed short wave solar radiation and of long wave departing radiation is called the radiation balance of the Earth-atmosphere system. The equation of the radiation balance has the form

$$R_s = Q_0(1 - A_s) - F_\infty$$

where Q_0 is the incoming solar energy beyond the limits of the atmosphere (solar constant); A_s is the albedo of the Earth-atmosphere system, equal to the ratio of short wave radiation Q_∞ reflected and diffused by the Earth into outer space to the incident solar energy Q_0; F_∞ is the departing long wave radiation.

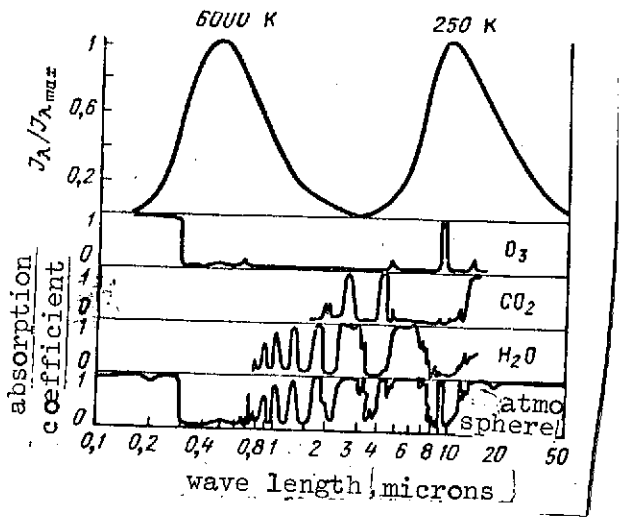

Fig. 1.1. Absorption spectra of H_2O, CO_2, O_3 and the absorption spectrum of the atmosphere at the level of the Earth's surface (middle and lower parts of the drawing); distribution of energy in the radiation spectrum of an absolutely black body at 6000°K (the temperature of the Sun) and 250°K (the average temperature of the troposphere).

The magnitude of the solar constant Q_0 at the present time is known with an accuracy of several per cent. Therefore, for the measurement of the radiation balance it is sufficient to measure short wave Q_∞ and long wave F_∞ departing radiation. Study of the radiation balance and of its components makes it possible to investigate regularities of the radiation of the Earth as a planet.

Long wave departing radiation consists of radiation of the underlying surface (the surface of continents and of oceans) and radiation of the atmosphere. The processes of the transfer of this radiation in the atmosphere substantially affect its spectral composition. The atmosphere is a medium consisting of a mixture of gases and of water vapor with various particles suspended in it. The basic components of the atmosphere that absorb infrared radiation and determine the spectral composition of long wave departing radiation are water vapor, carbon dioxide and ozone, which constitute an insignificant part of it.

For the overall characteristics of the absorption spectrum of the atmosphere, in Fig. 1.1 are depicted absorption bands of

water vapor, carbon dioxide and ozone and the absorption spectrum of the atmosphere at the level of the Earth's surface. From the drawing, it can be seen that water vapor most intensely absorbs infrared radiation in the range of wave lengths considered. The strongest absorption bands of water vapor are the parts of the spectrum the centers of which determine the absorption maximum and occur at wave lengths 2.68 and 6.3 microns. The centers of the basic bands of absorption of carbon dioxide occur at wave lengths 4.3 and 15 microns. As for absorption bands of water vapor 2.68 and of carbon dioxide 4.3 microns, their effect on absorption of long wave infrared radiation can be disregarded, inasmuch as they are located on the wing of the curve of spectral distribution of the intensity of radiation of a black body at temperatures that occur in the atmosphere (Fig. 1.1). Ozone, in the range of wave lengths considered has several absorption bands. In the atmosphere only the narrow, but intensive band with center at wave length 9.6 microns is sufficiently clearly observed. The remaining absorption bands of ozone overlap the more intensive bands of water vapor and carbon dioxide.

Water vapor enters the atmosphere as a result of evaporation of water from the Earth's surface and as a result of diffusion in the atmosphere due to mixing. The water vapor content in air varies from zero to several percent due to a number of causes, in part because of the temperature of air and because of atmospheric pressure; it decreases very quickly with altitude and already at an altitude of the order of magnitude of 8-10 kilometers becomes insignificantly small. Thus water vapor is concentrated, basically, in the troposphere. Let's recall that the troposphere extends to altitudes of 8-9 kilometers in temperate latitudes and to 16-17 kilometers in tropical latitudes. It is characterized by a uniform decrease of temperature with altitude, that comes to approximately 6.5 degrees/kilometer.

The volumetric concentration of carbon dioxide gas in the atmosphere, on the average equal to 0.033%, is assumed constant up to great altitudes. The maximum of the concentration of ozone is observed at altitudes of 20-25 kilometers. At higher and lower altitudes, the ozone content decreases.

In addition to the already enumerated water vapor, carbon dioxide and ozone, a number of secondary components of the atmosphere have absorbing properties. However, with respect to energy, absorption and radiation of long wave radiation by these components are negligibly small and are not of practical interest.

In absorption bands, radiation of the underlying surface and of lower layers of the atmosphere is partially absorbed by the overlying layers of the atmosphere that, in turn, themselves radiate. Departing long wave radiation is, thus, the total of radiations of the underlying surface and of the atmosphere. The greater the absorption coefficient of the atmosphere in a given part of the spectrum, the lesser the degree that the underlying surface and lower layers of the atmosphere will be represented in the departing radiation. On the other hand, in the low-absorbing parts of the spectrum, radiation of lower layers of the atmosphere and of the underlying surface will comprise the basic portion of departing radiation. /8

Such parts of the spectrum are called "windows of transparency" of the atmosphere. The most important for the energy balance of the Earth is the "window of transparency" in the range 8 - 12 microns. This range occurs in the maximum of the curve of spectral distribution of intensity of radiation of a black body with a temperature of 250°K (Fig. 1.1). Therefore, in the "window of transparency" of 8 - 12 microns, the Earth's radiation into outer space is very intensive, and only ozone absorption in the band 9.6 microns, that is located in this part of the spectrum, attenuates it somewhat.

1.2 Theoretical and Experimental Investigations of the Departing Radiation of the Earth.

Accurate theoretical calculations of the departing radiation, based on the use of the equation of the transfer of radiant energy, are fairly complex. The scantiness of data about the structure of the atmosphere, about physical processes that occur in its upper layers, leads to errors in the results of calculation. (For instance, knowledge about the dependence of the absorption of radiation on pressure and temperature, about the concentration of water vapor in the stratosphere.) This picture is even further complicated by the random nature of distributions of temperature and of the concentration of components that absorb radiation.

Therefore, for enhancing the accuracy of results of calculations, above all one strives to maintain the reliability of the initial data. Both average and concrete stratifications of the atmosphere are used. In calculations both cloudless conditions and the presence of cloud cover can be allowed for at various altitudes.

The solution of the transport equation is carried out numerically and graphically, in which case it is usually assumed that the Earth's surface and clouds are absolute black emitters. In the numerical method, a model of the atmosphere in the form of a set of horizontal layers, in the limits of each of which the temperature and density of gases that absorb radiation is assumed to be constant. Integrals that appear in the transport equation are replaced by sums according to the number of layers. For the graphical solution the so-called radiation nomograms are used, in which the intensities of radiation are interpreted by the area in a determined system of coordinates. First, the magnitude of the average flux F_∞ of radiation of the Earth into outer space was calculated by Abbot and Fowle at the beginning of our century [1]. Abbot and Fowle, having estimated the average value of the planetary albedo of the Earth, found that it radiates an average of 23 milliwatts/cm^2. If one considers that the Earth-atmosphere system radiates as an absolute black body, then the radiation temperature T_{rad} of this radiation is determined from formulas $T_{rad} = \sqrt[4]{F_\infty/\sigma}$, where σ is the Stefan-Boltzmann constant. (By radiation temperature is understood such a temperature of the surface of an absolute black body, in the case of the sighting of which on the output of a measuring apparatus the same signal is created as the one from the surface observed.) Temperature T_{rad} was found to be equal to 256°K. Inasmuch as such a temperature occurs at an altitude of about 4 kilometers, Abbott and Fowle arrived at the important conclusion that the radiation substances are the water vapor and carbon dioxide present in the troposphere.

/9

G. Simpson [2] in 1928 developed a method of determining the departing radiation according to the average values of basic meteorological elements. He used the following simplified scheme of the spectrum of absorption by water vapor: a) complete transparency in the range of wave lengths 8.5-11.0 and less than 4.0 microns; b) complete absorption in the range of wave lengths 5.5-7.0 and greater than 14.0 microns, if the mass in the absorbing layer is not less than 0.03 grams/cm^2; c) partial absorption in intervals of the spectrum 7.0-8.5 and 11.0-14.0 microns. The degree of approximation of this method is due to both the roughness of the approximation of the spectrum and to the absence of accountability of the distribution of temperature and of moisture according to altitude, and to the inaccuracy of the allowance for cloudiness. However, because of its simplicity, the Simpson method, with some refinement of the boundaries that separate spectral regions, is used by various authors right up to the present day [3].

Let's discuss some contemporary results of calculations of departing long wave radiation. K.Ya. Kondrat'yev and O.P. Filipovich [4] for calculations of average-width distribution of departing radiation of the northern hemisphere used radiation nomograms. In the calculations it was assumed that the radiating and absorbing components of the troposphere are only water vapor and carbon dioxide, and the magnitude of the departing radiation flux does not change in the case of its passage through an isothermal layer of the atmosphere. This second assumption, caused by the absence of necessary data on the stratification of the atmosphere at great altitudes, identifies departing radiation with the rising flux of thermal radiation at the level of the tropopause, that leads to a relative error that does not exceed 6%. /10

Results of calculations, performed in accord with different radiation nomograms, differ substantially. The basic cause of this discrepancy is the difference in approximations of functions of transmission (or of absorption), assumed in the plotting of nomograms.

In spite of the marked disparity of results of calculations performed in [4], they all show that the rising radiation flux at the level of the tropopause decreases from the equator to the pole and that cloudiness assists the decrease of the magnitude of the rising radiation flux. An analysis carried out by authors of [4], shows that the excess of magnitudes of rising flux at the equator above the magnitudes of the flux at the pole occurs mainly due to radiation of warm layers of the atmosphere with a high water vapor content.

D. London in article [6] arrives at similar results. He carried out calculations of the rising flux of thermal radiation at the level of the tropopause for four seasons of the year in the northern hemisphere under average conditions of cloudiness. The results of the calculations are presented in Table 1.1.

As follows from Table 1.1, the troposphere makes the basic contribution to long wave departing radiation. The contribution of the troposphere in the different seasons of the year comprises 86%-89%. Radiation of the Earth's surface (in windows of transparency) comprises less than 10% of the overall departing radiation, but the contribution of radiation of the stratosphere does not exceed 3%-6%. Seasonal variability of the components of departing radiation is very insignificant. The small variability of thermal radiation of

TABLE 1.1

Radiating Medium	Values of the Average Flux of Thermal Radiation, mW/cm^2				
	Winter	Spring	Summer	Autumn	Average Annual
Earth's Surface (in windows of transparency)	2.02	2.02	1.82	1.82	1.88
Troposphere	19.30	19.2	20.5	19.7	19.7
Stratosphere	0.77	1.12	1.32	0.7	0.98
Overall Departing Radiation	22.09	22.34	23.64	22.22	22.56

the Earth's surface is explained by the mutually compensating effects of the increase of the temperature of the Earth's surface from winter to summer and of the decrease of transparency of the atmosphere with the increase of its overall water vapor content, and likewise with the rise of the degree of cloudiness. However, these conclusions about the small variability of departing radiation pertain to magnitudes averaged over the whole northern hemisphere. /11

The dependence of the intensity of departing radiation on latitude for the northern hemisphere is presented in Fig. 1.2, borrowed from [6]. In this drawing the scale along the axis of ordinates is proportional to the area of latitudinal zones. The figures around each line signify the magnitudes of departing fluxes of thermal radiation at the level of the tropopause in calories/cm^2·min. At almost all latitudes the radiation maximum takes place in the summer, due to maximal temperatures during the summer. A characteristic special feature of the latitudinal distribution is the maximum of departing radiation in the subtropics, due to a decrease of cloudiness and an increase of the average temperature of the troposphere in subtropical zones of high pressure.

As can be seen from Fig. 1.2, the magnitudes of departing radiation decrease from 0.2 calories/cm^2·min. (13.9 mW/cm^2) in polar regions to 0.36 calories/cm^2·min. (25.4 mW/cm^2) in the

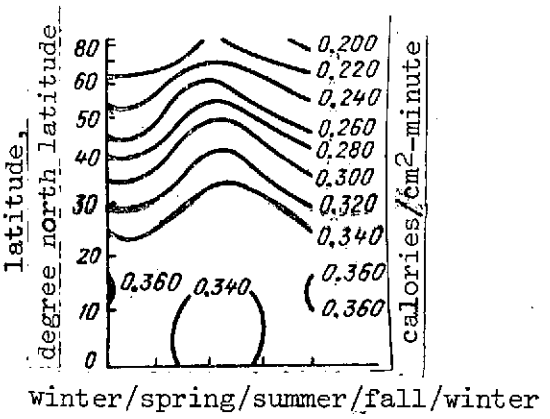

Fig. 1.2. Latitudinal variation of radiation according to the data of calculations of D. London.

sub-tropics. The average annual latitudinal distribution of departing radiation for the northern hemisphere in mW/cm^2 according to the results of calculations of London is presented in Table 1.2. In this same table latitudinal distributions are presented that were calculated by a number of other authors. The magnitude of the flux of departing radiation F_∞ averaged over the entire northern hemisphere and the radiation temperature T_{rad} that corresponds to it are presented in the lower part of Table 1.2

K.Ya. Vinnikov carried out calculations of departing radiation F_∞ on the basis of an approximation method proposed by him [11]. This method issues from a proposition about linear stratification of temperature, an exponential law of the distribution of density of water vapor with altitude in the troposphere and of isothermy in the stratosphere. Contemporary data on the integral function of transmission of atmospheric gases were used [12]. The method of K.Ya. Vinnikov makes it possible to determine departing radiation in the case of a cloudless sky and in the presence of clouds of various levels. Calculations of departing radiation of the Earth were accomplished with the help of an electronic computer for 260 points, located along the whole territory of the globe. Of those, 164 points were on land and 96 in the ocean. On the basis of results of calculations monthly (for January, April, July, October) and annual maps of the planetary distribution of departing radiation were plotted. From these maps it follows that the field of departing radiation is sufficiently homogeneous and the limits of variation of monthly and annual sums are comparatively small. On all maps an increase of the magnitude of F_∞ from the poles to the tropics is observed. The greatest magnitudes are noticed over deserts of low latitudes, for which insignificant cloudiness and high air temperature in the case of low moisture content are characteristic. Near the Equator in places with elevated cloudiness and significant humidity,

magnitudes of fluxes of departing radiation are appreciably reduced. However, along the Equator a continuous zone of reduced values of F_∞, that is on the maps of Simpson [2] is not observed.

Average yearly magnitudes F_∞ over the globe vary from 18 mW/cm^2 at high latitudes up to more than 25 mW/cm^2 above the North African and Arabian deserts. An appreciable effect on the magnitude of departing radiation is exerted by cold and warm ocean currents. A decrease of the magnitude of F_∞ is connected with cold currents; an increase of them is connected with warm currents. The great oceanity of the southern hemisphere and the shift of the thermal equator to the north of the geographical Equator leads to the fact that on the average thermal radiation of the southern hemisphere is less than that of the northern. /13

The absolute maximum of monthly magnitudes F_∞ (29 mW/cm^2) is located above the central part of the Sahara (July); the absolute minimum is found above Eastern Siberia (January), where the magnitude of departing radiation does not exceed 16 mW/cm^2.

Using data of maps of annual and monthly sums of departing radiation, K.Ya. Vinnikov calculated the average values of radiation fluxes for 10-degree latitudinal zones, that are presented in Table 1.2. As can be seen from the table, these data agree well with results of calculations of Houghton and D. London.

Experimental data that make it possible to estimate the degree of reliability of accepted hypotheses on the structure and nature of radiation of the atmosphere are of particular value for estimating the results of theoretical calculations.

For obtaining experimental data on the planetary distribution of the radiation balance and its components, the application of artificial Earth satellites is most promising. Artificial Earth satellites have an important advantage that lies in the fact that in a comparatively short time interval, measurements can be conducted from them at many points of the globe, over a large part of its surface, to study latitudinal, diurnal, local, seasonal dependences of one or another phenomenon. The value of information collected by satellites from extensive territories of oceans, of polar regions, of desert and mountainous regions, that constitute almost 80% of the Earth's surface, is especially great. Terrestrial measurements here

TABLE 1.2

Latitude, Degree	Values of Fluxes of Leaving Radiation, mW/cm^2					
	1	2	3	4	5	6
0-10	19.33	20.72	24.01	21.63	24.29	23.87
10-20	19.82	21.28	24.36	22.68	24.78	24.22
20-30	19.93	21.42	24.22	23.24	24.71	24.08
30-40	19.85	21.00	23.38	22.47	22.89	22.54
40-50	19.67	20.23	22.12	21.14	21.42	21.14
50-60	19.34	19.60	20.93	20.30	20.09	20.09
60-70	18.60	18.90	19.88	19.60	18.90	19.11
70-80	17.92	17.85	19.11		17.71	
80-90	17.61	17.29	18.27		17.15	
F_∞, mW/cm^2	19.6	20.6	23.0	21.5	22.8	22.3
T_{rad}, K	243	246	253	248	251	250

Note: 1. Simpson [2]. 2. Bagrov [3]. 3. Houghton [5]. 4. Berlyand [10]. 5. London [6]. 6. Vinnikov [11].

are very rare or altogether absent. Although the accuracy of satellite measurements of departing radiation is as yet comparatively low, in recent years one has succeeded in obtaining experimental data that characterizes the spatial and temporal variation of departing radiation and of the radiation balance of the system Earth-atmosphere.

Such measurements were conducted, in part, on American satellites "Tiros" and "Nimbus" and Soviet satellites "Kosmos" and "Meteor." Below, a summary is presented of some contemporary experimental and calculated data on the middle latitude distribution of leaving long wave radiation F_∞ for the winter and summer periods. This summary is represented in Figs. 1.3 and 1.4. As can be seen from the drawings, in all cases the minimum of leaving radiation is observed near the Equator, and /14 maxima are observed in subtropic zones with subsequent continuous decrease in the direction of the poles; in the summer

hemisphere, radiation is more intensive than at the corresponding latitudes in the winter hemisphere.

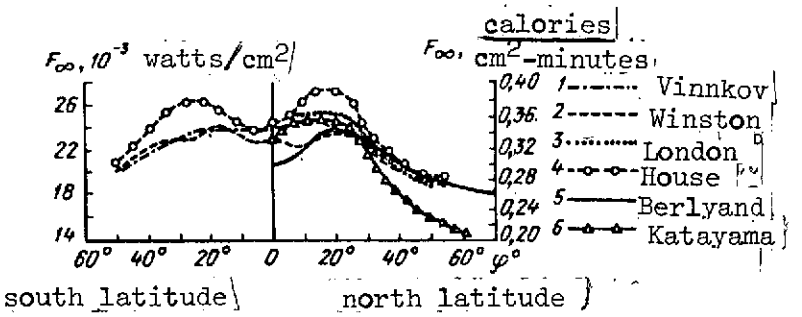

Fig. 1.3. Departing long wave radiation according to data of measurements and of calculations (winter period).

1 - Vinnikov. January (average multi-year, calculated); 2 - Winston, Rao. November - January (measurement from "Nimbus-II": 3 - London. Winter (calculated, average per season); 4 - House. February - April (measured from "Tiros-IV"); 5 - Berlyand, T.G. December (average multi-year, calculated); 6 - Katayama. January (average multi-year, calculated).

According to data of measurements from artificial Earth satellite "Nimbus-2", Ye. Raschke plotted maps of the distribution over the globe of departing long wave radiation, averaged along several two-week time intervals in May-July 1966 [13]. Comparison of these maps with calculated ones gives satisfactory agreement. Magnitudes of departing radiation are appreciably reduced in regions connected with cloud fields and elevated humidity of equatorial regions. /15

On the other hand, above deserts of low latitudes, where cloudiness is insignificant and the moisture content of the atmosphere is small, magnitudes of departing radiation are maximal. Correlation of magnitudes F_∞ with the temperature of the underlying surface is clearly observed. For instance, values of F_∞ are reduced near the South Pole, in Greenland and above the ice fields of the East Siberian Sea. Both in calculated data and in satellite measurements, the zonal location of isolines above cold and warm ocean currents is appreciably disrupted.

From what was discussed above, one can conclude that calculated data completely satisfactorily represent qualitative

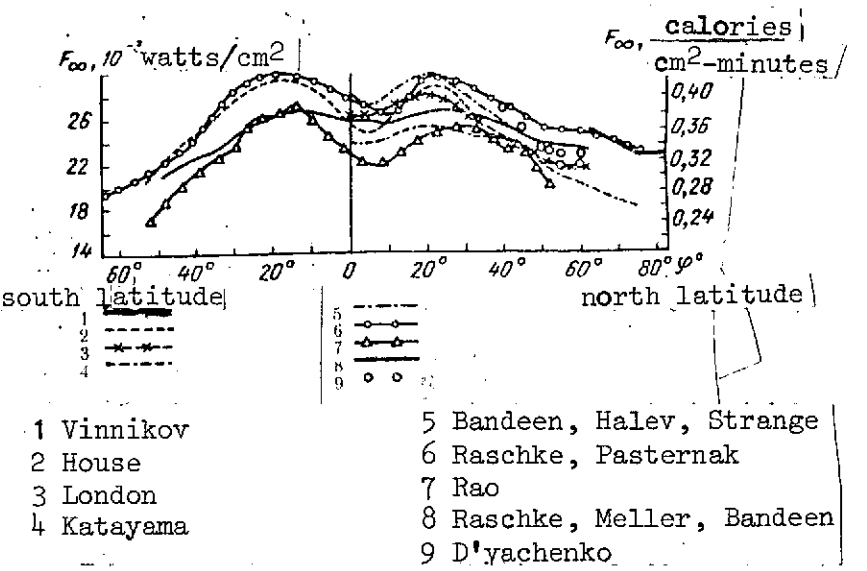

Fig. 1.4. Departing long wave radiation according to data of measurements and calculations (summer period).

1- Vinnikov. July (average multi-year, calculated); 2 - House. April - June (measured from "Tiros-IV); 3 - London. Summer (calculated, average per season); 4 - Katayama. July (average, multi-year, calculated); 5 - Bandeen, Halev, Strange. June 1963 - May 1964, region of the spectrum 8-12 microns, measured from "Tiros-VII"; 6 - Raschke, Pasternak, 1-25 June 1966 (measured from "Nimbus-II"); 7 - Rao. July (10 days, measured from "Tiros-III"); 8 - Raschke, Meller, Bandeen. May-July (measured from "Nimbus-II"); 9 - D'yachenko "Kosmos-122", 26-29 July, data for the USSR.

special features of the geographical distribution of departing radiation. Significant quantitative discrepancies between experimental and theoretical data can be explained both by the degree of approximation of theoretical calculations, and by errors of measurements. To enhance the accuracy of the determination of the magnitude of the radiation balance of the system Earth-atmosphere, above all a decrease of errors of measurements is required, and likewise refinement of calculating methods.

In recent years in connection with the development of satellite meteorology, great consideration is given to the spectral and angular structure of the field of departing long wave radiation. These data are necessary for the investigation of the structure and composition of the atmosphere, and likewise for the solution of a number of applied problems

connected with the design of satellite navigation systems, by calculations of the thermal regime of satellites, etc.

In theoretical articles these questions are comparatively extensively elucidated; however, theoretical calculations can only give approximate estimates. A fully adequate solution of the problem can be achieved only on the basis of experiment. Nevertheless, in the experimental data published up to now, questions of the spectral and angular structure of departing radiation are scarcely touched upon. The statistical characteristics of departing long wave radiation of the Earth in separate parts of the spectrum are totally uninvestigated; there is no data on the combined distributions of spectral intensities of the radiation of the Earth. These and some other questions are considered in the following chapters on the basis of experimental material, obtained with the help of artificial Earth satellites of the "Kosmos" series.

CHAPTER TWO

THE APPARATUS, THE METHOD OF CALIBRATING IT AND THE RECORDING OF INFORMATION [14]

2.1 Description of the Apparatus.

Experiments in the investigation of the distribution of energy in the spectrum of thermal radiation of the Earth were carried out on artificial Earth satellites "Kosmos-45" and "Kosmos-65." Elements of orbits of these satellites were respectively the following: angle of inclination of the plane of the orbit to the plane of the Equator 65°, initial periods of revolution 89.69 and 89.80 minutes, altitudes at the perigree 206 and 210 kilometers, altitudes at the apogee 327 and 342 kilometers (the first figures pertain to satellite "Kosmos-45," the second to satellite "Kosmos-65"). Satellite "Kosmos-45" was put in orbit around the Earth in September, 1964; satellite "Kosmos-65" in April, 1965.

Measurements were conducted continuously for a period of 65 hours on artificial Earth satellite "Kosmos-65." In the course of the entire time of operation of the apparatus on artificial satellite "Kosmos-45" and for a large part of the time on artificial Earth satellite "Kosmos-65" radiation of the Earth was investigated at an orientation of the optical axis to the nadir; for the rest of the time on artificial earth satellite "Kosmos-65" observations were conducted of radiation from the region near the horizon of the Earth. Measurements were conducted by the method of comparison of radiation of the Earth with radiation of outer space. Since radiation from outer space in the infrared region of the spectrum is insignificantly little, one can consider that the absolute values of the flux of thermal radiation of the Earth were recorded by the apparatus.

A diffraction scanning spectrophotometer, that is an electronic optical mechanical apparatus intended for measurement of the flux of the thermal radiation of the Earth in the spectral range 7-38 microns, was used in experiments. [14] For operation in such a wide range, the apparatus had two spectral sub-ranges: the first from 7 to 20 microns; the second from 14 to 38 microns.

The dispersing elements of monochromators of the apparatus were plane reflecting diffraction gratings with 24 lines/

millimeter in the first, and with 12 lines/millimeter in the second spectral sub-range, with maximum of energy concentration in the spectrum of the first order at wave lengths 10 microns in the first and 20 microns in the second spectral sub-range.

Expansion of each spectral sub-range is inadvisable for two reasons: first, this is determined by the nature of the distribution of light by wave lengths by means of diffraction gratings, the reflecting capacity of which quickly falls on both sides from the wave length of the reflection maximum; and, second, because of the necessity of excluding overlapping of the third and higher orders of spectra on the operating spectrum of the first order. /17

Magnitudes of spectral resolution of the apparatus $\Delta\lambda$ (by the half-width of the apparatus function), obtained by means of calculation for both spectral sub-ranges, are presented in Table 2.1.

TABLE 2.1

λ, Microns	$\Delta\lambda$, Microns	
	7-20 Microns	14-38 Microns
7	1.4	-
10	1.3	-
14	1.2	2.8
18	1.1	2.7
22	-	2.6
27	-	2.4
36	-	2.1

During the recording of radiation in spectral invervals equal to the magnitudes of $\Delta\lambda$, the satellite travelled a distance comparable with the magnitude of spatial expansion of the apparatus ($\sim$10 kilometers). This means that the recorded fluxes of radiation of neighboring elements of the spectral expansion can be considered independent.

The angle of the instantaneous field of vision of the optical system of the apparatus is 1°46' by 2°20'. At such an angle of the field of vision and at an average altitude of flight of 250 kilometers, the image of a part of the radiating surface with dimensions 7.5 by 10 kilometers fills the inlet slits. The wide side of the slit is located along the direction of flight. The optical axis of the apparatus was oriented to the nadir. In the case of observation of the horizon on artificial satellite "Kosmos-65," the optical axis of the apparatus was oriented in the direction of motion of the satellite somewhat lower than the horizontal direction; scanning took place in a field of vision at an angle $\pm 8°30'$ in a vertical plane from this direction. As receivers of radiation semiconducting bolometers with a sensitive area equal to 1 mm^2 (1 by 1) were used.

The cycle of operation of the apparatus consisted of the following successively carried out operations (Fig. 2.1): /18

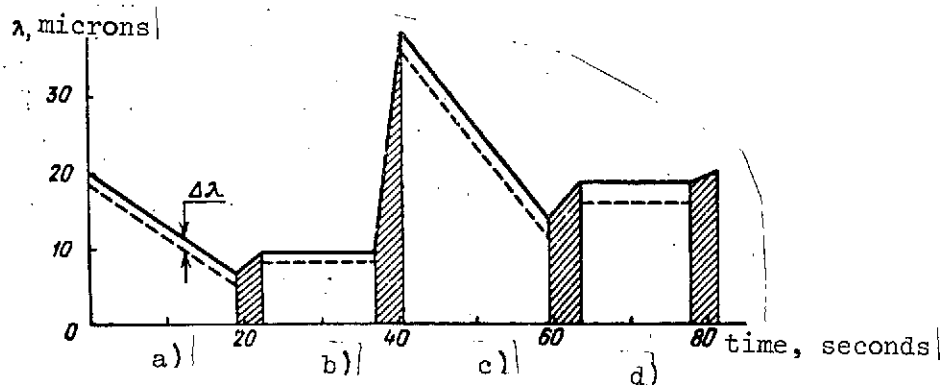

Fig. 2.1. Cycle of operation of the spectrophotometer.

a) measurement of the distribution of energy in the spectrum from 7 to 20 microns during 18.5 seconds;

b) sighting along the trajectory of motion of the satellite at a wave length λ = 9.5 and 10 microns during 14.4 seconds for satellites "Kosmos-45" and "Kosmos-65" respectively;

c) measurement of the distribution of energy in the spectrum from 14 to 38 microns during 18.5 seconds;

d) sighting along the trajectory of motion of the satellite at wave length λ = 18.5 and 19 microns during 14.4 seconds for satellites "Kosmos-45" and "Kosmos-65" respectively.

The remaining time in the cycle was occupied with transitions between operating regimes. The duration of one full operating cycle of the apparatus constituted 81 seconds.

If in parts a and c there took place recording of energy in separate spectral intervals $\Delta\lambda$ every 640 kilometers, i.e. the macrostructure of the field of Earth's radiation was investigated, then in parts b and d the microstructure of the field of radiation was investigated by scanning the field of vision throughout 120 kilometers in wave lengths of scanning. Moreover, parts b and d perform another role: if readings on neighboring parts remain constant, i.e. uniformity of conditions in the atmosphere occurs, then the probability is great that such a uniformity will be observed also during recording of the spectrum located between parts b and d. This signifies that special features in the spectrum in parts a and c are determined by processes of the radiation transfer in the atmosphere, and not by the variations of the synoptic situation along the path of the satellite.

Henceforth, for brevity of the discussion, the parts of the records on traces that correspond to cycles b and d of the operation of the spectrophotometer we will designate with the term "scans." /19

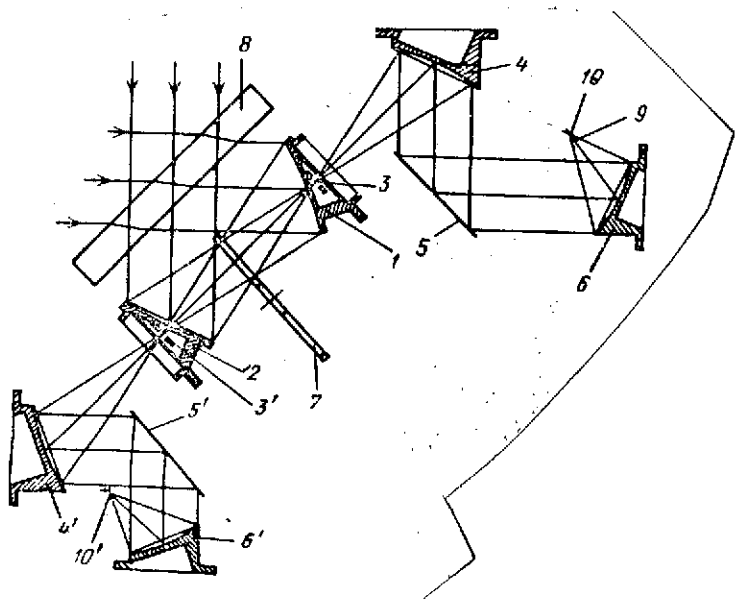

Fig. 2.2. Optical scheme of the spectrophotometer.

The optical scheme of the spectrophotometer is shown in Fig. 2.2. Radiation of the Earth and of outer space enters through inlet window 8, that ensures the pressurization of the whole volume of the apparatus. The window is made of crystal KRS-5. Mirror two-sided gold-plated modulator 7 with 4 blades ensures successive substitution, with a frequency 27 Hertz on inlet slits of monochromators, of the radiant flux from the surface to be investigated to the flux from the background of comparison and vice versa.

Mirror objective lens 1 reflects a part of the surface to be investigated on the inlet slit of monochromators 3 and 3'; the same objective lens 2 is oriented to the background of comparison into outer space. Both objective lenses have a focal distance 55 millimeters and aperture ratio 1:2. Both diffraction monochromators are equipped with collimators and cameras with identical mirror objective lenses (4 and 4', 6 and 6'); objective lenses of cameras have focal distances 20 millimeters and aperture ratio 1:1.

To ensure minimal external dimensions of the apparatus, all mirror objective lenses were realized as extra-axial paraboloids. They are all gold-plated with the exception of 4', made of lithium fluoride without coating. Objective lenses 1 and 2 are located in such a manner that radiant fluxes from the surface to be investigated and from the background of comparison pass through one and the same place of inlet window 8, excluding by this noises due to non-uniformities of the inlet window. /21

As cutoff filters in the optical system there were used: in the first spectral sub-range -- plate 9 made of indium antimony 0.15 millimeters in thickness, that does not transmit radiation shorter than 7 microns; in the second spectral sub-range there is no transparent light filter, but lithium fluoride crystal from which is produced collimator objective lens 4', does not reflect radiation shorter than 14 microns, and reflects radiation well in the whole range from 14 to 38 microns.

Radiation fluxes from the surface to be investigated and from the background of comparison arranged along the spectrum are simultaneously focussed by objective lenses 6 and 6' on sensitive areas of two radiation receivers in such a manner that if radiation of the surface to be investigated is incident on the receiver of the first spectral sub-range, then radiation of the background of comparison is incident on the receiver of the second spectral sub-range and vice versa.

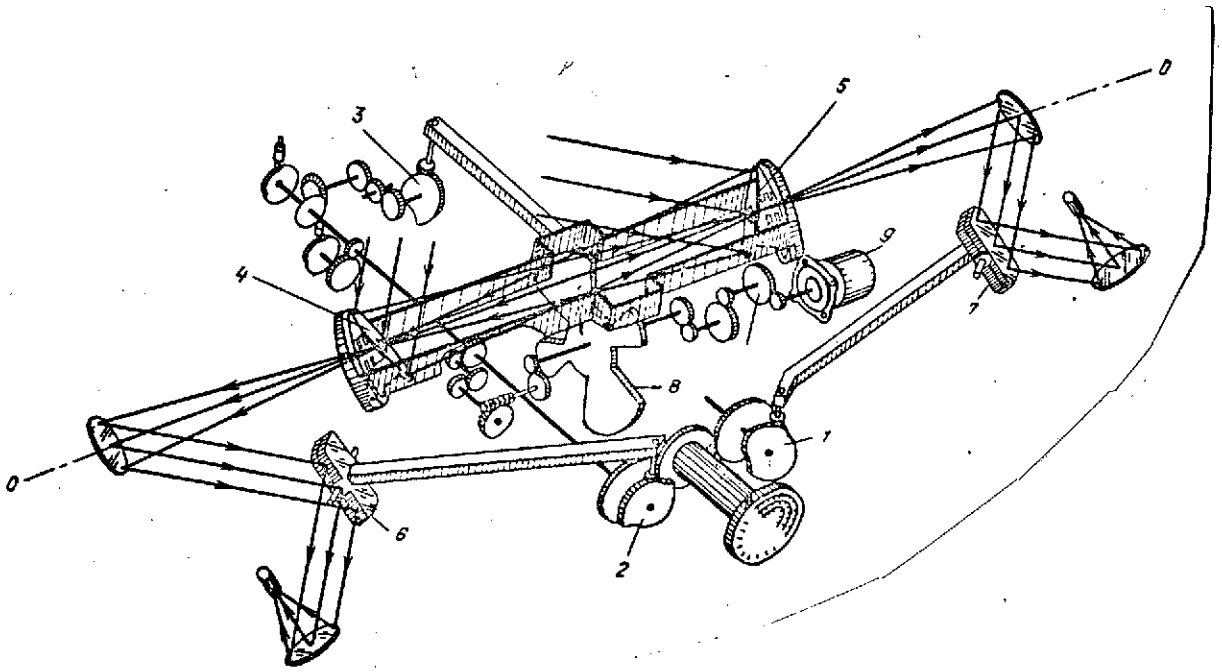

Fig. 2.3. Kinematic scheme of the spectrophotometer.

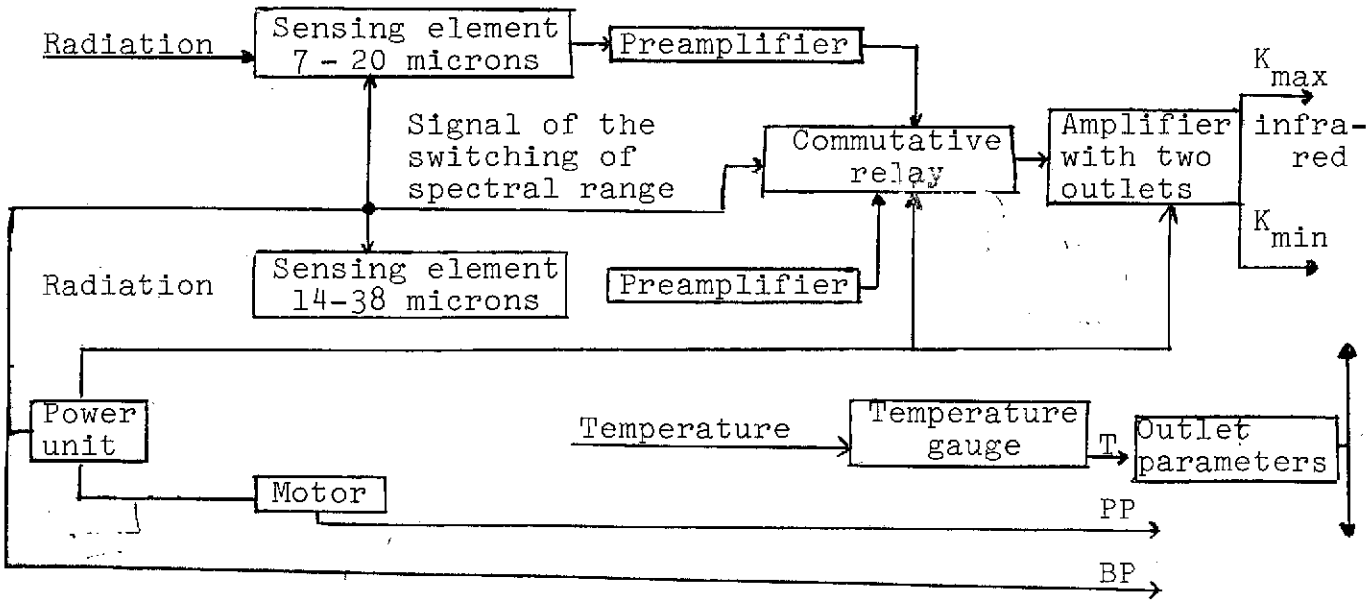

Fig. 2.4. Block diagram of the electronic part of the spectrophotometer.

Fig. 2.3 illustrates the kinematic scheme of the spectrophotometer. Scanning over the spectrum is accomplished by rotation of diffraction gratings 6 and 7 around axes parallel to the direction of lines on gratings, using the corresponding cam mechanisms. Scanning over a locality at an angle ±8°30' /22
is carried out by rotation of mirror objective lenses 4 and 5 around axis 00 with the help of cam mechanism 3. The drive of cam mechanisms and of modulator disc 8 is realized using electric motor 9.

A block diagram of the electronic part of the spectrophotometer is presented in Fig. 2.4.

For the measurement of radiation, separated by the optical system of the apparatus into two spectral sub-ranges, the amplifying circuit contains two channels, each of which has a preamplifier. Channels other than sensitive elements and preamplifiers have one overall amplifier. Signals after the preamplifier are supplied through a device for switching of spectral sub-ranges (a commuting relay) into the intake of the amplifier alternately every 40.5 seconds. The commuting relay is controlled by a cam, kinematically connected with the motor of the apparatus. To expand the limits of measurements, the amplifier is divided into two units with different amplifying coefficients and separate outlets. The ratio of amplifying coefficients of the units is 1:3.

In addition to the basic signals (infrared in Fig. 2.4) from outlets of the amplifier units, auxiliary information was likewise given on the recorder -- signals of the control of the work of the motor (parameter PP), of the control of the work of the power unit (parameter BP), of the control of temperature of the apparatus (T).

2.2 Calibration of the Spectrophotometer.

To obtain the distribution of absolute radiation fluxes along the spectrum, one must convert the ordinates of traces on the film to the units of energy that correspond to them. To do this, before the beginning of the experiment the spectrophotometer is calibrated by radiation of the source with a known distribution of energy in the spectrum. A simulator of an absolutely black body with a large aperture [15] is such a source.

Two simulators were arranged in front of the spectro-

photometer in such a manner that radiation from them fell on the inlet window of the spectrophotometer in the same direction in which it entered the apparatus from Earth and from outer space in the conditions of the experiment. Thus, radiation from each of the simulators alternately entered both receivers and the signal at outlet was proportional to the difference of the energy fluxes of the simulators in the given spectral interval.

Records of the spectra were produced at constant temperature of the simulator of cosmic radiation and at various temperatures of the simulator of the radiation of Earth on the same recorder, that was used in the experiment. This eliminated mistakes connected with the difference of sensitivities and with possible non-linearities of recorders. The temperature of simulators was maintained at a given level with an accuracy of $\pm 0.5°C$. /23

Samples of obtained calibration traces are presented in Fig. 2.5. These traces were recorded at temperature of the simulator of cosmic radiation equal to 294°K and temperatures of the simulator of Earth's radiation 303, 313, 323, 333, 342°K. In the traces overlapping of the spectrum of the second order can be clearly seen. In the first spectral sub-range, overlapping occurs in the region from 15 to 20 microns and in the second spectral sub-range in the region from 28 to 34 microns. At large wave lengths the intensity of the spectrum of the second order quickly decreases, whereas the spectrum of the first order still remains sufficiently intense. In short wave parts of sub-ranges ($\lambda<28$, $\lambda<14$) overlapping is completely absent due to the use of the above-mentioned cutoff filters with transmission boundaries 14 and 7 microns respectively.

Spectral transmission coefficients of all elements of the optical system of the apparatus, with the exception of diffraction gratings, were measured on standard spectrophotometers.

The distribution of intensity of radiation along the spectrum, that results from the diffraction grating in the region of high concentration, was calculated according to data of article [16]. The overall transmission coefficient of the whole optical system K, equal to the product of the transmission coefficients of all its elements taking into account the spectral distribution of light of the diffraction grating, as a function of wave length, is represented in Fig. 2.6a and 2.6b. In case of scanning over the spectrum, coefficient K /24

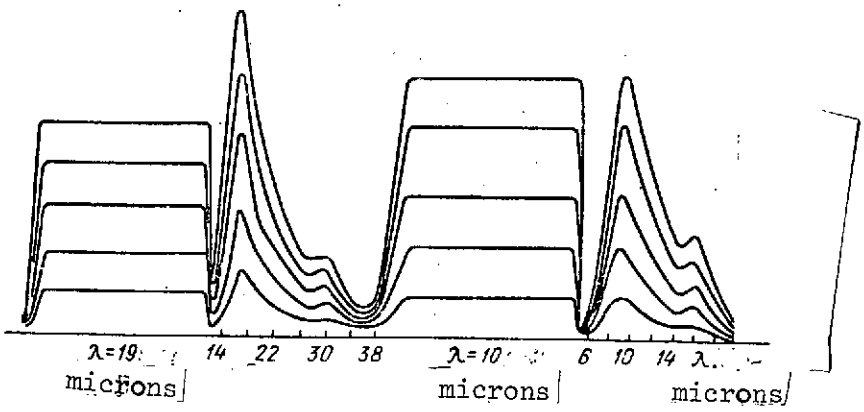

Fig. 2.5. Calibration of a trace of a complete cycle of operation of a spectrophotometer.

varies as a function of the wave length; in case of scanning over a locality, naturally, it remains constant. Discontinuities of the curve of the coefficient of transmission in the intervals between scanning over the spectrum and over a locality correspond to the times of rapid shifting of the diffraction grating from the position that corresponds to the end of scanning over the spectrum, to the position at which scanning over a locality is conducted or, vice-versa, from this latter position to the initial position before the start of scanning over the spectrum. Some special features of the trace on these transitional parts (in particular, ordinates of minimum A and of maximum B, recorded on the short wave scan) of instrumental origin make it possible to control the accuracy of the work of the apparatus.

The signal in the outlet of the apparatus does not completely correspond to the actual distribution of energy along the spectrum at the inlet. Errors are introduced by elements of the optical system of the apparatus, the transmission coefficients of which depend on the wave length, by the inlet and outlet slits (the outlet slit is the sensitive area of the receiver), and likewise by the amplifier channel.

Reconstruction of the true spectral distribution of energy by the known signal at the outlet and the known apparatus function of the spectrophotometer by analytical means is possible in principle, but entails great mathematical difficulties. /25
Therefore, another method was chosen, based on the use of

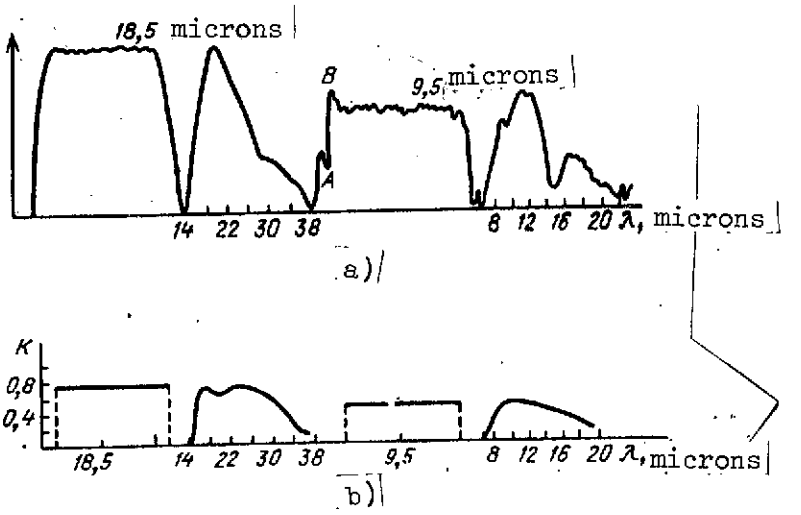

Fig. 2.6. Characteristic trace of a spectrophotometer and the dependence of the transmission coefficient of the optical system on wave length.

standard spectra with a known distribution of energy, the results of the measurement of which by a spectrophotometer were compared with spectra of leaving radiation, obtained from satellites. Results of the processing of the spectra investigated were expressed finally in intensities and temperatures of the equivalent radiation of an absolutely black body.

In case of bulk processing of spectra it proved to be convenient to project the image of traces on a screen, on which was drawn as a grid the family of curves of the radiation of absolutely black bodies of different temperature or intensity. Families of curves of the radiation of black bodies with temperatures 200-300°K for both spectral sub-ranges are represented in Fig. 2.7. These families of curves are plotted only for regions of the first orders of magnitude in each of the spectral sub-ranges (7-15 microns in the first and 14-28 microns in the second sub-range). Along the axes of ordinates are plotted linear units of ordinates of traces on the screen of the projector. Onto these families are projected traces (heavy curves), obtained from outer space.

In the first spectral range a band of ozone with center at $\lambda = 9.6$ microns and a blend of bands of carbon dioxide and ozone with center about 15 microns can be seen. /26

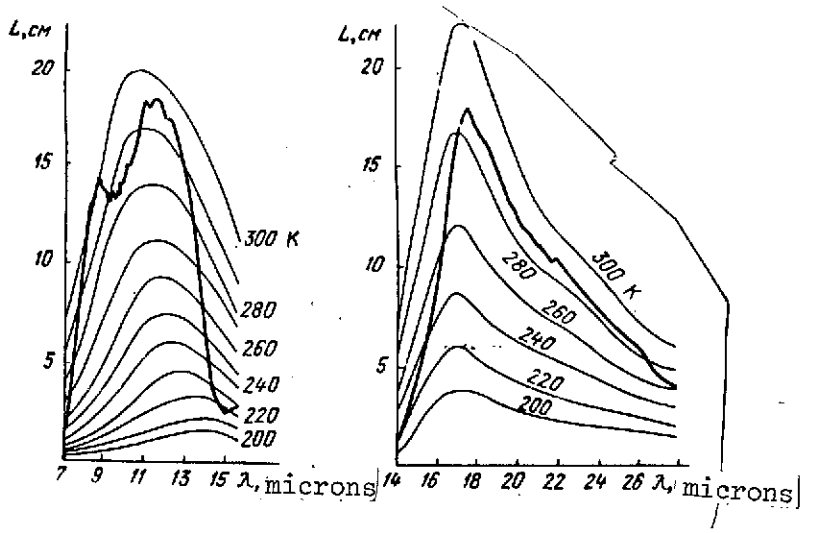

Fig. 2.7. Families of curves of equal temperatures of radiation of absolutely black bodies.

To express the results of the processing of spectra in intensities of the equivalent radiation of an absolutely black body, families of curves of equal temperatures were reorganized into families of curves of equal intensities, presented in Fig. 2.8.

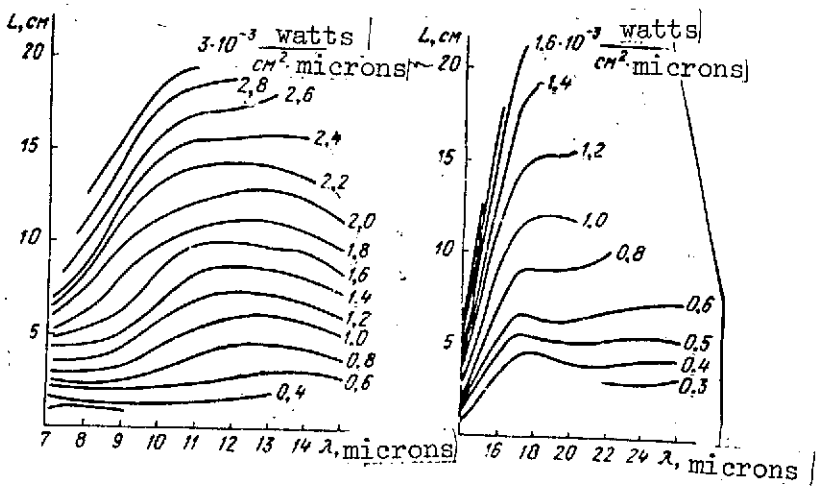

Fig. 2.8. Families of curves of equal intensities of radiation of absolutely black bodies.

While calibrating a spectrophotometer by energies, joining of traces by wave lengths was simultaneously carried out along lines of reflection of quartz 8.8 and 21 microns, lines of absorption of transparent solid films (lavsan, solid phthalate, polystyrene) and lines of absorption of liquid filters (chloroform, bromobenzene, pyridine, toluene, chlorobenzene).

It should be mentioned that due to the finite resolving power of a spectrophotometer over wave lengths, some closely arranged absorption bands are not resolved. So, for instance, two absorption bands of polystyrene with center 13.2 and 14.2 microns (Fig. 2.9) are visible on traces as one absorption band with a center at 13.7 microns. In this same drawing are represented traces of spectra of the reflection of quartz and of the transmission of toluene.

The accuracy of the obtained results is determined basically by errors of calibration, by mistakes of measurements, by mistakes of joining spectra by wave lengths. The largest errors arise due to the finite resolving power of the apparatus over wave lengths. The spectrophotometer was calibrated by radiation of a black body and due to the fact that the true spectral distribution of energy is smoothed by the apparatus, the discrepancy of spectral distributions of energy of the radiation to be investigated and of an absolutely black body leads to an error, that grows with magnitude $\Delta\lambda$. As analysis /27

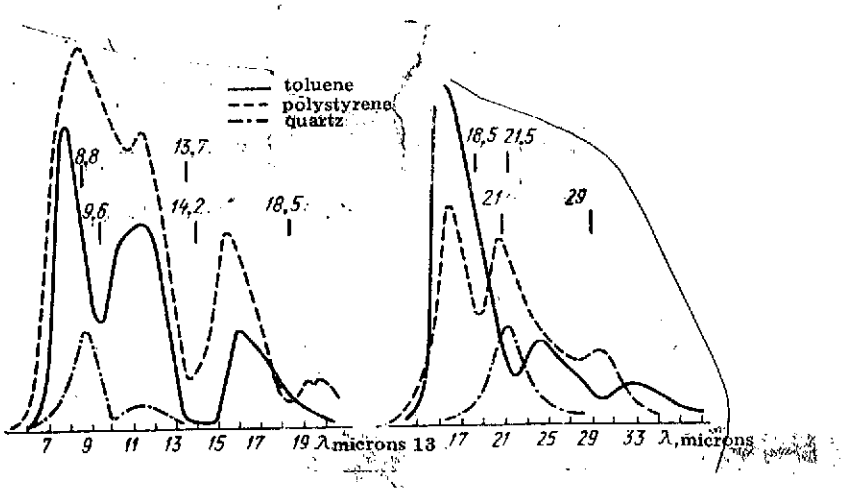

Fig. 2.9. Traces of transmission spectra of polystyrene, toluene and reflection spectrum of quartz.

showed, the greatest errors of this sort arise in the interval of wave lengths 13-16 microns (the absorption band of CO_2) and in the absorption band of ozone with center 9.6 microns. In the center of the CO_2 band the error has a systematic nature and leads to overestimation of the true value of radiation energy of approximately 8%. At other wave lengths (excluding the O_3 band) the error does not exceed 3%.

2.3 Recording Information

Recording information in case of calibrations and in flight was accomplished with the help of an edge multi-loop oscillograph on 35-mm motion picture film. The maximal time of uninterrupted recording consisted of about 4 days. The used film was delivered to Earth in a discharged container. The joining of traces to locality was performed by the readings of clocks, the image of the dial of which every 112 seconds was printed on film. For determining the accuracy of the movement of the clocks, verification of them was performed by signals of universal time before and after flight. Coordinates of the sections of the Earth's surface to be investigated were determined by the known time of measurement taking account of the accuracy of the movement of clocks and by orbital data of the satellite. /28

In Fig. 2.10 a sample of a film record obtained in the case of sighting of the day side of the Earth from the artificial Earth satellite "Kosmos-45." Traces with two outlets of the amplifier can be seen well -- their amplitudes differ approximately three-fold. On traces it is easy to distinguish four regimes: photographing of spectra 14-38 microns (a), scanning by locality at a wavelength of 18.5 microns (b), photographing of spectra 7-20 microns (c) and scanning by locality at wave length 9.5 microns (d). These regimes successively replace one another; each of them has its characteristic form.

A smoothly varying uninterrupted line in the upper part of the record represents the signal of the photometer of the range 0.6 - 0.8 microns. This photometer was basically intended for distinguishing clouds from the surface of seas and continents by a method independent of infrared measurements. In red light 0.6 - 0.8 the albedo of clouds reaches 60-70%, and water surfaces and sections of dry land covered by forest seem almost black. Even deserts have an albedo that sharply differs from clouds. The resolving power of the photometer on a locality is about 30 kilometers.

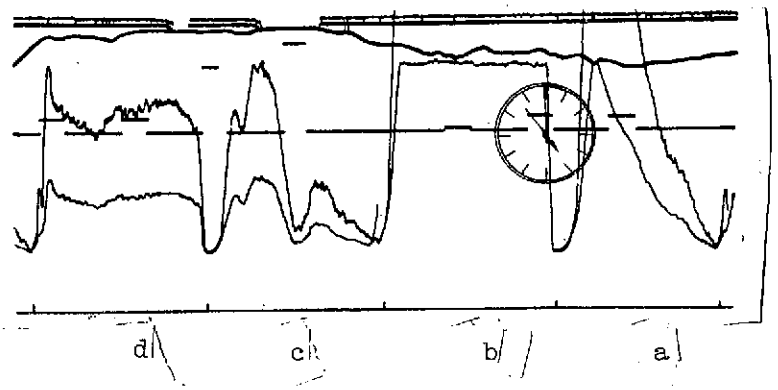

Fig. 2.10. Sample of the record of a spectrogram on film.

Besides these informative signals, signals of the control of the operation of the motor of the spectrophotometer, of the power source and the signal of the thermal data unit were recorded.

CHAPTER THREE

/29

STATISTAL CHARACTERISTICS OF DEPARTING RADIATION OF THE EARTH IN SEPARATE SECTIONS OF THE SPECTRUM

3.1 Method of Deciphering Traces of Spectra.

The intensity of radiation of the Earth leaving into outer space in various ranges of the spectrum is determined by a number of factors, which are random at any moment at any point on the Earth. Consequently, the intensity of radiation is a random magnitude dependent both on time and on the geographical position of each section of the surface of the Earth that is to be considered. Therefore, in the estimation of the intensity of leaving radiation of the Earth, the most advisable approach is a statistical one, in which the intensity of radiation is considered as a random function, given in the form of a sequence of discrete values -- of separate results of measurements in each of the sections of the spectral range to be investigated. The whole set of values of intensity of radiation in a determined section of the spectral range can be considered as a global (overall) set, that characterizes radiation of the whole surveyed surface of the Earth. Selections, pertaining to separate latitudinal zones, or united by some other general feature to the determined assembly, can characterize radiation of determined objects (surfaces of oceans, of continents, etc.)

It should be mentioned that the treated part of the measurements conducted does not include the whole surface of the Earth. However, by force of the randomness of the "selection" of sections of the surface of the Earth, significantly distant from one another, and of a sufficiently great number (about 1200) of measurements, one can assert with determined reliability that on the remaining unexamined sections of the surface in the limits of latitudes considered ($\pm 65°$), radiation can be characterized by those same laws that are obtained on the basis of the measurements conducted.

In accordance with the overall aim of the experiment, investigation of the spectral distribution of energy of departing radiation of the Earth, in deciphering traces the spectrum was /30 divided into a number of equal sections, the width of which was chosen taking into account the spectral resolving power of the spectrophotometer [18]. So, in the range of wave lengths λ = 7–15 microns, the spectrum was divided into sections

$\Delta\lambda$ = 1 micron in width; and in the range of wave lengths λ = 14–26 microns, the spectrum was divided into sections $\Delta\lambda$ = 2 microns in width. For each section of the spectrum in accordance with the obtained calibration dependences (see Fig. 2.8), the mean intensity of radiation, that pertained to the center of each spectral section $\Delta\lambda$, was determined.

For the simplification of the process of photographing readings with the help of a projector in accordance with a recommendation of mathematical statistics [19,20] the whole scale of intensities I was divided into categories: in the range λ = 7–15 microns, $\Delta I \approx 0.2 \times 10^{-3}$ watts·cm^{-2}·microns^{-1} and in the range λ = 14 to 26 microns, $\Delta I \approx 0.1 \times 10^{-3}$ watts·cm^{-2}·microns^{-1}. To decipher the traces by the size of the screen of the projector, a deciphering grid was made, in the limits of each section of the spectral range of which were drawn the boundaries of categories of intensities ΔI. If when projecting traces onto this grid, the curve fell in the limits of some category, then the mean value of the category was attributed to the intensity of radiation I in the given section of the spectral range. Recording of traces of a relatively deciphered grid by wave length was accomplished with the help of so-called "apparatus peaks" that appear in each cycle of operation of the spectrophotometer.

Results of the deciphering of traces of spectra were recorded in a table and then transferred to punch cards to be statistically processed on an electronic computer.

3.2 Global Differential Laws of the Distribution of Spectral Intensities of Radiation of the Earth.

As was already indicated, the intensity of radiation of the Earth in each section of the spectral range is a random magnitude. Therefore, for investigating it, the most advisable approach is a probabilistic statistical one, which requires a large number of measurements, which make it possible to judge with sufficient reliability the magnitude of intensity of radiation and its possible fluctuations for each section of the spectral range. The most complete characteristic of a random magnitude, as is well known, is the law of its distribution. Therefore, in addition to the numerical characteristics: mathematical expectation $\bar{I}$, the second μ_2 (dispersion), the third μ_3, and the fourth μ_4 of the central moments, the bar graphs of the differential laws of distribution were determined during the statistical processing of the results of measuring the /31

radiation intensity in specific sections of the examined range of a spectrum of width $\Delta\lambda = 1$. These graphs are presented in Figures 3.1 and 3.2.

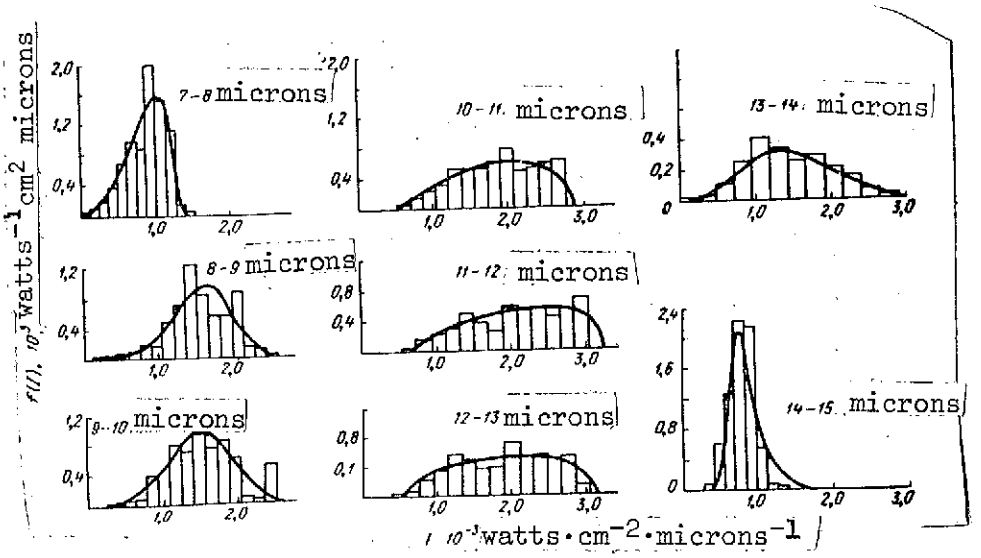

Fig. 3.1. One-dimensional differential laws of the distribution of radiation intensities in specific sections of the $\Delta\lambda = 1$ micron zone of the spectrum from 7 to 15 microns.

In the drawings the value of random magnitude I (the intensity of radiation in a given spectral section) is plotted along the abscissa and along the ordinates, the probability density (watts^{-1} ·cm^2 ·microns):

$$f(I_i) = \frac{n_i}{N\Delta I_i}, \qquad (3.1)$$

where n_i is the number of observations of random magnitude I in the i^{th} division; N - the total number of processed spectra; ΔI_i - the extent of the i^{th} division, watts·cm^{-2} · microns^{-1}.

The area of a rectangle, constructed at each of the divisions is equal to the experimentally obtained frequency of the given category

$$p_i = f(I_i)\,\Delta I_i \qquad (3.2)$$

As usual, the total area of the bar graph equals 1, i.e. /32

$$\sum_{i=1}^{m_0} p_i = 1, \qquad (3.3)$$

where m_0 is the number of divisions into which the whole range of observed values of random magnitude I is divided. It is usually recommended to select the number of categories within the limits $10 \leq m_0 \leq 20$ [19]. In the range of wave lengths of 7 to 15 microns, the number of categories m_0 was selected as equal to 18, and in the range of wave lengths of 14 to 26 microns, $m_0 = 10$. Magnitudes N for the same ranges of wave lengths equalled respectively 1176 (7 to 15 microns) and 1278 (14 to 26 microns).

In the experimentally obtained statistical distribution of radiation intensity of the Earth, there unavoidably are present elements of randomness, connected, above all, with the limited number of observations. Therefore, in the processing of statistical material for each statistical series, a theoretical curve of distribution is usually selected that expresses the essential features of the given statistical material and that is cleansed of probabilities connected with an insufficient amount of experimental data. Such a problem is called a problem of compensating of statistical series. /33

For the compensating of the acquired experimental data, the universal system of Pearson curves is used [20], that makes it possible to compensate not only symmetric, but also asymmetric statistical distributions which have appreciable excess. Each Pearson curve depends on four parameters: A_1, A_2, M_1, M_2 (or m, v, a, α), which are selected in such a manner that the first four moments of statistical distribution (mathematical expectation, dispersion, μ_3 and μ_4) are maintained.

In the given work, for the compensation of the statistical distribution of the intensity of radiation of the Earth, two

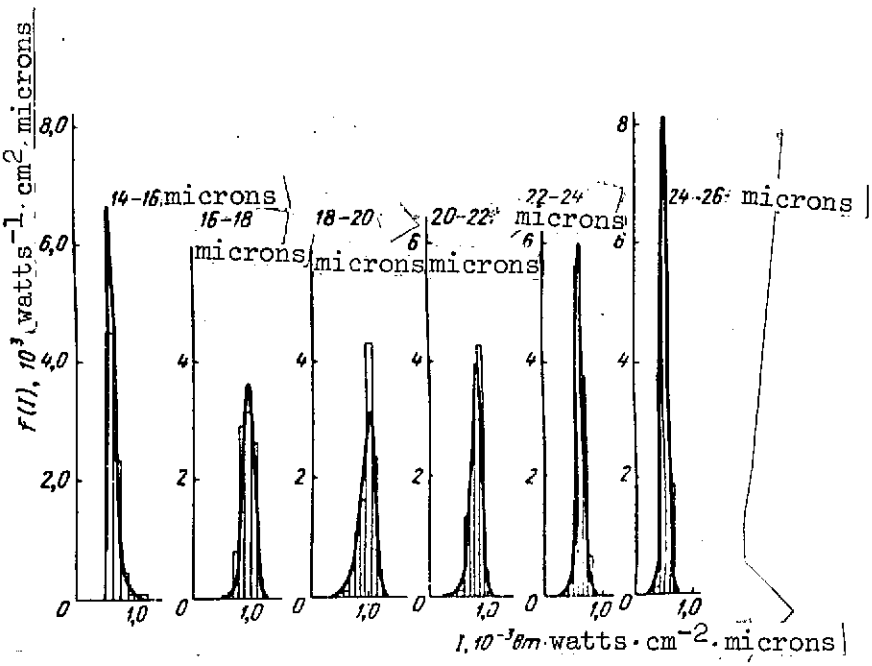

Fig. 3.2. One-dimensional differential laws of the distribution of radiation intensities in specific sections of the $\Delta\lambda$ = 2 micron zone of the spectrum from 14 to 26 microns.

Pearson equations were used

$$f(I)=y_0^*\left(1+\frac{I-M}{A_1}\right)^{M_1}\left(1-\frac{I-M}{A_2}\right)^{M_2}, \tag{3.4}$$

$$f(I)=y_0^*\left[1+\frac{(I-\alpha)^2}{a^2}\right]^{-m}\exp\left[-\nu\,\mathrm{arctg}\left(\frac{I-\alpha}{a}\right)\right], \tag{3.5}$$

where M is the mode of random magnitude I (the most probable value), watts·cm^{-2}·microns^{-1};

$$M=\bar{I}-\frac{\mu_3(r+2)}{2\mu_2(r-2)}; \tag{3.6}$$

$\bar{I}$ is the mathematical expectation of random magnitude I, watts·cm^{-2}·microns^{-1}:

$$\bar{I} = \sum_{i=1}^{m_0} I_i p_i; \tag{3.7}$$

μ_2 is the second central moment (dispersion) of random magnitude I, (watts·cm^{-2}·microns^{-1})^2:

$$\mu_2 = \sum_{i=1}^{m_0} (I_i - \bar{I})^2 p_i; \tag{3.8}$$

μ_3 is the third central moment of random magnitude I, that characterizes the asymmetry or skewness of the distribution, (watts·cm^{-2}·microns^{-1})^3:

$$\mu_3 = \sum_{i=1}^{m_0} (I_i - \bar{I})^3 p_i; \tag{3.9}$$

$$M_{1,2} = \frac{1}{2}\left[r - 2 \pm r(r+2)\left(\frac{\beta_1}{\beta_1(r+2)^2 + 16(r+1)}\right)^{1/2}\right], \tag{3.10}$$

$$r = \frac{6(\beta_2 - \beta_1 - 1)}{6 + 3\beta_1 + 3\beta_2}; \quad \beta_1 = \frac{\mu_3^2}{\mu_2^3}; \quad \beta_2 = \frac{\mu_4}{\mu_2^2}; \tag{3.11}$$

μ_4 is the fourth central moment of random magnitude I, that characterizes the "steepness," i.e. the peaks or flatness of the distribution, (watts·cm^{-2}·microns^{-1})^4:

$$\mu_4 = \sum_{i=1}^{m_0} (I_i - \bar{I})^4 p_i. \tag{3.12}$$

At $\mu_3 < 0$ in equation (3.10) a negative root is assumed for M_2.

$$A_1 + A_2 = \frac{\sigma}{2}\sqrt{\beta_1(r+2)^2 + 16(r+1)},$$
$$A_1 = \frac{A_1 + A_2}{1 + M_2/M_1}; \quad y_0^* = \frac{y_0}{N}. \tag{3.13}$$

where $\sigma = \sqrt{\mu_2}$ is the root-mean-square deviation of the random magnitude, watts·cm^{-2}·microns^{-1};

$$y_0 = \frac{M_1^{M_1} M_2^{M_2} N \Gamma(M_1 + M_2 + 2)}{(M_1 + M_2)^{(M_1+M_2)}(A_1 + A_2)\,\Gamma(M_1 + 1)\,\Gamma(M_2 + 1)};$$

$$\alpha = M + \frac{\mu_3 r}{4\mu_2};$$

$$a = \frac{\sigma}{4}\sqrt{16(s-1) - \beta_1 (s-2)^2}; \qquad (3.14)$$

$$s = -r,\ a > 0,\ m = -\frac{1}{2}(r-2) = \frac{1}{2}(s+2);$$

$$\nu = -\frac{\mu_3 s (s+2)}{4\mu_2 a}.$$

For equation (3.5)

$$y_0^* = \frac{1}{aF(s, \nu)};$$

$$F(s, \nu) = \int_{-\pi/2}^{\pi/2} \cos^s \theta e^{-\nu\theta}\, d\theta; \qquad (3.15)$$

$\Gamma(M_1+1)$, $\Gamma(M_2+1)$, $\Gamma(M_1+M_2+2)$ are the gamma functions of the corresponding arguments.

The presented system of equations (3.6) - (3.15), that determine the coefficients in the Pearson equations (3.4), (3.5), was solved with the use of electronic machine BESM-2M. Pearson curves, that equalize the experimental statistical distribution, are drawn with bold lines in Figs. 3.1 - 3.2.

Presented in Table 3.1 are values of the most important numerical characteristics of the random magnitude, the intensities of radiation of the Earth, that are described by equation (3.4). Sections of the spectrum, for which the Pearson equation (3.5) was used, are marked with an asterisk. For them, instead of values M_1, M_2, A_1, A_2, the corresponding values m, v, a, α are given in the table.

TABLE 3.1

λ, microns	$\bar{I}\cdot 10^{-3}$, watts/cm²·microns	$\sigma 10^{-3}$, watts/cm²·microns	$\mu_2\cdot 10^{-6}$, watts²/cm⁴·microns²	$\mu_3\cdot 10^{-11}$, watts³/cm⁶·microns³	$\mu_4\cdot 10^{-13}$, watts⁴/cm⁸·microns⁴	$M\cdot 10^{-3}$, watts/cm²·microns	$y^*_{O_2}\cdot 10^3$, cm²·microns/watts	M_1	M_2	$A_1\cdot 10^{-3}$, watts/cm²·microns	$A_2\cdot 10^{-3}$, watts/cm²·microns
7—8	0.88	0.25	0.062	—1.09	0.13	1.01	1.59	6.09	1.31	1.57	0.34
8—9	1.60	0.41	0.17	—3.1	0.94	1.69	0.99	176	14.3	19.6	1.59
9—10	1.54	0.44	0.19	0.64	1.1	1.53	0.99	46.7	71.8	3.9	6.02
10—11	1.88	0.55	0.30	—4.0	2.02	2.1	0.62	1.16	0.57	1.62	0.8
11—12	2.07	0.64	0.41	—8.05	3.54	2.77	0.55	0.68	0.13	2.1	0.42
12—13	1.89	0.61	0.37	—4.2	2.79	2.23	0.53	0.52	0.23	1.66	0.72
13—14	1.45	0.53	0.28	5.37	2.02	1.32	0.71	3.06	6.94	1.25	2.83
14—15*	0.79	0.18	0.034	0.0093	0.18	0.75	0.18	2.98	—5.76	0.28	0.47
14—16	0.67	0.09	0.0082	0.11	0.0039	0.59	6.64	0.24	15.7	0.023	1.52
16—18	0.93	0.11	0.012	—0.03	0.0035	0.95	3.60	13.4	7.04	0.71	0.37
18—20*	0.93	0.12	0.014	—0.017	0.011	1.02	$0.48\cdot 10^{-4}$	7.15	19.81	0.26	1.39
20—22	0.84	0.10	0.01	—0.07	0.0035	0.88	3.94	13.1	2.38	0.93	0.17
22—24*	0.65	0.073	0.0053	—0.01	0.0011	0.66	4.56	5.74	2.45	0.21	0.7
24—26*	0.51	0.057	0.0032	—0.0064	0.0006	0.52	6.85	3.48	1.56	0.11	0.54

It must again be emphasized that all the obtained characteristics are global, i.e., represent the radiation of the Earth as a whole, without subdivision of the aggregate of radiation for the shaded and lighted sides, for clouded or cloudless places, for dry land or sea, etc. Any selection of intensity of radiation according to any specific feature will be confined to the boundaries of global laws of distribution presented in Figs. 3.1 and 3.2.

For the practical use of results of the experiment, the plotting of such differential laws of distribution of radiation intensity for wider sections $\Delta\lambda$ of the range of the spectrum under consideration is of great interest.

In the plotting of these distribution laws, radiation intensities I were averaged in several neighboring sections of the spectral range. This average value was taken as the intensity of radiation in a wider section of the spectrum. With such an approach, naturally, one does not take account of the fact that in case of intermittent scanning of the spectrophotometer and in case of movement of the satellite, intensities of radiation in separate sections of the spectrum can be related to different parts of the Earth's surface and of the upper atmosphere.

Results of the calculation of bar graphs of laws of the distribution of the intensity of radiation in the spectral range 7 to 15 microns for latitudinally different sections of the spectrum are presented in the appendix in Fig. P.3.1 - P.3.5, in which the width of average sections varies from 2 to 8 microns. /37

These bar graphs were likewise equalized with the help of Pearson curves. Values of numerical coefficients in Pearson equation (3.4) for this series of laws are presented in Table 3.2.

Consideration of these differential laws of distribution makes it possible to draw the conclusion that many of them, for instance for 8 to 10 microns, 9 to 11 microns, 7 to 11 microns, 9 to 13 microns, 10 to 14 microns and some others, are close to normal. For these laws comparatively small values of the third and fourth central statistical moments are characteristic.

It is likewise characteristic that for an overwhelming number of spectral ranges the intensity of radiation practically does not exceed magnitude 3×10^{-3} watts$\cdot$cm$^{-2}\cdot$microns^{-1}.

Let's note that for the spectral range under consideration (7 to 15 microns) radiation is caused, mainly, by intrinsic thermal radiation of the system Earth-atmosphere; and, therefore, curves presented in Figs. P.3.1 - P-3.5 are correct both for day and for night sides of the globe in the case of observation of it from outer space.

In the presence of dense cloud cover, radiation beyond the limits of the atmosphere in the window of transparency is determined by radiation of upper edges of clouds.

Processing of experimental data with a "slipping" spectral interval of variable extension was also carried out for the 14 - 26 micron part of the spectrum. This range corresponds to the intense absorption band of water vapor, and radiation in it is determined, mainly, by radiation of the most upper layers of the atmosphere, located higher than the usual limits of clouds and of mountain tops. Some effect can here be exerted on the variation of intensity of radiation in the day time by atmospheric formations, located higher than the indicated boundaries, and namely: those having very small density and rarely formed noctilucent clouds (80 kilometers), dust layers of vulcanic or meteorite origin, etc. However, as a whole, radiation of the Earth in this spectral range can be considered homogeneous. The intensity of radiation practically does not depend on the change of day and night and on the nature of Earth's underlying surface, since only a very small part of the radiation of the Earth's surface can escape to outer space because of strong atmospheric absorption. /38

In Figs. P.3.6 - P.3.8 in the form of bar graphs are presented intensities of radiation of the Earth in different ranges of the spectrum from 14 to 26 microns with variable width of sections of the spectral interval from $\Delta\lambda$ = 4 microns to $\Delta\lambda$ = 12 microns.

From consideration of the bar graphs it follows that in the given spectral range, practically independent of the width of sections of the spectral interval (up to $\Delta\lambda$ = 12 microns inclusively) the intensity of radiation has substantially smaller amplitude in comparison with radiation /39
of sections of the same width in the range 7 to 14 microns.

The obtained one-dimensional differential laws of distribution and their numerical characteristics sufficiently fully describe the intensity of radiation of the Earth in the range of wave lengths 7 to 26 microns.

TABLE 3.2

$\Delta\lambda$ μ	λ · μ	$\bar{I}\cdot 10^{-3}$, $\frac{\text{watts}}{\text{cm}^2\cdot\mu}$	$\sigma 10^{-3}$, $\frac{\text{watts}}{\text{cm}^2\cdot\mu}$	$\mu_2\cdot 10^{-6}$, $\frac{\text{watts}^2}{\text{cm}^4\cdot\mu^2}$	$\mu_3\cdot 10^{-11}$, $\frac{\text{watts}^3}{\text{cm}^6\cdot\mu^3}$	$\mu_4\cdot 10^{-13}$, $\frac{\text{watts}^4}{\text{cm}^8\cdot\mu^4}$	$M\cdot 10^{-3}$ $\frac{\text{watts}}{\text{cm}^2\cdot\mu}$	β_1	β_2	r	M_1	M_2	$A_1\cdot 10^{-3}$ $\frac{\text{watts}}{\text{cm}^2\cdot\mu}$	$A_2\cdot 10^{-3}$ $\frac{\text{watts}}{\text{cm}^2\cdot\mu}$	$y_0^*\cdot 10^3$ $\frac{\text{cm}^2\cdot\mu}{\text{watts}}$
2	7—9	1,20	0,294	0,088	—1,76	0.28	1,30	0.420	3,509	51.42	44.44	4,986	6.07	0,678	1,385
	8—10	1,55	0.425	0,181	—1,03	0.75	1,58	0,018	2,975	113,25	74.98	36,27	6,50	3,156	1,030
	9—11	1,69	0.487	0,238	—0,75	1.37	1,72	0,004	2,404	6,97	2,66	2,30	1,48	1,28	0.735
	10—12	1,95	0.582	0.344	—4,74	2.50	2,24	0,056	2,118	3.29	0,894	0.399	1.69	0,76	0,573
	11—13	1,94	0,615	0.378	—4,75	2.26	2,58	0,041	1,947	2,44	0,367	0,074	1,91	0,38	0,532
	12—14	1,65	0,543	0.293	—0,16	1.96	1,69	$2.59\cdot 10^{-5}$	2,208	4,57	1,302	1,271	1,31	1,27	0,663
	13—15	0,96	0,308	0.096	+0,93	0.23	0,96	0,113	3,044	49,35	11,058	36,296	1.18	3,92	12,85
3	7—10	1.32	0.340	0.016	—1,65	0.41	1,40	0,174	3,011	22,04	15,12	4,92	2,78	0,907	1,170
	8—11	1,67	0.474	2.205	—1,86	1.06	1,74	0,040	2,546	8.789	4,14	2.64	1,75	1,12	0,815
	9—13	1,83	0.521	0,271	—2,86	1.68	1,95	0,041	2,274	4.702	1,680	1,02	1,88	1,20	0.764
	10—14	1,97	0,583	0.338	—4,55	2.43	2,22	0,053	2,113	3.292	0,886	0.406	1.67	0,767	0,567
	11—15	1,32	0,406	0,165	+0,32	0,61	1,30	0,002	2,228	4.748	1,218	1,450	0.911	1,030	0.850
4	7—11	1.45	0.378	0,143	—1,83	0.34	1,52	0,113	2,867	17,345	10.744	4,591	3.176	1,356	1,070
	9—13	1.84	0,535	0,291	—2,40	1.87	1,94	0,023	2,227	4.467	1,468	0,999	1,511	1,025	0,638
	10—14	1,82	0,565	0,319	—1,80	2.20	1,90	0,010	2,170	4.115	1,197	0,918	1,531	1,020	0.654
	11—15	1,51	0.451	0,204	—0,82	0.89	1,58	0,008	2,131	3.821	1,024	0,797	1.151	0,897	0,717
5	7—12	1,54	0.420	0,175	—2,42	0,75	1,71	0,109	2,454	5,680	2,517	1,163	1,531	0,706	0.861
	8—13	1,80	0,507	0,257	—2,63	1,53	1,91	0,0401	2,339	5,388	2,087	1,300	1,592	0,981	0,697
	9—14	1.81	0,537	0,288	—1,77	1,80	1,90	0,013	2,166	4,050	1,180	0,870	1,391	1,029	0,631
	10—15	1,60	0.471	0,220	—1,42	1,01	1,75	0,019	2,072	3,305	0.797	0,508	1,205	0,768	0,710
6	7—13	1,62	0,444	0,197	—2,58	0,92	1,77	0,087	2,358	4,944	1,980	0,964	1,491	0,725	0,800
	9—15	1,60	0,460	0,213	—1,19	1,02	1,67	1,471	2,232	4,626	1,508	1,118	1,261	0,936	0,737
7	7—14	1,64	0,451	0,204	—2,00	0,96	1,74	0,047	2,316	5,039	1,907	1,132	1,418	0,837	0,780
	8—15	1,61	0,445	0,199	—1,52	0,90	1,70	0,029	2,282	4,932	1,763	1,169	1,318	0,872	0,780

On the basis of obtained data generalized characteristics of the spectral intensity of radiation of the Earth were plotted (in the case of observation from a given orbit of an artificial Earth satellite). In Fig. 3.3 graphs of magnitudes $\bar{I} = \bar{I}(\lambda)$, $M = M(I_\lambda)$, $\sigma = \sigma(I_\lambda)$ over the spectrum are presented (left scale). It can be seen that minima in the intensity of radiation (of magnitudes $\bar{I}$ and M) correspond to absorption bands of atmospheric gases (ozone with center at 9.6 microns and carbon dioxide with center at 15 microns), to which likewise correspond minima of fluctuations of intensity of radiations (minimum of magnitude σ), especially in the band of carbon dioxide. For the long wave region of the spectrum ($\lambda > 14$ microns), in general, a lower level of fluctuations of radiation (small values of magnitudes σ) is characteristic.

/40

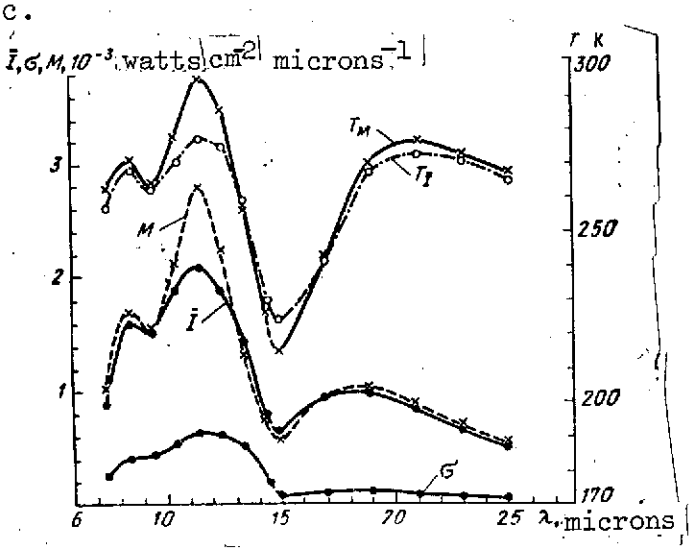

Fig. 3.3. Generalized statistical characteristics of the spectral intensity of radiation of the Earth.

From the obtained data it follows that in the window of transparency of the Earth's atmosphere, the intensity of radiation varies within wide limits, and the law of distribution is close to uniform. This is explained by the fact that in a given case both earth and water surfaces at different latitudes and variable cloudiness were observed through the atmosphere. Thus, in this range of the spectrum the intensity of radiations depends substantially on the coordinates of the sections to be observed. At the boundaries of the

windows of transparency (at sections 7 to 8 and 13 to 14 microns) the distribution contracts.

In Fig. 3.3 (the first scale) are likewise indicated values of radiation temperatures, that correspond to the spectral density of radiation: $T_{\overline{I}}$ is the temperature calculated by the magnitude of the mathematical expectation, T_M is the temperature calculated by the value of the mode. At wave length λ microns "contraction" of the curve of distribution is observed which corresponds to temperature T_M, approaching -60°C, /41 is observed. This is explained by the fact that in the center of the spectral band of carbon dioxide the atmosphere is least transparent, and at these wave lengths only high layers of the atmosphere that have such temperature are observed.

In the range from 14 to 26 microns the distribution of intensity of radiation has a small variance by amplitude, i.e. the flux of leaving radiation in case of a variation of coordinates varies little.

Beyond the long wave boundary of the carbon dioxide band in the interval from 18 to 26 microns, temperatures T_M and $T_{\overline{I}}$ are very close to one another and vary little with wave length. Values $T_{\overline{I}}$ are enclosed in this spectral interval in the limits 265-272°K, and values T_M are enclosed in the limits 267-276°K.

Consequently, on the average the spectrum of departing radiation in this interval of wave lengths is close to the spectrum of an absolutely black body with a temperature of about -5°C.

3.3 Latitudinal Dependences of the Statistical Characteristics of Spectral Intensities of Radiation of the Earth.

Data on the regularities of distribution of energy of radiation of the Earth will be incomplete if limited to statistical characteristics of the radiation field of the planet as a whole. Due to the difference of the albedo of different sections of the Earth's surface (first of all because of the large value of the albedo of cloudiness), the geographical distribution of solar energy absorbed by the Earth will not correspond to the geographical distribution of incident energy. Moreover, due to various factors (shifts of air masses,

sea and ocean currents) there occurs a redistribution over the surface of solar energy obtained by the Earth. Therefore, the geographical distribution of intrinsic infrared radiation of the Earth does not correspond to the geographic distribution of solar radiation.

By the present time extensive theoretical calculations of latitudinal dependences of departing radiation of the earth have been conducted. The experimental study of latitudinal dependences of departing radiation was accomplished with the use of satellites; however, published results pertain to wide sections of the spectrum. Thus, with the help of a satellite of the "Tiros" series the integral departing radiation and the radiation in the spectral ranges 8 to 12 and 8 to 30 microns were studied. Information about the distribution of departing radiation of the Earth is of considerable interest. Results of measurements of spectral intensities of departing radiation of the Earth, carried out from satellites "Kosmos-45" and "Kosmos-65," were used for the plotting of latitudinal dependences of the radiation of the Earth into outer space at various wave lengths. Results of the processing of measurements are presented below. /42

The same spectrograms that were used for the obtaining statistical characteristics of radiation of the earth into outer space and were presented in §3.2 (1278 spectrograms, obtained from artificial Earth satellite "Kosmos-45," and 782 spectrograms from "Kosmos-65"), underwent processing. As usual, those parts of the spectrograms were used for processing, that are undistorted by overlapping of spectra of the second order (7 to 15 microns in the first spectral subrange and 14 to 26 microns in the second) [42].

Between measurements of intensities in one wave length 80 seconds elapsed. During this time the satellite moved in the region of the Equator along a latitude approximately at 5°, and with an increase of the latitude this magnitude decreased, approaching 0 at latitude 65°. Spectrograms were attached along latitudes. The accuracy of the attaching constitutes $\pm$0.5° at the Equator and improved in proportion to movement to high latitudes. The latitude of mean wave length (11 to 20 microns) of the used part of the spectrogram was attributed to all the remaining wave lengths of the given spectrum.

All processed spectrograms were divided into the following latitudinal intervals: 0-10°,

10-20°, 20-30°, 30-40°, 40-48°, 48-55°, 55-61°, 61-65-61°. The first spectral interval 7 to 15 microns, as a result of the method of processing, was an exception on satellite "Kosmos," where latitudinal intervals were 0-15°, 15-30°, 30-43°, 43-55°, 55-63°, 63-65-63°. The number of spectrograms in each of the latitudinal intervals comprised up to 20 at the Equator and up to 108 at high latitudes. In each of the indicated latitudinal intervals mathematical expectations of spectral intensities (average values of intensities) $\overline{I}_\lambda$ and the root-mean-square deviations $\sigma(I_\lambda)$ were calculated. Average values of intensities were attributed to the middle of the corresponding latitudinal interval. $\overline{I}_\lambda$ and $\sigma(I_\lambda)$ were calculated on an electronic computer. Results obtained by the described method are presented in Figs. 3.4 - 3.5 and in Tables 3.3 and 3.4. In Tables 3.3 and 3.4 in the last column is the quantity of spectrograms recorded in the corresponding latitudinal zones.

In Fig. 3.4 curves are presented for seven spectral intervals, of width 1 micron each, from 7 to 14 microns; in Fig. 3.5 curves are presented for seven spectral intervals 2 microns wide from 14 to 26 microns. Along the axis of abscissas are plotted latitudes from 65° south latitude in the order that the satellite passed them. South latitudes are signified by a minus sign. On axes of ordinates is plotted the mathematical expectation of the intensity of radiation $\overline{I}_\lambda$.

The dependence of the intensity of radiation on latitude can be clearly seen. As should be expected, at high latitudes intensities are minimal and they grow toward the tropics. This dependence is more strongly expressed in intervals of wave lengths 8 to 13 and 16 to 20 microns (windows of transparency of the atmosphere) and less clearly in others, especially in the absorption band of CO_2, 14 to 16 microns. In the window of transparency 8 to 13 microns, intensities vary in separate spectral intervals from (1-1.5) X 10^{-3} at latitude 65° to (2-2.5) X 10^{-3} watts/cm^2·microns in the subtropics. In spectral intervals 7 to 8 and 16 to 22 microns, intensities vary from (0.7-0.8) X 10^{-3} to (1-1.1) X 10^{-3} watts/cm^2·microns at the same latitudes, and in wave lengths 14 to 16 and 22 to 26 microns almost do not depend on latitude and are enclosed in the limits (0.5 - 0.7) X 10^{-3} watts/cm^2·microns.

/48

/49

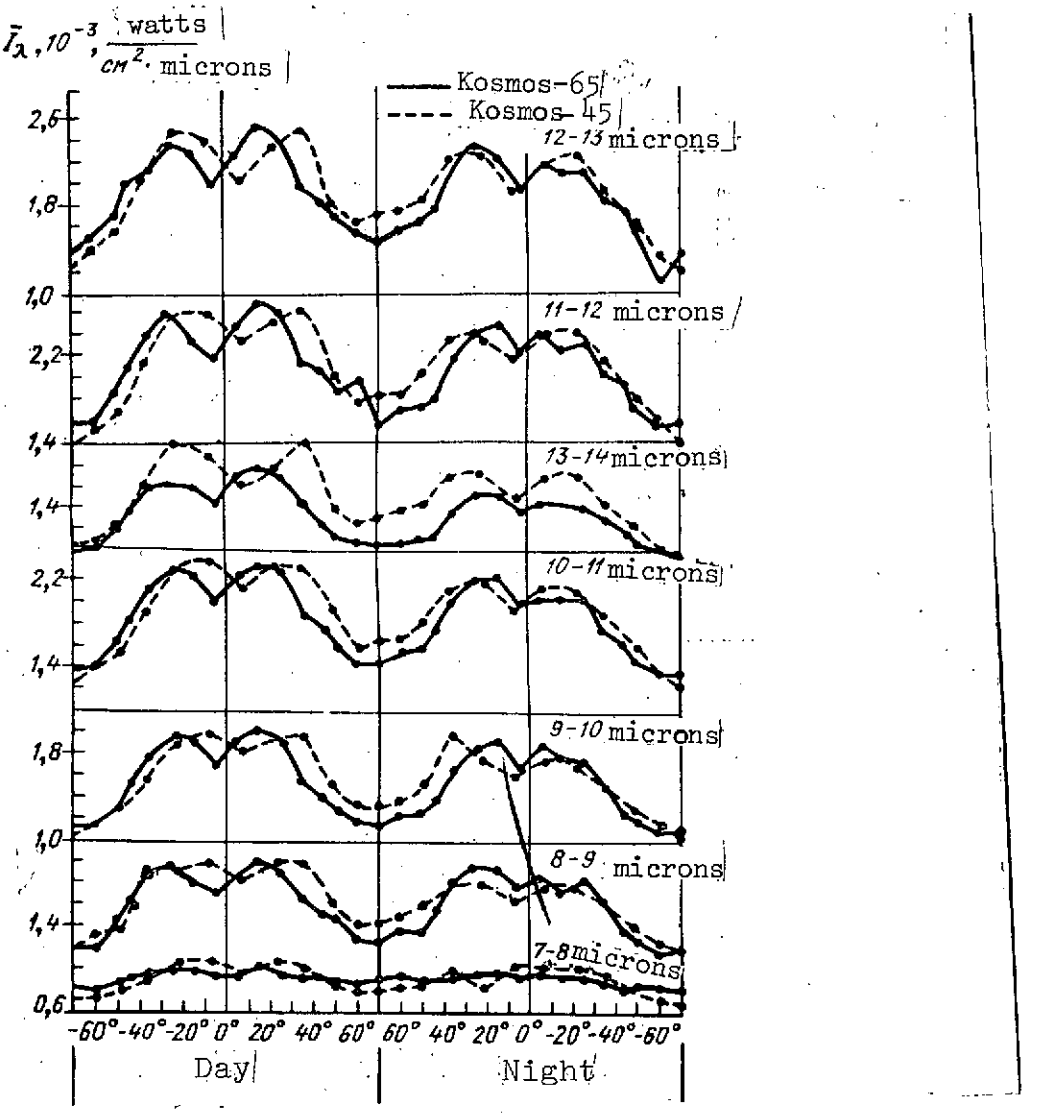

Fig. 3.4. Latitudinal dependences of the intensity of radiation in sections of the range of the spectrum from 7 to 14 microns.

TABLE 3.3

Latitudes	Intensity of radiation I and root-mean-square deviations σ10^{-3} watts/cm^2-microns for spectral intervals from 7 to 15 microns ("Kosmos-45", September 1964).																Number of measurements
	7–8 microns		8–9 microns		9–10 microns		10–11 microns		11–12 microns		12–13 microns		13–14 microns		14–15 microns		
	$\bar{I}$	σ	$\bar{I}$	σ	$\bar{I}$	σ	$\bar{I}$	σ	$\bar{I}$	σ	$\bar{I}$	σ	$\bar{I}$	σ	$\bar{I}$	σ	
Northern Hemisphere																	
Day	0–15°	0,94	0,26	1,80	0,49	1,82	0,51	2,12	0,62	2,34	0,67	2,07	0,68	1,61	0,61	0,80	0,20	57
	15–30°	1,04	0,24	1,97	0,48	1,94	0,52	2,33	0,57	2,52	0,69	2,32	0,65	1,75	0,51	0,78	0,18	57
	30–43°	0,98	0,23	1,94	0,39	1,95	0,48	2,33	0,52	2,61	0,57	2,47	0,55	1,99	0,60	0,88	0,30	57
	43–55°	0,85	0,27	1,57	0,41	1,51	0,43	1,91	0,54	2,01	0,64	1,81	0,58	1,42	0,46	0,82	0,14	57
	55–63°	0,79	0,25	1,40	0,28	1,32	0,26	1,58	0,42	1,77	0,51	1,62	0,44	1,24	0,36	0,82	0,14	57
Night	63–63°	0,80	0,19	1,44	0,17	1,32	0,21	1,64	0,28	1,86	0,37	1,71	0,37	1,29	0,29	0,84	0,11	69
	63–55°	0,84	0,17	1,48	0,24	1,36	0,24	1,66	0,40	1,86	0,40	1,73	0,44	1,35	0,36	0,84	0,12	57
	55–43°	0,88	0,24	1,58	0,38	1,51	0,36	1,83	0,46	2,04	0,55	1,84	0,50	1,42	0,44	0,82	0,13	54
	43–30°	0,97	0,21	1,78	0,31	1,97	0,22	2,13	0,47	2,34	0,57	2,18	0,58	1,68	0,58	0,79	0,19	60
	30–15°	0,98	0,23	1,80	0,40	1,77	0,37	2,21	0,50	2,45	0,61	2,25	0,61	1,68	0,17	0,76	0,15	60
	15–0°	1,02	0,16	1,64	0,54	1,61	0,52	1,98	0,63	2,19	0,74	1,94	0,72	1,47	0,57	0,73	0,28	57
Southern Hemisphere																	
Day	0–15°	1,04	0,17	1,95	0,34	1,96	0,36	2,37	0,38	2,60	0,46	2,38	0,47	1,89	0,49	0,82	0,16	57
	15–30°	1,03	0,15	1,91	0,24	1,89	0,32	2,31	0,31	2,57	0,39	2,42	0,40	1,91	0,49	0,90	0,16	57
	30–43°	0,86	0,26	1,60	0,37	1,53	0,39	1,90	0,48	2,13	0,57	2,00	0,55	1,59	0,45	0,84	0,14	57
	43–55°	0,77	0,20	1,36	0,27	1,28	0,26	1,54	0,36	1,68	0,43	1,56	0,43	1,22	0,35	0,80	0,17	57
	55–63°	0,73	0,19	1,27	0,24	1,15	0,21	1,38	0,30	1,53	0,35	1,38	0,35	1,04	0,30	0,72	0,19	60
Night	63–63°	0,71	0,21	1,19	0,22	1,07	0,19	1,26	0,24	1,38	0,26	1,22	0,23	0,95	0,22	0,65	0,16	63
	63–55°	0,72	0,23	1,23	0,26	1,15	0,23	1,37	0,31	1,50	0,34	1,33	0,32	1,02	0,27	0,67	0,12	57
	55–43°	0,81	0,23	1,40	0,29	1,30	0,29	1,60	0,38	1,79	0,44	1,61	0,45	1,24	0,43	0,79	0,29	57
	43–30°	0,92	0,21	1,58	0,31	1,49	0,30	1,90	0,40	2,15	0,47	1,90	0,48	1,44	0,40	0,78	0,14	57
	30–15°	1,00	0,17	1,77	0,25	1,70	0,21	2,11	0,38	2,42	0,38	2,23	0,35	1,70	0,40	0,78	0,14	57
	15–0°	1,00	0,20	1,79	0,32	1,76	0,34	2,15	0,46	2,39	0,55	2,16	0,54	1,68	0,50	0,74	0,16	57

TABLE 3.3 continued

Latitudes	14–16 μ $\bar{I}$	14–16 μ σ	16–18 μ $\bar{I}$	16–18 μ σ	18–20 μ $\bar{I}$	18–20 μ σ	20–22 μ $\bar{I}$	20–22 μ σ	22–24 μ $\bar{I}$	22–24 μ σ	24–26 μ $\bar{I}$	24–26 μ σ	Number of measurements
Northern Hemisphere													
Night I Day 0–10°	0,67	0,10	0,95	0,13	0,97	0,12	0,88	0,08	0,66	0,08	0,52	0,05	38
10–20°	0,68	0,09	0,96	0,12	0,96	0,11	0,88	0,07	0,65	0,08	0,52	0,04	38
20–30°	0,66	0,08	1,00	0,10	1,00	0,09	0,90	0,07	0,69	0,05	0,54	0,04	38
30–40°	0,71	0,12	1,00	0,11	1,00	0,35	0,91	0,07	0,69	0,06	0,54	0,04	38
40–48°	0,68	0,10	0,96	0,08	1,00	0,06	0,88	0,06	0,66	0,04	0,52	0,04	38
48–55°	0,68	0,09	0,93	0,09	0,96	0,08	0,86	0,08	0,64	0,06	0,51	0,05	38
55–61°	0,66	0,09	0,88	0,07	0,94	0,10	0,82	0,08	0,62	0,05	0,49	0,04	38
61–61°	0,66	0,09	0,89	0,07	0,93	0,09	0,79	0,07	0,62	0,04	0,49	0,04	100
61–55°	0,66	0,09	0,89	0,10	0,94	0,08	0,79	0,08	0,64	0,04	0,51	0,05	36
55–48°	0,68	0,08	0,95	0,10	0,95	0,10	0,81	0,10	0,64	0,07	0,50	0,05	36
48–40°	0,68	0,09	0,95	0,10	0,96	0,10	0,84	0,09	0,64	0,09	0,51	0,04	40
40–30°	0,68	0,07	0,98	0,13	0,99	0,12	0,84	0,09	0,66	0,08	0,52	0,06	40
30–20°	0,66	0,08	0,94	0,12	0,96	0,14	0,83	0,12	0,66	0,08	0,51	0,06	40
20–10°	0,64	0,06	0,90	0,11	0,89	0,16	0,77	0,15	0,60	0,10	0,49	0,07	38
10–0°	0,66	0,07	0,93	0,14	0,91	0,15	0,78	0,13	0,62	0,08	0,49	0,06	38
Southern Hemisphere													
Night I Day 0–10°	0,67	0,08	1,00	0,10	1,00	0,08	0,91	0,06	0,70	0,06	0,55	0,05	38
10–20°	0,68	0,10	1,00	0,09	1,10	0,04	0,94	0,04	0,74	0,07	0,56	0,05	38
20–30°	0,68	0,10	1,02	0,10	1,05	0,09	0,93	0,07	0,73	0,09	0,56	0,05	38
30–40°	0,65	0,08	0,94	0,11	0,99	0,12	0,90	0,09	0,69	0,09	0,53	0,07	38
40–48°	0,66	0,07	0,92	0,08	0,98	0,07	0,88	0,07	0,66	0,05	0,51	0,05	38
48–55°	0,64	0,07	0,88	0,08	0,93	0,10	0,81	0,10	0,63	0,07	0,50	0,05	40
55–61°	0,66	0,07	0,87	0,07	0,92	0,08	0,80	0,07	0,62	0,04	0,49	0,04	40
61–61°	0,65	0,07	0,83	0,06	0,85	0,07	0,73	0,05	0,60	0,04	0,47	0,04	108
61–55°	0,66	0,09	0,84	0,06	0,86	0,08	0,73	0,07	0,60	0,04	0,47	0,04	38
55–48°	0,66	0,07	0,88	0,08	0,91	0,08	0,78	0,08	0,63	0,05	0,49	0,04	38
48–40°	0,68	0,10	0,91	0,08	0,94	0,09	0,80	0,07	0,63	0,05	0,50	0,04	38
40–30°	0,69	0,09	0,95	0,09	0,96	0,09	0,84	0,09	0,66	0,06	0,52	0,05	38
30–20°	0,69	0,11	1,00	0,06	1,00	0,05	0,89	0,05	0,71	0,06	0,55	0,05	38
20–10°	0,71	0,14	0,99	0,08	1,00	0,09	0,83	0,08	0,70	0,06	0,54	0,06	38
10–0°	0,70	0,12	0,98	0,11	0,99	0,10	0,86	0,09	0,67	0,07	0,53	0,05	38

TABLE 3.4

Latitudes	Intensity of radiation $\bar{I} \cdot 10^{-3}$, watts/cm^2-microns for spectral intervals from 7 to 26 microns ("Kosmos-65", April 1965).													Number of measurements
	7–8 μ	8–9 μ	9–10 μ	10–11 μ	11–12 μ	12–13 μ	13–14 μ	14–15 μ	14–16 μ	16–18 μ	18–20 μ	20–22 μ	22–24 μ	24–26 μ	
Northern Hemisphere															
Day 0–10°	0,92	1,85	1,90	2,20	2,46	2,25	1,66	0,75	0,72	1,05	1,08	0,92	0,71	0,54	20
Day 10–20°	1,02	1,99	2,00	2,33	2,68	2,50	1,74	0,79	0,73	1,10	1,13	0,96	0,71	0,53	20
Day 20–30°	0,94	1,90	1,91	2,30	2,58	2,36	1,67	0,77	0,70	1,04	1,07	0,91	0,68	0,52	21
Day 30–40°	0,92	1,63	1,52	1,88	2,14	1,96	1,41	0,76	0,66	0,94	0,99	0,83	0,65	0,52	24
Day 40–48°	0,90	1,49	1,39	1,76	2,03	1,84	1,22	0,78	0,68	0,90	0,99	0,83	0,65	0,52	24
Day 48–55°	0,86	1,44	1,27	1,60	1,89	1,69	1,12	0,75	0,64	0,90	0,95	0,82	0,64	0,52	24
Day 55–63°	0,87	1,29	1,17	1,46	1,99	1,53	1,06	0,76	0,66	0,88	0,86	0,79	0,61	0,50	36
Day 63–63°	0,89	1,25	1,14	1,42	1,57	1,48	1,04	0,78	0,66	0,87	0,82	0,79	0,61	0,52	39
Night 63–55°	0,92	1,34	1,22	1,54	1,70	1,57	1,06	0,76	0,68	0,92	0,84	0,82	0,62	0,52	36
Night 55–48°	0,86	1,36	1,24	1,57	1,72	1,64	1,08	0,75	0,66	0,90	0,78	0,80	0,60	0,49	24
Night 48–40°	0,90	1,53	1,39	1,75	1,78	1,74	1,12	0,75	0,69	0,94	0,89	0,82	0,65	0,52	24
Night 40–30°	0,93	1,80	1,64	2,05	2,18	2,08	1,33	0,75	0,72	1,00	0,93	0,86	0,68	0,53	24
Night 30–20°	0,95	1,92	1,82	2,22	2,42	2,32	1,52	0,76	0,72	1,10	0,96	0,87	0,88	0,54	24
Night 20–10°	0,97	1,91	1,91	2,26	2,48	2,20	1,54	0,76	0,71	0,95	0,87	0,82	0,64	0,52	24
Night 10–0°	0,92	1,75	1,67	2,00	2,22	1,94	1,38	0,75	0,67	0,91	0,86	0,79	0,64	0,52	20
Southern Hemisphere															
Day 0–10°	0,91	1,70	1,68	2,00	2,18	1,95	1,41	0,74	0,70	0,98	0,97	0,82	0,66	0,51	22
Day 10–20°	0,97	1,78	1,91	2,21	2,32	2,24	1,56	0,76	0,65	1,02	1,01	0,99	0,68	0,51	22
Day 20–30°	0,98	1,92	1,93	2,30	2,58	2,34	1,60	0,76	0,71	1,02	1,01	0,87	0,68	0,51	23
Day 30–40°	0,92	1,86	1,75	2,10	2,36	2,22	1,58	0,76	0,71	1,02	1,03	0,91	0,71	0,53	24
Day 40–48°	0,88	1,61	1,50	1,84	2,10	1,98	1,34	0,76	0,69	0,98	0,98	0,87	0,68	0,53	24
Day 48–55°	0,86	1,40	1,29	1,60	1,87	1,69	1,18	0,75	0,69	0,92	0,90	0,82	0,65	0,51	24
Day 55–63°	0,78	1,21	1,13	1,40	1,57	1,49	0,98	0,73	0,67	0,88	0,85	0,79	0,65	0,51	24
Day 63–63°	0,81	1,17	1,10	1,35	1,59	1,35	0,94	0,71	0,64	0,83	0,77	0,75	0,59	0,48	36
Night 63–55°	0,81	1,18	1,10	1,37	1,57	1,41	1,00	0,73	0,65	0,81	0,74	0,75	0,54	0,47	44
Night 55–48°	0,86	1,28	1,19	1,50	1,72	1,56	1,07	0,73	0,66	0,86	0,78	0,75	0,62	0,49	36
Night 48–40°	0,81	1,35	1,28	1,65	1,92	1,71	1,17	0,74	0,67	0,91	0,85	0,78	0,61	0,50	24
Night 40–30°	0,89	1,61	1,46	1,78	2,03	1,86	1,28	0,79	0,68	0,91	0,86	0,88	0,63	0,52	24
Night 30–20°	0,93	1,81	1,72	2,07	2,32	2,10	1,39	0,81	0,71	0,95	0,93	0,84	0,66	0,51	24
Night 20–10°	0,92	1,75	1,76	2,06	2,70	2,10	1,43	0,71	0,69	0,96	0,93	0,83	0,62	0,52	24
Night 10–0°	0,97	1,86	1,86	2,06	2,39	2,14	1,43	0,72	0,68	0,96	0,91	0,83	0,69	0,51	24

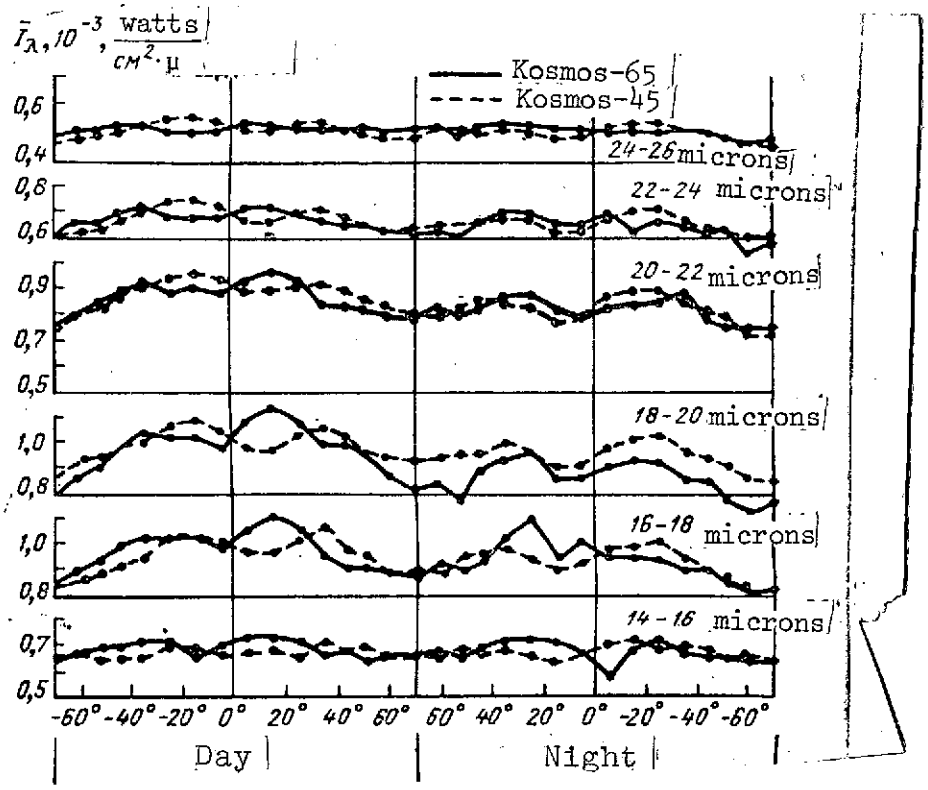

Fig. 3.5. Latitudinal dependences of the intensity of radiation in sections of the range of the spectrum from 14 to 26 microns.

In windows of transparency of the atmosphere, leaving radiation appears to be radiation of the underlying surface and of lower layers of the troposphere. Their average temperatures increase from the poles to the tropics, leading to an increase of intensities with a decrease of latitude. In the interval of wave lengths 7 to 8 microns, the effect of the oscillating absorption band of water vapor with center at $\lambda = 6.3$ microns appears. For wave lengths $\lambda > 20$ microns, the presence of a very intense rotational absorption band of water vapor with center around 50 microns is characteristic. As is well known, the moisture content in the atmosphere increases with a decrease of latitude. Therefore the portion of radiation of the underlying surface and of the lower troposphere, absorbed by water vapor in the atmosphere increases with a decrease of latitude. /50

As a result, latitudinal dependence in intervals of wave lengths λ = 7–8 and λ > 20 microns becomes less distinct, than in windows of transparency. The attenuation of the latitudinal dependence with increase of wave length at λ > 20 microns is caused by the increase of the absorption coefficient of water vapor with an increase of λ. In the absorption band of CO_2 at λ = 14–16 microns, radiation is formed in the upper troposphere and stratosphere and almost does not have latitudinal variation. /51

Cloudiness has a substantial effect on latitudinal variation $\bar{I}_\lambda$. This effect appears in all the considered spectral intervals. The greatest effect of cloudiness appears in the windows of transparency of the atmosphere, since in these wave lengths radiation of a relatively warm Earth's surface and of lower layers of the troposphere is replaced by radiation of the colder upper boundaries of clouds. In windows of transparency the effective temperature of radiation in the absence of clouds is close to the temperature of soil, and in the presence of clouds is close to the temperature of their upper surface, often differing 20–30° from the soil temperature. Therefore, there should be and there in fact is a close negative correlation between intensities measured in this range of wavelengths by a spectrophotometer and luminances at a point under the satellite, measured by a photometer for visible radiation.

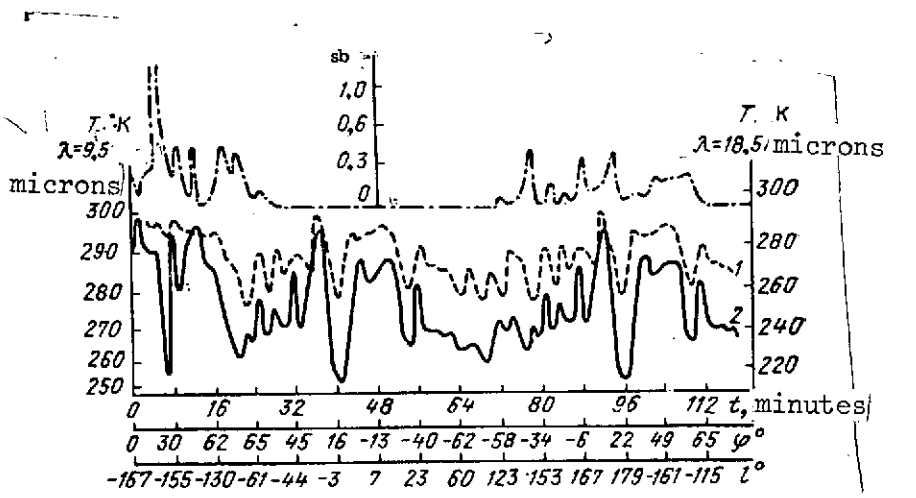

Fig. 3.6. Comparison of the geographical distribution of radiations at wave lengths 9.5 microns, 18.5 microns, and in the visible region of the spectrum.

Fig. 3.6 can serve as an obvious case, in which for one of the loops of satellite "Kosmos-45" are compared latitudinal dependences of average radiation temperatures for wave lengths 18.5 and 9.5 microns (curves 1 and 2 respectively) with the trace of a photometer for visible radiation (upper curve). Calculations of the latter equal zero on the night side of the Earth and strongly correlate with both radiation temperatures on the day side of the Earth. /52

In Fig. 3.7 is shown the latitudinal dependence of radiation temperature at wave length 9.5 microns according to data of scanning over locality in one of the loops (satellite "Kosmos-45"). Along the axis of abscissas is plotted the time from the moment when the satellite crosses the Equator, and likewise through each 8 minutes of latitude ϕ and of longitude ι of the point under the satellite (longitude is considered positive to the east of Greenwich). In the drawing three curves are represented: the upper corresponds to the greatest intensities of radiation in each of the scans, the lowest corresponds to the least intensities, and the middle corresponds to the average by area limited curve of scanning. It can be seen that the curves undergo sharp jumps, that is explained by the presence of cloudiness. From the drawing it can be seen that the behavior of curves is various: curves now approach close to one another, and then move far apart. This is explained by the different degree of non-uniformity of the field of radiation. In those cases, when the field of radiation during the time of a scan by locality (14.4 seconds) did not vary substantially, curves came close to one another.

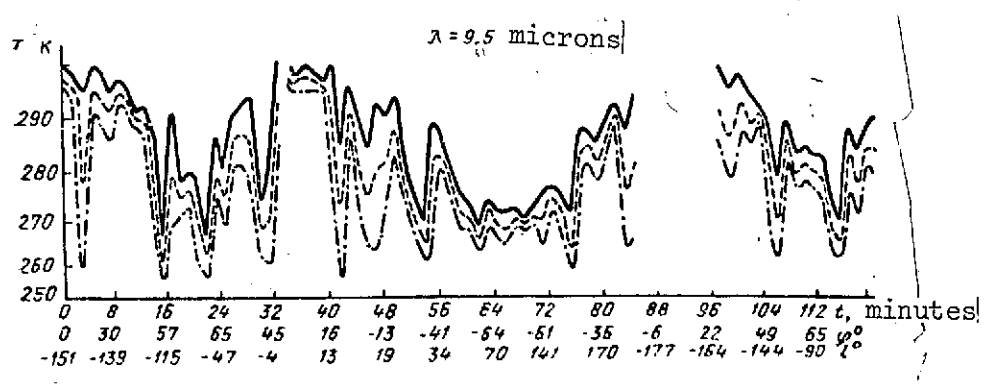

Fig. 3.7. Latitudinal dependence and local fluctuations of radiation at wave length 9.5 microns.

When curves diverge, it attests to variations in the nature of the underlying surface, most often of the sequence of clouds and of the gaps between them. Often sharp troughs are observed in radiation at wave 9.5 microns, when the radiation temperature falls to 250-260 °K. At these moments of time cloudiness falls into the field of vision of the apparatus. Sections of discontinuity of curves correspond to off-scale readings of the apparatus, i.e. radiation temperatures of radiation higher than 300 °K. /53

A similar picture is observed in graphs of Fig. 3.8, plotted similarly to graphs of Fig. 3.7 for wave length 18.5 microns of the same loop. Vibrations of curves in graphs of Fig. 3.7 are explained mainly by variations of radiation of the underlying surface, and not by variation of the ozone content of the atmosphere, since the width of the band recorded by the apparatus $\Delta\lambda$ = 1.2 microns is wider than the width of the absorption band of ozone.

Let's return to Figs. 3.4 - 3.5. In the region of the Equator occurs the relative minimum $\bar{I}_\lambda$ [sic], that is explained by the increase of the degree of cloudiness in the region of location of an intertropical zone of convergence. On both sides of these equatorial minima are located almost identical (north and south of the Equator) subtropical maxima of intensity of radiation. These maxima result from a decrease of cloudiness in subtropical zones of high pressure. One should note that equatorial minima of radiation $\bar{I}_\lambda$, measured in September from satellite "Kosmos-45", at any time of the day are located north of the Equator, in April ("Kosmos-65") the latitude of these minima varies in the course of a day: at night they are located north of the Equator and during the day south of it. In all cases the distance of minima $\bar{I}_\lambda$ from the Equator

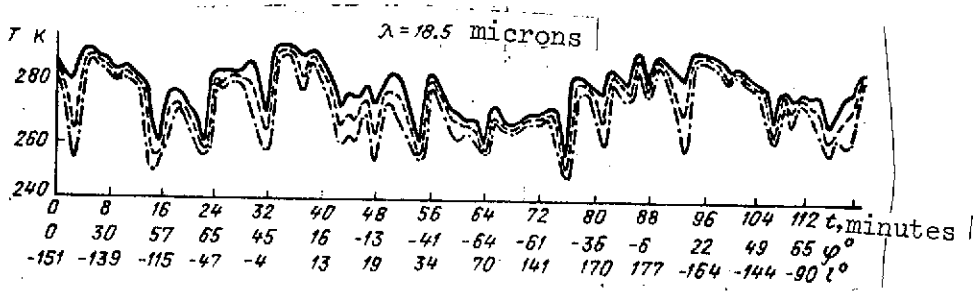

Fig. 3.8. Latitudinal dependence and local fluctuations of radiation at wave length 18.5 microns.

comprises 5 - 10°. Values of latitudes, in which subtropical maxima are located at various spectral intervals, are presented in Table 3.5.

As can be seen from Figs. 3.4, 3.5 and Table 3.5, these maxima in the northern hemisphere are located at higher latitudes in September than in April, and in the southern hemisphere in September are closer to the Equator in the day, whereas at night they are at the same latitudes both in April and in September. It is interesting to note that magnitudes of intensities of radiation in these maxima in September are the same north and south of the Equator, and in April in the north they are greater than in the south. /54

A sufficiently clear representation of the effect of cloudiness on latitudinal dependences $\bar{I}_\lambda$ is given in Fig. 3.9, where according to data of satellite "Kosmos-45" there are represented latitudinal dependences of root-mean-square deviations $\sigma(I_\lambda)$, that result from the variance of averaged spectral intensities of a given latitudinal interval. Along the axis of abscissas latitudes are plotted; along the axis of ordinates magnitudes $\sigma(I_\lambda)$.

Comparing Fig. 3.9 with Figs. 3.4, 3.5, it is easy to notice that minima $\sigma(I_\lambda)$, correspond to equatorial minima of magnitude $\bar{I}_\lambda$, and minima $\sigma(I_\lambda)$ correspond to subtropical maxima $\bar{I}_\lambda$. With an increase of wave length at $\lambda > 20$ microns and in the interval of wave lengths 14 to 16 microns dependences $\sigma(I_\lambda)$ on latitude become less distinct. The variation of curves can be explained by the fact that when there is a high degree of cloudiness in the tropics, the variance of intensities of radiation from spectrum to spectrum inside the limits of a given latitudinal interval increase as a result of large values $\sigma(I_\lambda)$. In the subtropics, on the other hand, at little cloudiness the spectral intensities inside the limits of the given latitudinal interval differ little, i.e. will be less than magnitude $\sigma(I_\lambda)$. At $\lambda = 14$–16 and $\lambda > 20$ microns the departing radiation is formed in the upper troposphere and stratosphere, and therefore the effect of cloudiness becomes little noticeable.

The effect of cloudiness on latitudinal dependences of intensities of radiation $\overline{I}_\lambda$ is expressed even more clearly in Fig. 3.10 where curves of ratio $\sigma(I_\lambda)/\overline{I}_\lambda$ for satellite "Kosmos-45" are plotted as a function of geographical latitude. Equatorial maxima and subtropical minima are here more pronounced than in Fig. 3.9. A decrease of ratio $\sigma(I_\lambda)/\overline{I}_\lambda$ at high latitudes is caused by sufficiently uniform temperature of the radiation surface, resulting, apparently, from little cloudiness. /55

TABLE 3.5

Latitudes	Time of day	"Kosmos-45" (September)	"Kosmos-65" (April)
Northern	Day	30–40°	10–20°
	Night	25–35°	15–25°
Southern	Day	10–25°	20–30°
	Night	15–20°	15–20°

The Earth loses energy due to long wave infrared radiation from the whole Earth's surface, and obtains energy from the side of the surface turned to the Sun. Therefore, intensities of radiation of the day and night sides of the Earth should differ. If one compares the intensity of radiation at identical latitudes on the sides of the Earth illuminated and /56
unilluminated by the Sun, one finds that in September ("Kosmos-45") the intensity by day is greater than at night in the region that extends from the Equator to 40-50° latitude, and at /57
higher latitudes the day and night intensities practically coincide. Another picture is observed in April ("Kosmos-65"). Curves of latitudinal distributions of day and night are as if shifted from the Equator 5° to different sides: by day to the south, by night to the north. This leads to the fact that in southern latitudes intensities of radiation in the region from the Equator to 65° south latitude are greater by day than by night. North of the Equator there is such a difference only up to 20° north latitude, and further up to 65° north latitude intensities are approximately the same night and day. The special features presented here occur in all

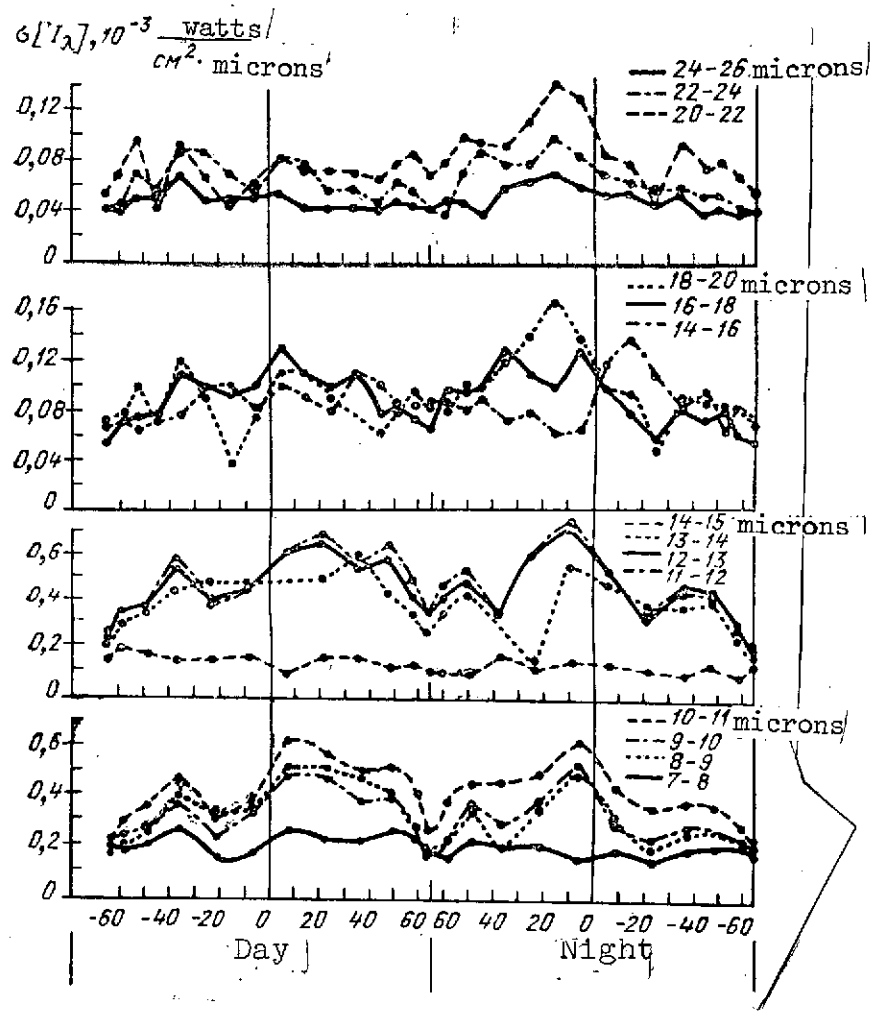

Fig. 3.9. Latitudinal dependence of root-mean-square deviations $\sigma[I_\lambda]$.

spectral intervals, except ranges 7 to 8 and 14 to 16 microns where the difference between day and night sides is unappreciable.

Finally, let's compare the intensities of radiation at identical latitudes north and south of the Equator. In September both day and night intensities are greater in

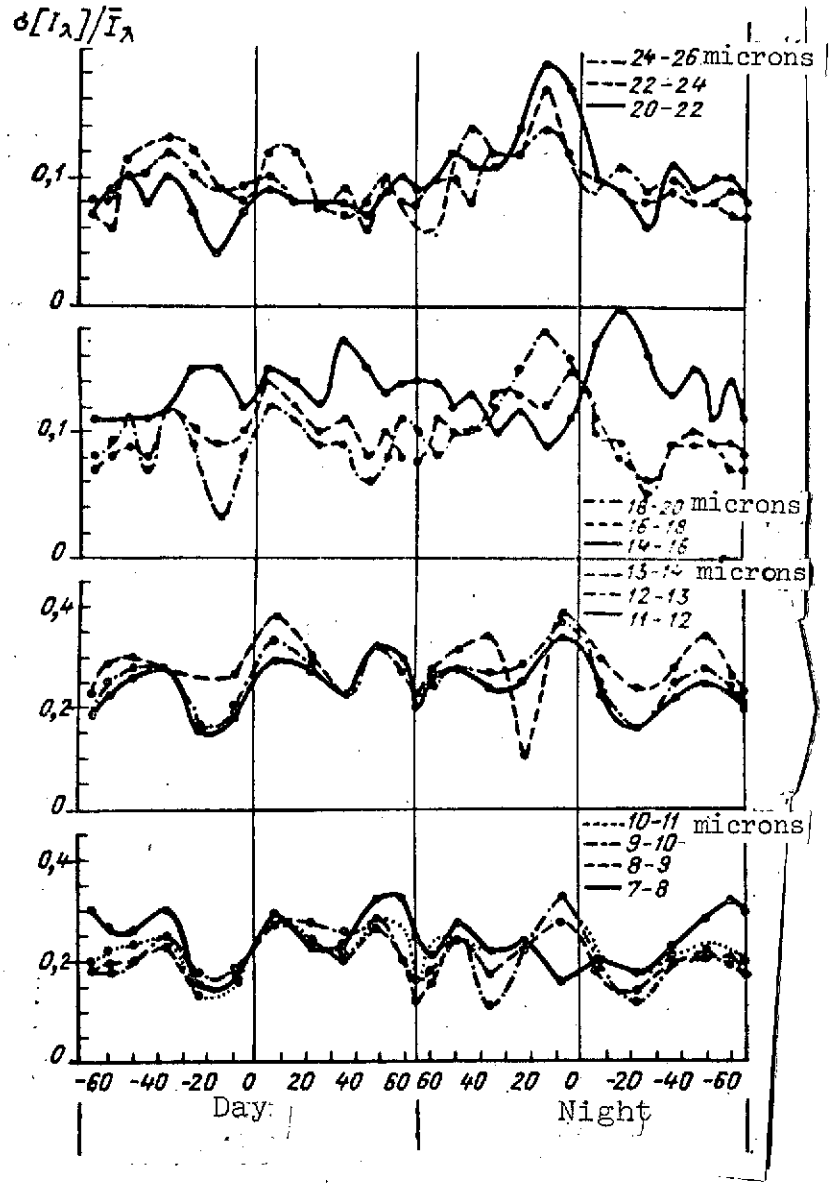

Fig. 3.10. The latitudinal dependence of ratio $\sigma(I_\lambda)/\bar{I}_\lambda$.

northern latitudes than in southern, with the exception of the band 25° to both sides of the Equator, where the picture is reversed. If intensities of radiation at latitudes 65° north latitude and 65° south latitude are compared, then in the north they are greater (1.25 times) in the spectral interval 8 to 14 microns and approximately the same in the remaining spectral intervals.

In April intensities of radiation north and south of the Equator have approximately the same values. Latitudes adjacent to the Equator up to 25° north and south of the Equator are an exception. By day in these latitudes intensities to the north of the Equator are greater. By night in the band of latitudes ±10° on both sides of the Equator, intensities are greater to the south, and further, like in the day, up to 25° north latitude and 25° south latitude intensities have large values in the region north of the Equator.

The basic causes of the differences of the field of departing radiation that were noted between the northern and southern hemispheres, and likewise between the day and night sides are cloudiness and the unevenness of temperatures of the Earth's surface. The shift of the thermal Equator to the north from the geographical and the great oceanity of the southern hemisphere are likewise expressed in the distribution of radiation.

On the basis of data of Figs. 3.4 - 3.5 curves of spectral distributions of intensities of departing radiation were plotted in the range of wave lengths 7 to 26 microns on the day side of Earth for six latitudinal zones (at three on each side of the Equator). Curves of the spectral distributions are presented in Fig. 3.11. The above noted regularities of latitudinal distributions can be seen even here. Curves of spectral distributions of various latitudinal zones differ strongly among themselves in windows of transparency of the atmosphere. This difference decreases in spectral ranges 7 to 8, 14 to 16, and at $\lambda > 22$ microns. /59

Above (see §3.2) the average spectral distribution of the Earth in the range of latitudes ±65° was obtained along the trajectory of the satellite. Such a spectral distribution differs from the average spectral distribution of radiation of the Earth in the interval of latitudes ±65°. This is explained by the fact that in the case of motion of the satellite along the trajectory for a great part of the time it is found at high latitudes.

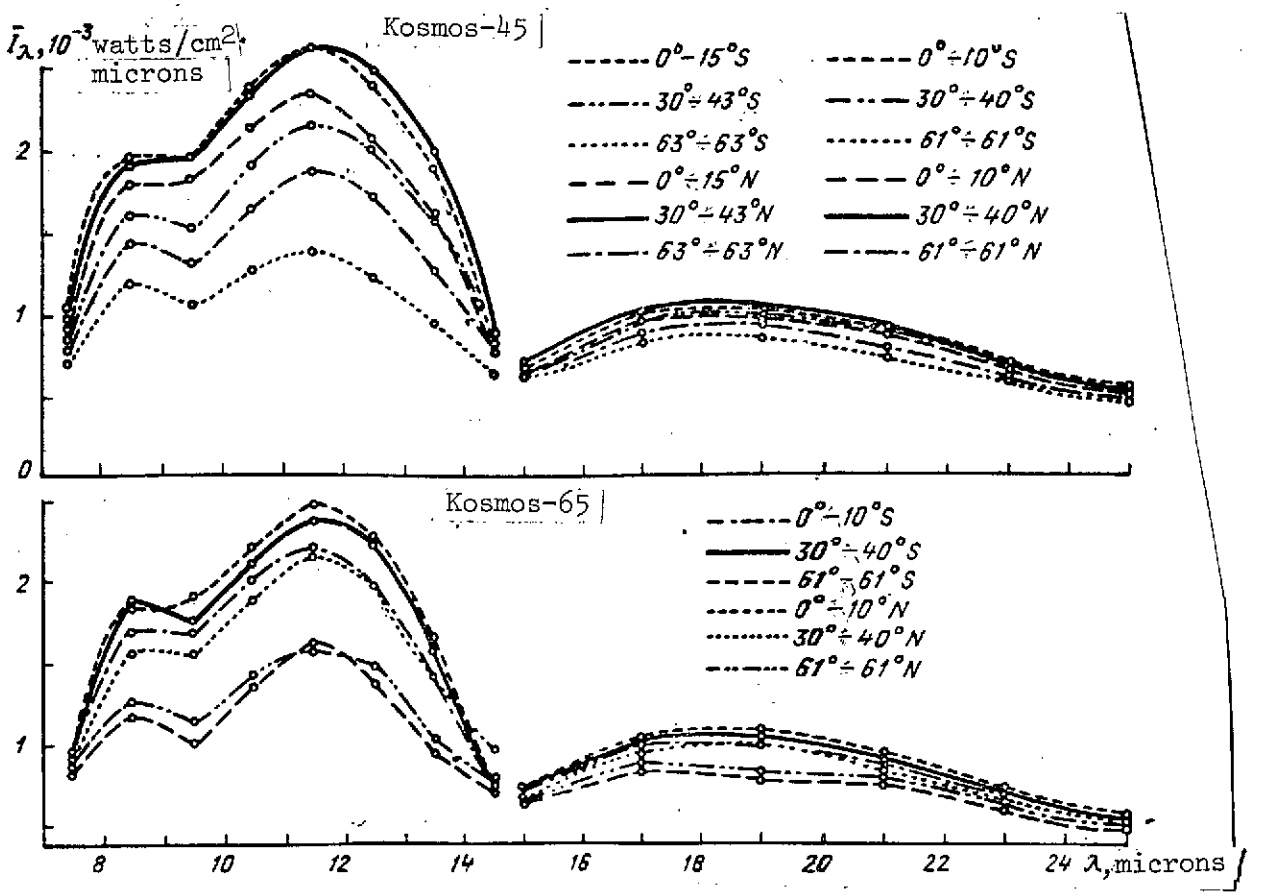

Fig. 3.11. The spectral distribution of intensity of radiation for six latitudinal zones.

The spectrum of radiation of the Earth in the interval of latitudes ±65° can be plotted in accord with results of spectral distributions in separate latitudinal zones. Characteristics of such a spectrum, calculated in accord with data of satellite "Kosmos-45," are presented in Table 3.6. In this table are presented average spectral distributions for the northern and southern hemispheres from the Equator to 65° latitude and the average spectrum of radiation of the Earth from 65° north latitude to 65° south latitude. Intensities I obtained by summing the intensities from Table 3.3 according to latitudes taking into account the area of latitudinal zones. In each latitudinal zone from Table 3.3 average intensities were taken on the day and night sides of the Earth. /60

TABLE 3.6

Parameters of radiation	Spectral intervals Δλ, microns						
	7–8	8–9	9–10	10–11	11–12	12–13	13–14
$\bar{I}$ northern hemisphere	0,95	1,73	1,72	2,08	2,29	2,09	1,60
$\bar{I}$ southern hemisphere	0,93	1,67	1,62	1,98	2,21	2,03	1,57
$\bar{I}$ average	0,94	1,70	1,67	2,03	2,25	2,06	1,58
σ average	0,25	0,41	0,44	0,55	0,64	0,61	0,53

Parameters of radiation	Spectral intervals Δλ, microns					
	14–16	16–18	18–20	20–22	22–24	24–26
$\bar{I}$ northern hemisphere	0,67	0,95	0,96	0,84	0,65	0,51
$\bar{I}$ southern hemisphere	0,68	0,96	0,99	0,87	0,68	0,53
$\bar{I}$ average	0,67	0,95	0,97	0,85	0,67	0,52
σ average	0,09	0,11	0,12	0,10	0,07	0,06

As follows from Table 3.6, the average spectral distributions of the hemispheres practically coincide. In Table 3.6 are likewise presented magnitudes of the root-mean-square deviation $\sigma(I_\lambda)$ for the Earth in the interval of latitudes +65°. Comparison of Tables 3.1 and 3.6 shows that in the interval of wave lengths 8 to 13 microns, intensities in the first are 5 to 8% lower than in the second.

One should note that the average spectral distribution of radiation of the Earth as a whole, taking account of polar regions will differ insignificantly from the distribution presented in Table 3.5, because the area of polar regions in the range of latitudes 65-90° constitutes in all 10% of the overall area of the Earth. One should expect the greatest difference, evidently, in the spectral inverval of the window of transparency 8 to 14 microns, where the variation of the intensity of radiation with latitude is especially great. Let's take, for example, the spectral interval 12 to 13 microns. The average intensity of radiation of the Earth

in the range of latitudes ±65°, according to the data of Table 3.5, comprises 2.06 X 10^{-3} watts/cm^2·micron. If one extrapolates the curve of latitudinal distribution of the given spectral interval into the region of polar latitudes up to the poles, then in this case the average intensity for the whole Earth appears to be equal to 2.02 X 10^{-3} watts/cm^2·micron. Such a variation (2%) does not exceed errors of the experiment. The variation of intensities in spectral intervals outside of the window of transparency 8 to 14 microns is still less.

Latitudinal dependences of integral intensities of departing radiation in the range of wave lengths 7 to 26 microns, obtained by summing spectral intensities (Figs. 3.4 - 3.5), are presented in Fig. 3.12 (upper curves). These curves sufficiently fully characterize the latitudinal distribution of integral radiation, inasmuch as in the indicated spectral interval the basic mass of energy of the radiation of the Earth into outer space is concentrated. The above noted special features of latitudinal distributions of spectral intensities of radiation are here too. Magnitudes of intensities in the interval 7 to 26 microns vary from 16 X 10^{-3} at 65° to (23 – 25) X 10^{-3} watts/cm^2 in the subtropics. Intensities at 65° north latitude exceed intensities at 65° south latitude 1.2 times in September and 1.13 times in April.

If subtropical maxima on both sides of the Equator are the same in September, then in April their difference is conspicuous; they are greater in northern latitudes than in southern. The latitudinal distribution in the window of transparency 8 to 12 microns looks similar (lower curves in Fig. 3.12). From a comparison of the upper curves with the lower, /61
one can note that the average intensity over latitudes from 65° south latitude and up to 65° north latitude in the interval of wave lengths 8 to 12 microns constitutes about 35% of the similarly obtained average value of the intensity in the interval of wave lengths 7 to 26 microns.

Let's compare the regularities of latitudinal variation of departing radiation obtained on artificial Earth satellite "Kosmos-45" and "Kosmos-65" with similar results of other experiments. In the period from 1960-1965, 10 American satellites of the "Tiros" series were launched. On four of them (Tiros-II, III, IV, VII, with launching dates Nov. 23, 1960, July 12, 1961, February 8, 1962, and June 19, 1963 respectively) there was an apparatus for the measurement of leaving radiation. The orbits of these satellites were almost

circular with average altitudes 630 to 770 kilometers. The angle of inclination of the plane of the orbit to the plane of the Equator in the first three came to about 48°, in "Tiros-VII" it constituted 58°. "Tiros" satellites were not oriented relative to the Earth. They were stabilized in space by rotation around an axis that maintained unchanged orientation relative to stars.

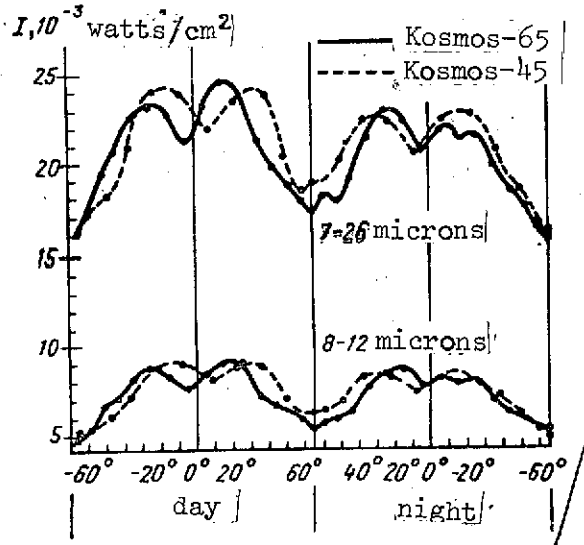

Fig. 3.2. Latitudinal dependences of integral intensities of departing radiation in the range 7 to 26 and 8 to 12 microns.

Integral departing radiation was investigated with the help of receivers with an angle of view of 50° and from hemispherical receivers with an angle of view of 180°. Measurements of departing radiation in different spectral intervals were conducted with the help of a five-channel radiometer with a field of view 5° X 5°. The optical axis of the radiometer was located at an angle of 45° to the angle of rotation of the satellite. Scanning was generated due to the rotation of the satellite around its axis, with a speed of about 10 revolutions/minute and due to the motion along the orbit. The radiometer operated in the following regions of the spectrum: channel 1 5.7 - 6.9 microns (the absorption band of water vapor); channel 2 7.5 - 12 microns (a window of transparency of the atmosphere); channel 3 0.2 - 5.5 microns (reflected solar radiation); channel 4 7.5 - 30 microns (the integral long wave departing radiation); channel 5 0.55 - 0.75 microns (reflected solar radiation in the region of the spectrum where television tubes are sensitive). Thermal departing

/62

radiation was investigated in accord with data of channels 1, 2, and 4.

On satellite "Tiros-IV" channel 4 was not included, and on satellite "Tiros-VII" in channel 1 the region of sensitivity was selected in the spectral interval 14.8 to 15.5 microns (the absorption band of CO_2). Detailed characteristics of all these experiments can be found in references [21-26]. Reconstruction of the integral fluxes of over radiation in accord with data of channels 2 and 4 of the five-channel radiometer was performed by the method discussed in [27].

As follows from the data obtained on these satellites, the latitudinal dependence of departing radiation appears tobbe as follows: a relative minimum in the region of the Equator, a maximum in the subtropics on both sides of the Equator, after which there is a continuous decrease to the sides of high latitudes. Such a dependence is explained by the distribution of cloudiness and of temperature of the Earth's surface. An increase of the degree of cloudiness in the region of the Equator leads to smaller values of departing radiation in comparison with the subtropics, where combination of high temperatures of the Earth's surface with comparatively little cloudiness gives an absolute maximum of departing radiation.

In [25] the middle-latitude distribution of departing radiation during 26 days between November 26, 1960, and January 6, 1961 is plotted in accord with data of satellite "Tiros-II." This distribution is presented in Fig. 3.13. Data of measurements pertain to angles of not less than 56° relative to the nadir. Authors obtained different meridian profiles over oceans and continents. Over oceans the tropical minimum is more weakly expressed than over continents: subtropical maxima on both sides of the Equator above oceans are almost identical and equal approximately 500 calories/cm^2·day, and above continents equal 540 and 475 calories/cm^2·day in summer and winter hemispheres respectively. Such a difference in slightly cloudy subtropics should be explained by the effect of the underlying surface. /63

One should note that the absolute magnitudes of departing radiation, obtained from satellite "Tiros-II", are too low in comparison with data of satellite "Explorer-VII," "Tiros-VII" and actinometric radiosondes, that is explained, apparently, by the difference in calibrations of the apparatus.

The same authors tried to discover the daily variation of departing radiation [26]. However, the discovery of appreciable daily variation above oceans with sufficiently stable surface temperature makes it impossible to consider the conclusions of the authors reliable.

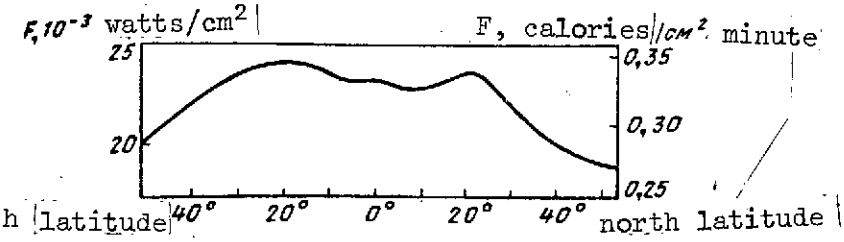

Fig. 3.13. Middle-latitude distribution of departing radiation in accord with data from satellite "Tiros-II."

On satellite "Tiros-VII" was conducted the most complete investigation of regularities of variation of the field of departing radiation, spanning 14 months of uninterrupted measurements, beginning in June 1963. In the processing of results records of signals of a channel 8 to 12 microns of a five-channel radiometer were used [28]. Reconstruction of the integral fluxes of departing radiation in accord with this data was performed on the basis of the method discussed in [27]. As was noted above, the angle of inclination of the plane of the orbit of satellite "Tiros-VII" to the plane of the Equator constituted 58°. However, because of the fact that the optical axis of the radiometer was inclined to the axis of rotation of the satellite, the field of vision fell in the band of latitudes $\pm 63.5°$.

For comparison with data of "Tiros-VII," integral fluxes of departing radiation were calculated on the basis of the above presented intensities in the range of wave lengths 7 to 26 microns (Fig. 3.12). It was assumed that in the range of wave lengths 7 to 26 microns was included 84% of all departing radiation. The given assumption was made from the following considerations: the quantity of radiation in the range of wave lengths 26 to 36 microns was estimated as a result of processing some spectrograms, and at wave lengths greater than 36 microns was estimated by extrapolation of experimental data. Inasmuch as our measurements of departing radiation were conducted at an orientation of the optical angle of the apparatus

to the nadir, for obtaining the integral flux of departing radiation it is necessary to take account of the effect of the decrease of the intensity of radiation toward the edge of the Earth. The calculation of the flux was carried out in accord with formula /64

$$F = 2\pi \int_0^{\pi/2} \frac{I_{(\theta=0)}}{\pi} k(\theta) \sin\theta \cos\theta d\theta \qquad (3.16)$$

where $I_{(\theta=0)}$ is the integral intensity of departing radiation in the range of wave lengths from 7 microns to ∞ at zenith distance $\theta = 0$; F is the integral flux of departing radiation; $k(\theta)$ is the coefficient, taking account of the effect of the degree of intensity toward the edge of the Earth.

In case of integration of expression 3.16, the graph of function $k(\theta)$ is taken in accord with data of measurements from satellite "Tiros-VII" [29]. The azimuthal asymmetry of the field of departing radiation was not taken into account by us.

Results of comparison are presented in Figs. 3.14-3.15. In Fig. 3.14 are presented curves of the latitudinal variation of departing radiation, measured from satellite "Kosmos-45" and for a three-month period (September - November, 1963) from satellite "Tiros-VII"; in Fig. 3.15 from satellite "Kosmos-65" and for the period March - May, 1964 from satellite "Tiros-VII." Curves of satellites "Kosmos-45" and "Kosmos-64" are continuous, those of "Tiros-VII" are dot-dash lines. Along the axis of ordinates are plotted fluxes of departing radiation F; along the axis of abscissas are plotted latitudes; the scale is proportional to the area of the latitudinal zones. Inasmuch as in the cited results from satellite "Tiros-VII" there is no division into day and night sides of the Earth, data of satellites "Kosmos-45" and "Kosmos-65" obtained by day and by night were averaged. Dashed curves up to 90° are the extrapolation of data in the band of latitudes where there were no measurements. As can be seen from Fig. 3.14-3.15, curves of satellites "Kosmos-45", "Kosmos-65" and "Tiros-VII" are close to one another. In Fig. 3.14 (September - November) according to results of satellites, the tropical minimum is located north of the Equator approximately at 10° north latitude, the subtropical maxima in regions of high pressure are identical in magnitude to the north and south of the Equator, the magnitudes of fluxes of departing radiation in the measured latitudes is greater to the north of the Equator than to the south. /65

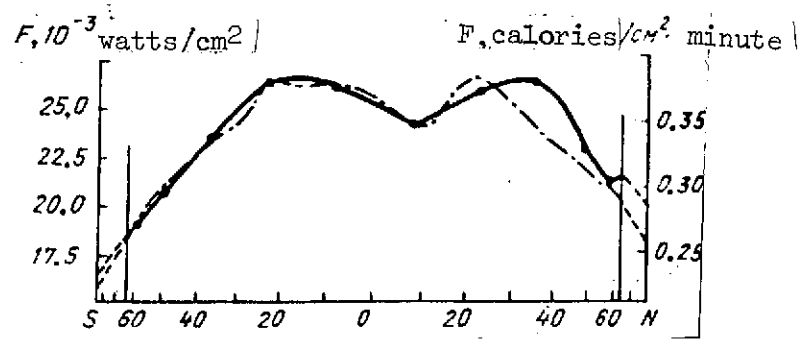

Fig. 3.14. Curves of the latitudinal variation of the flux of departing radiation, measured from satellites "Kosmos-45" and "Tiros-VII."

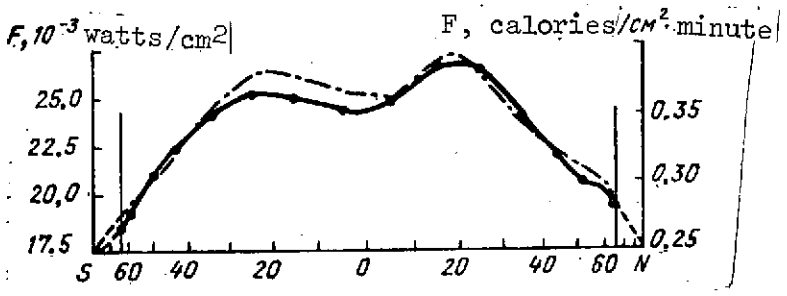

Fig. 3.15. Curves of the latitudinal variation of the flux of departing radiation, measured from satellites "Kosmos-65" and "Tiros-VII."

In Fig. 3.15 in accord with data of satellites "Kosmos-65" and "Tiros-VII" the subtropical maximum to the north of the Equator is greater in magnitude than to the south; in the measured latitudes north and south of the Equator fluxes of departing radiation are close to one another. The average magnitude over the whole Earth of the integral flux of departing radiation F taking account of sections of extrapolation, obtained from Figs. 3.14 - 3.15, is presented in Table 3.7. Here for comparison are presented magnitudes of the average flux of departing radiation in the autumn and in the spring for

TABLE 3.7

Parameters of radiation	"Kosmos-45" (September, 1964)	"Tiros-VII" (Sept.-Nov., 1963)	"Kosmos-65" (April, 1965)	"Tiros-UP" (March-May, 1964)	Data of article [6]	
					Fall	Spring
$\overline{F}$, 10^{-3} Watts/cm^2	23.63	23.42	23.28	23.49	22.24	22.37
T_{rad}, K	254	253.5	253	253.7	250	251

the northern hemisphere, calculated in [6]. In the lower line of Table 3.7 are presented radiation temperatures of the radiation of the Earth T_{rad}, that correspond to magnitudes $\overline{F}$. Magnitudes T_{rad}, were determined from the formula $T_{rad} = \sqrt[4]{\overline{F}/\sigma}$, where σ is the Stefan-Boltzmann constant. As can be seen from Table 3.7, all the magnitudes F and T_{rad}, obtained from satellites are very close to one another, in spite of the fact that they were measured in different years and seasons. These magnitudes are somewhat greater than those calculated theoretically in [6]. /67

In Table 3.8 are presented sums of integral fluxes of departing radiation in units 10^{15} watts in 10-degree zones, and likewise separately for the northern and southern hemispheres and for the entire Earth as a whole in accord with data of satellites "Kosmos-45," "Kosmos-65" and "Tiros-VII," obtained with the help of curves of Figs. 3.14 - 3.15. Comparison of total fluxes of both hemispheres between themselves and of departing radiation of the whole Earth (the two right columns in Table 3.8), obtained from the satellites under consideration, indicates their insignificant variability.

In accord with date of Table 3.8, curves were plotted of the dependence from latitude ϕ of the portion of the flux of departing radiation in the band of latitudes from the Equator to given latitude ϕ on the overall flux of each hemisphere:

$$\sum \overline{F}_{\Delta\varphi}(<\varphi)/\Sigma F)_{hem}$$

These dependences showed good agreement of results of measurements for all three satellites. Curves do not fall outside the limits of the hatched region in Fig. 3.16, and it is shown that 50% of all departing radiation in each hemisphere is included in the latitudinal interval from the Equator to 21-24° latitude, 90% from the Equator to 55° latitude. In the range from 80° to 90° latitude in each hemisphere the magnitude of departing radiation constitutes 1% of the full flux of departing radiation of the hemisphere.

One should note that the presented figures pertain to fluxes of integral radiation. For different spectral inervals the latitudinal distribution of the portion of radiation of separate latitudinal zones in the departing radiation of a given spectral interval will be different. In fact, in a

TABLE 3.8

Name of satellite	Integral fluxes of departing radiation (in units 10^{15} watts) in intervals of latitudes										
	0–10°	10–20°	20–30°	30–40°	40–50°	50–60°	60–70°	70–80°	80–90°	whole hemi-sphere	whole earth
Northern Hemisphere											
Kosmos-45	10,79	10,25	10,44	9,50	7,64	5,51	3,59	2,49	0,75	60,96	120,05
Tiros-VII Sept.-Nov. 1963	11,05	10,56	10,63	8,85	7,23	5,37	3,36	2,35	0,75	60,15	120,24
Kosmos-65	11,01	10,96	10,62	8,90	6,93	5,20	3,28	2,31	0,75	59,94	117,91
Tiros-VII Mar.-May 1964	11,28	11,20	10,64	8,90	7,10	5,41	3,35	2,35	0,81	61,04	121,73
Southern Hemisphere											
Kosmos-45	11,46	10,96	10,44	8,66	6,79	5,04	2,98	2,11	0,65	59,09	120,05
Tiros-VII Sept.-Nov. 1963	11,67	11,09	10,48	8,63	6,97	5,19	3,10	2,22	0,74	60,09	120,24
Kosmos-65	10,66	10,43	10,04	8,81	7,09	5,06	3,01	2,18	0,70	57,97	117,91
Tiros-VII Mar.-May 1964	11,25	11,00	10,68	9,06	7,16	5,21	3,24	2,33	0,76	60,69	121,73

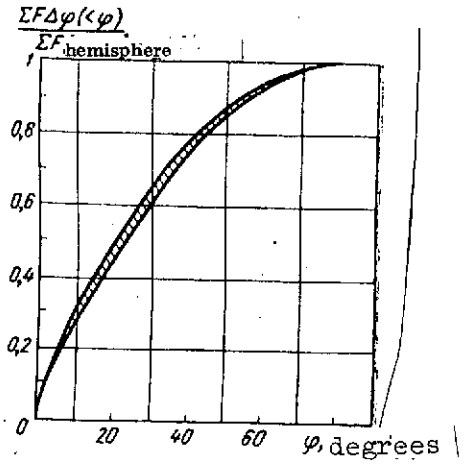

Fig. 3.16. The dependence on latitude of the portion of the flux of departing radiation in the band of latitudes from the Equator to a given latitude on the overall flux of each hemisphere.

window of transparency of the atmosphere, where there is a clearly expressed latitudinal variation of intensity of radiation (see Figs. 3.4 - 3.5), the portion of radiation of latitudes near the Equator in departing radiation in comparison with polar latitudes will be greater than in absorption bands, where the latitudinal variation of intensity of radiation is expressed less clearly. For instance, 50% of the departing radiation of the northern hemisphere in the spectral interval 11 to 12 microns, according to data of satellite "Kosmos-65", is enclosed in the latitudinal zone 0 - 22.5° north latitude, and in the spectral interval 14 to 16 microns is enclosed in a latitudinal zone 0 - 27° north latitude. /68

From the presented comparison, one can draw the conclusion that the portion of radiation of separate latitudinal zones in the integral departing radiation of the Earth and the total fluxes of departing radiation of each hemisphere and of the entire Earth as a whole remain almost constant for the seasons of different years considered.

In September, 1964, on satellite "Kosmos-45," P.A. Bazhulin, A.V. Kartashev, and M.N. Markov measured the departing radiation in various spectral intervals [3]. To obtain

the spectral distribution a method of modulation spectrometry with the use as a modulator of materials with different position of the edge of the absorption band [31] was developed. The angle of vision of the optical system of the apparatus was equal to 2×10^{-3} rads. This angle was scanned for about 0.1 seconds, in the course of which four spectral intervals in the range 0.8 - 38 microns were considered (0.8 - 38; 4.5 - 38; 8.5 - 38; 12.5 - 38 microns). As a result of subsequent treatment three more intervals were distinguished: 0.8 - 4.5; 4.5 - 8.5; 8.5 - 12.5 microns. The accuracy of the recording of the integral radiation in the interval 4.5 - 38 microns constituted 1%.

The apparatus operated during one loop of the satellite, during which characteristics of the field of radiation were obtained in seven regions of the globe. For the region of angles, not very strongly differing from the nadir, the magnitude of the integral flux on the average over the planet constitutes 245 watts/m^2, that corresponds to radiation temperature 255°K (the flux is obtained on the assumption of isotropic distribution of it over angles). It is interesting to note that these magnitudes vary little at wide variations of conditions of observation (day - night; mainlands - oceans; northern - southern hemisphere). In spite of the fact that the latitudinal variation is determined very roughly, the authors note that in the region of the subtropics (±15° from the Equator) the average magnitude of the integral flux is about 290 watts/m^2 (T_{rad} = 265°K), at middle latitudes 200-260 watts/m^2 and at high latitudes about 200 - 210 watts/m^2 [30]. Comparison of these results with ours shows good agreement of them.

The magnitude of the flux of departing radiation in the window of transparency 8.5 to 12.5 microns on the average over the planet constitutes 62 watts/m^2 (T_{rad} = 276°K) whereby variations of fluxes and of T_{rad} in the case of changes of the conditions of observations are the greatest here. /69

3.4 Angular Distribution of Infrared Radiation of the Earth into Outer Space Near the Horizon.

To date, a large number of theoretical calculations of the angular distribution of long wave infrared radiation of the Earth into outer space have been performed [32-27].

With the help of rockets and satellites measurements have been conducted of the angular distribution of intrinsic radiation of the Earth in various intervals of the spectrum [30-31, 38-40]. These measurements qualitatively confirm the theoretical calculations. However, all these measurements were conducted in relatively wide spectral intervals.

On satellite "Kosmos-65" measurements were conducted of the departing long wave radiation of the Earth from a region close to the horizon of the Earth. The transition to a regime of observation of radiation from a region near the horizon of the Earth, from a regime of observation to the nadir was brought about by the introduction into the field of vision of the apparatus of a supplementary gold-plated flat mirror. The optical axis of the apparatus was oriented forward in the direction of motion of the satellite.

In the recording of the spectra during the observation of the horizon, lines of sighting were located near it at different distances. During the recording of one spectrum the direction of sighting practically did not change relative to the horizon. The angle of the field of vision of the apparatus was identical at both orientations (to the nadir and to the horizon) of the optical axis and was equal to 1°46' X 2°20'. In the observation of the horizon, angle 2°20' was oriented in the vertical plane, angle 1°46' in the horizontal.

For making the distances from the horizon more precise, during which errors of measurement of spectra were generated, scanning the field of vision was carried out in a vertical plane at two wave lengths 10 and 19 microns after the recording of the corresponding spectrum: at wave length 10 microns after the recording of the spectrum in the interval 7 to 20 microns, and at wave length 19 microns after recording of the spectrum in the interval 14 to 38 microns.

Scanning occurred in a vertical plane at 8°30' to both sides of the direction of the optical axis, in which it was

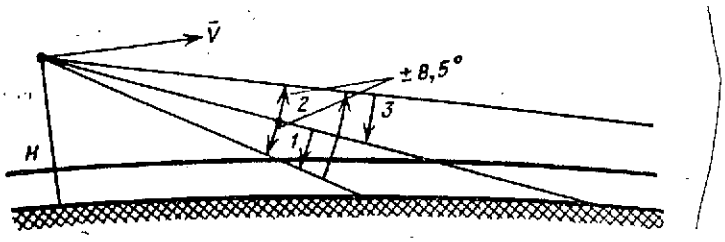

Fig. 3.17. The scheme of scanning the field of vision in a vertical plane in the case of observation of the horizon.

located during the recording of the preceding spectrum. Scanning consisted of three successive motions (Fig. 3.17):

1. Uniform shift of the optical axis down from the initial position to 8°30' in the course of 6.4 seconds.

2. Rapid and irregular shift of the optical axis to the highest position.

3. Uniform shift in 6.4 seconds to the initial position. /70

In Fig. 3.17 vector $\bar{V}$ is the direction of satellite's motion; H--the altitude of satellite above the Earth.

In Fig. 3.18 three typical traces of the full cycle of the spectrophotometer, taken in outer space at different angular distances from the horizon, of angles ϕ to be determined. Aside from these traces on the presented prints are visible curves of the record of other apparatuses, of the representation of the dial of a clock. To the right on the traces the short wave spectrum 7 to 20 microns is located with the section of scanning the field of vision at wave length 10 microns. Following it on the traces the long wave spectrum 14 to 38 microns is seen with the section of scanning the field of vision at wave length 19 microns.

In sections of the record of spectra scales of wave lengths are presented. In sections of scanning the field of vision, the three successive intervals of motion of the optical axis, indicated above are marked by numbers 1, 2, 3. In section 1 the optical axis of the apparatus shifts down to the side of the Earth and ordinates on the traces increase. In section 2, when the optical axis rapidly proceeds

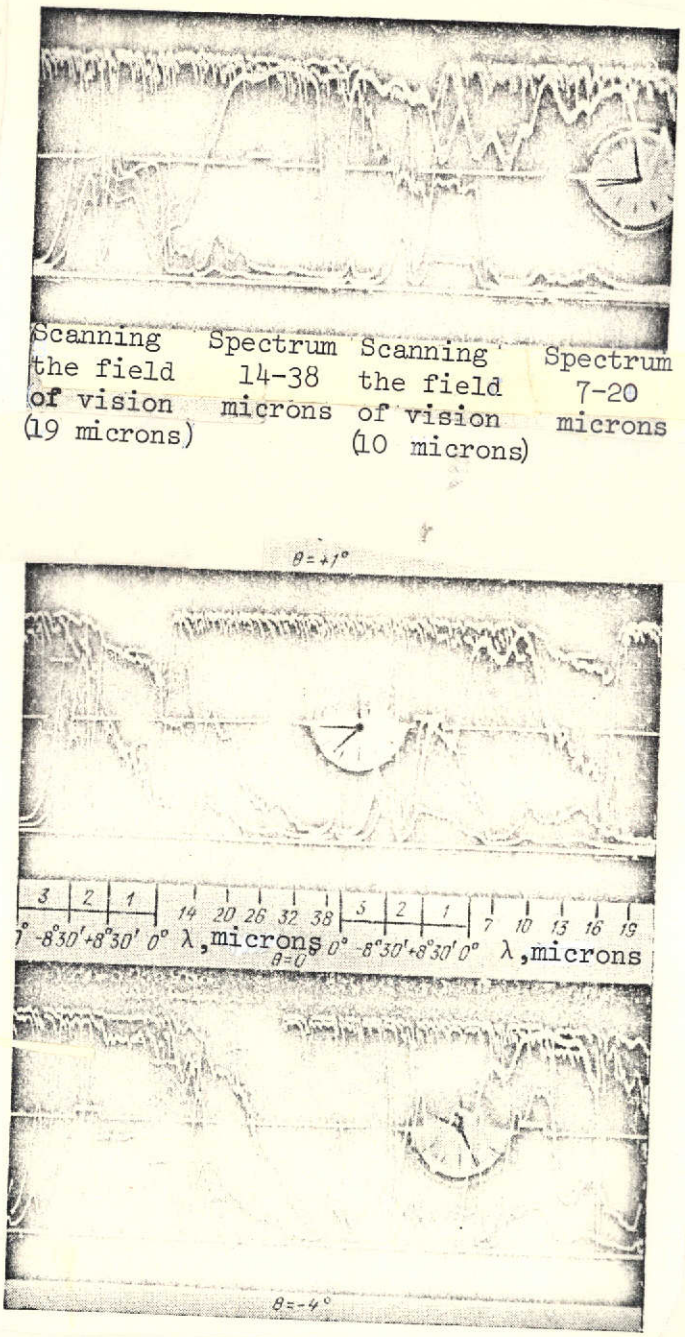

Fig. 3.18. Typical traces of a full cycle of a spectrophotometer, taken at different angular distances from the horizon.

from the lowest to the highest position, the ordinates decrease. However, due to the fact that the edge of the satellite falls into the field of vision of the apparatus in the highest position, a peak is seen on the traces with center at the boundary of sections 2 and 3. In section 3 the optical axis shifts down to its initial position; and as a function of the distance to the horizon, ordinates either remain zero or begin to increase.

Wave length 10 microns is located in a window of transparency of the atmosphere. Therefore, the apparatus "sees" in it the edge of the disc of the planet in clear weather or /72
the upper boundary of clouds in case of continuous cloudiness in the field of vision. At altitudes of flight of the satellite of about 250 kilometers, the angular distance between directions of the optical axis of the apparatus in these two cases in the case of the upper boundary of clouds being at an altitude of 9 kilometers does not exceed 0.25°.

In the case of scanning the field of vision, the optical axis of the apparatus crosses the line of the horizon, expressed by a sharp jump of the ordinates on traces. It was assumed that the position of the optical axis, corresponding to the middle of this jump of ordinates at wave length 10 microns, is equivalent to the direction of sighting edge of the Earth. Sections 1 and 3 of uniform shift of the optical axis were used in this case. At wave length 19 microns the boundary of the atmosphere, determinable at the middle of the jump of ordinates on sections of scanning, is located on the average at 0.25° higher than at wave length 10 microns. This conclusion is based on an analysis of traces obtained on satellite "Kosmos-92," where the recording of both spectral intervals and of the corresponding sections of scanning the field of vision was conducted in parallel fashion. From the direction that corresponds to the middle of the jump of the ordinates at both wave lengths, the direction of sighting at the recording of the preceding spectrum is reckoned. The direction of sighting to the visible edge of the Earth was taken as zero ($\theta = 0°$), and the directions of sighting higher and lower than zero were taken with plus and minus sign respectively. Inasmuch as the exact position of the visible horizon was not known, one should consider presented angles θ as tentative. 222 spectrograms obtained in April, 1965 on artificial Earth satellite "Kosmos-65" were used for processing. As usual, only the part of the spectrograms was processed where there was no overlapping of spectra of the second order on spectra of the first: 7 to 15 microns in the first spectral

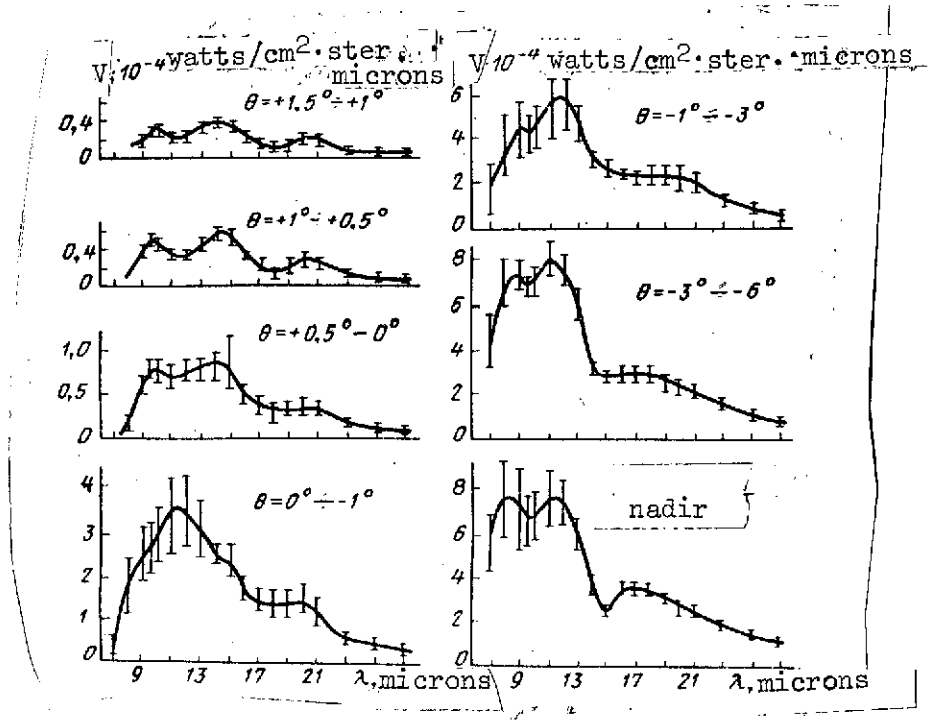

Fig. 3.19. Angular distribution of energy luminance in the case of directions of sighting close to the horizon.

range and 14 to 27 microns in the second. During these measurements the satellite was located in the range from 45 to 15° north latitude above the Atlantic and Pacific Oceans on the day side of the Earth. In this case during the observation of the horizon, the optical axis of the apparatus was directed to the side of the Equator. 154 spectrograms in the case of observation of the horizon were processed, as were 68 spectrograms, recorded on the same satellite in the same latitudinal interval in the case of orientation of the optical axis to the nadir. Spectra were grouped according to angle θ. In each group the average values of energies from spectra of the given group at wave lengths from 7 to 21 microns were determined one micron apart, and from 21 to 27 microns every two microns apart.

Obtained results are presented in Fig. 3.19. Along the axis of abscissas wave lengths in microns are plotted, and along the axis of ordinates energy luminance in units 10^{-4} watts/cm^2-ster.-microns. /73

Each point of Fig. 3.19 represents values of the root-mean-square deviations from the average, that result from variance of ordinates of separate spectra of the given group. This variance of points is caused by the real dispersion of averaged magnitudes, and not by errors of the measuring apparatus. In the case of positive angles θ (the optical axis is oriented above the visible edge of the Earth), emission bands with centers at 9.6, 15, 20 microns are a characteristic special feature of spectra. These bands are separated from one another by sections with smaller values of ordinates with centers at wave lengths 11 and 18 microns. These are windows of transparency of the atmosphere. Emission is explained by intrinsic radiation of gases of the atmosphere that absorb in the infrared region of the spectrum: O_3 (9.6 microns), CO_2 (15 microns), and water vapor (20 microns). Absorption of water vapor rapidly increases with an increase of wave length from 20 microns, that should also lead to an increase of departing radiation at $\lambda > 20$ microns. However, in curves of Fig. 3.19, after 20 microns a decrease begins that is caused by the Planckian nature of the distribution of energy in the radiation spectrum of the atmosphere. In the case when θ approaches 0°, values of departing radiation increase, in which case the relative increase in windows of transparency is greater than in emission bands. In case of switching to negative values of θ, there occurs a rearrangement of maxima in clearly expressed minima in bands of O_3 and CO_2 [41]. /74

This phenomenon is difficult to explain. In the case of a direction of the optical axis of the apparatus higher than the visible horizon ($\theta > 0°$), in spectral intervals of bands of atmospheric gases, the intrinsic radiation of these gases is of predominant significance. In windows of transparency the atmosphere almost does not radiate, and values of energies different from zero at $\theta > 0°$ are explained by the terminal resolution by wave length and angle of vision. With an approach of θ to zero the Earth's surface falls into the field of vision. The quantity of energy that enters the apparatus in windows of transparency is proportional to the portion of the field of vision occupied by this surface. In bands of absorption of atmospheric gases, "warm" radiation

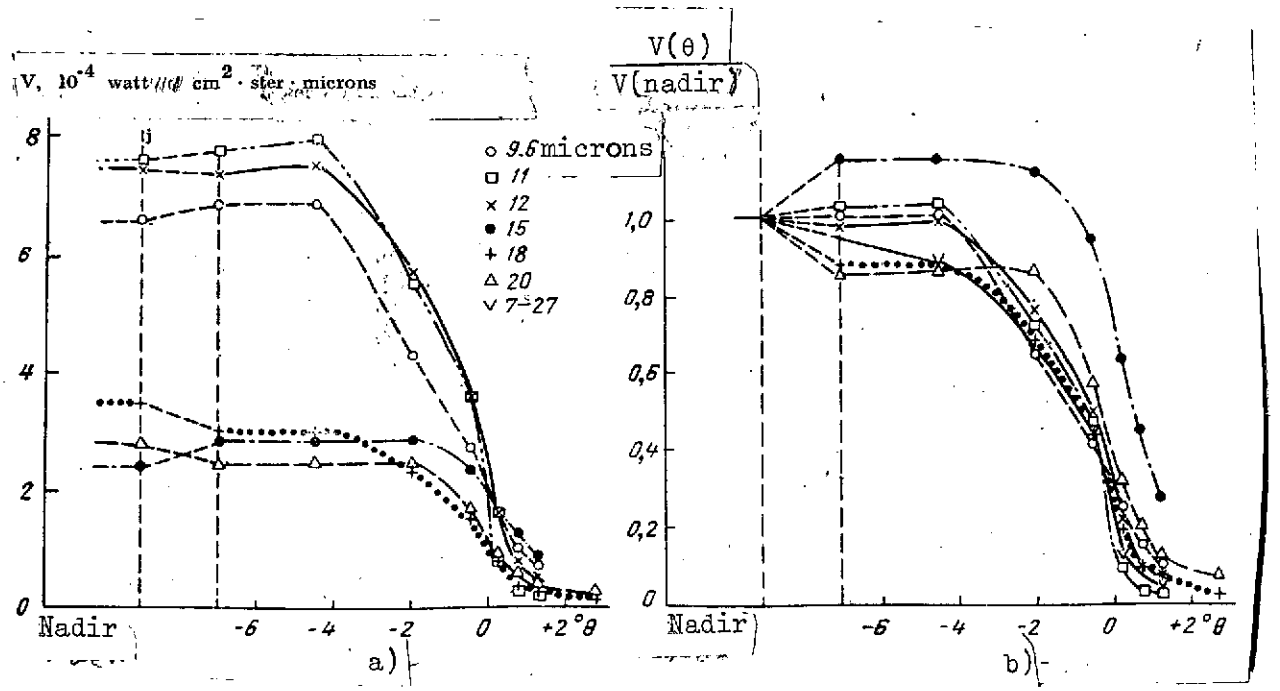

Fig. 3.20. Variation of the magnitude of departing radiation with the variation of the angle of sighting for some wave lengths.

of the Earth's surface and of lower layers of the atmosphere, that depend to a greater or lesser degree on the magnitude of the absorption coefficient and the quantity of absorbing gases, is replaced by "cold" radiation of these gases. In the band of ozone with center 9.6 microns this substitution is not so significant; whereas in the band of carbon dioxide with center 15 microns, practically all the radiation into outer space is formed high in the atmosphere. Therefore, at $\theta < 0°$ there occurs an almost constant value of departing radiation in the band 15 microns. The spectrum in case of θ from -3° to -6° already practically does not differ from the spectrum to the nadir.

The nature of the variation of departing radiation with the variation of angle θ is traced well in Fig. 3.20. Along the axis of abscissas angle θ is plotted; along the axis of ordinates is plotted the energy luminance in absolute units (3.20.a) and in relative units (3.20.b), normalized to one at an angle of sighting that corresponds to the direction to the nadir. Dependences are traced for six wave lengths: 9.6; 11; 12; 15; 18; 20 microns. Moreover, in Fig. 3.20.b the curve for departing integral radiation in the spectral interval 7 to 27 microns is presented. In addition, at the indicated wave lengths, spectra from $\theta > -6°$ that are related to the value $\theta = -7°$ were processed. The root-mean-square deviations in Fig. 3.20 are not shown. As can be seen from Fig. 3.20b, darkening of the disc of Earth toward the edge is different at different wave lengths. At wave length 15 microns brightening toward the edge is observed. However, these differences can be unreal, since they lie within the limits of statistical variance, explained by the presence of cloudiness in the field of vision of the spectrophotometer. In the case of flight of a satellite, monitoring of cloudiness was carried out at a point beneath the satellite with the help of a photometer in the spectral interval 0.6 - 0.8 microns. The photometer indicated the presence of cloudiness almost on all sections of the trajectory of the satellite used in the processing. /76

On the other hand, all theoretical calculations are constructed from conditions either of a clear sky or of continuous cloudiness at different levels. Therefore, there is no quantitative agreement of data of theoretical calculations with experimental results. As theoretical calculations show [33, 36, 37], an apparatus, that has an infinitely narrow field of vision, would show various profiles of the angular distribution of the intensity of radiation near the horizon

of the Earth and at different wave lengths. An apparatus with a finite field of vision smooths out various fine non-uniformities of the angular distribution, that leads to uniformity of profiles of the horizon at different wave lengths. Such a conclusion is arrived at by the authors of [32], where results are given of theoretical calculations of the angular distribution of fluxes of departing radiation in a three-degree cone in the region of large zenith angles. This is confirmed by results of the given experiment. At angles $\theta > 0°$ the slope of the decrease of the magnitude of departing radiation is approximately the same for all wave lengths.

The effective edge of the Earth for radiation at wave length 15 microns is located higher than at other wave lengths (Fig. 3.20.b). Its approximate excess in this wave length above the edge of the Earth, taken at λ =11 microns at level 0.5 of intensity of radiation to the nadir, constitutes 27 kilometers. This qualitatively corresponds to theoretical concepts [37]. In the band of ozone 9.6 microns a similar effect is obtained, that is completely natural, since the width of the band of ozone is comparable in magnitude with the resolving capacity of the apparatus over wave lengths in this region of the spectrum, and neighboring sections of the window of transparency make a substantial contribution to the energy to be recorded at λ = 9.6 microns.

Thus, the obtained results make it possible to draw a conclusion about their qualitative agreement with data of present-day theoretical concepts concerning the angular distribution of infrared radiation of the Earth into outer space. For quantitative agreement theoretical calculations must be performed that take into account real meteorological circumstances, mainly cloudy conditions.

CHAPTER FOUR

ANALYSIS OF COMBINED DISTRIBUTION OF SPECTRAL INTENSITIES OF THE RADIATION OF THE EARTH

4.1 Two Dimensional Differential Laws of Distribution.

The results of statistical processing of experimental material that were presented in the preceding chapter make it possible to estimate the average expected value of the magnitude of intensity of radiation and its variance in one spectral interval $\Delta\lambda = 1$ micron in width for $\lambda = 7-15$ microns and $\Delta\lambda = 2$ microns from $\lambda = 14-26$ microns. However, for calculation of the expected variance of the total intensity of radiation in several spectral intervals both neighboring and far along the spectrum from one another, it is insufficient to know the mathematical expectation and dispersion of the intensity of radiation in each spectral interval; it is necessary to know as well the correlation between them. This correlation can be established in the estimating of the combined distribution of intensities of radiation, measured simultaneously in two spectral intervals. A section of a trace during scanning along the spectrum can be considered as the result of simultaneous measurements, necessary for the calculation of combined distribution. In this case we disregard the variation of sections of the radiating surface in the field of vision of the spectrophotometer due to motion of the satellite itself. However, as will be shown in §4.2, this allowance is completely acceptable, inasmuch as measurement of the correlations between intensities of radiation in different spectral intervals due to motion of the satellite is insignificant.

As is well known, the most complete characteristic of the combined distribution of two random magnitudes is a two-dimensional law of their distribution.

In the plotting of the combined distribution, the intensity of radiation of the Earth I_i in each of two sections of the spectral range is considered as an uninterrupted random magnitude. The density of distribution of the system of two random magnitudes I_1, I_2 (the differential law) is the limit of the ratio of probability of incidence of a random point to a small rectangle in the system of coordinates

I_1, I_2 to the area of this rectangle, when both of its dimensions approach zero: /78

$$f(I_1, I_2) = \lim_{\substack{\Delta I_1 \to 0 \\ \Delta I_2 \to 0}} \frac{n(I_1, I_2)}{N \Delta I_1 \Delta I_2}, \tag{4.1}$$

where $f(I_1, I_2)$ is the density of distribution of random magnitudes I_1, I_2; $n(I_1, I_2)$ is the number of hits of a random point in a rectangle with center at point I_1, I_2 and with sides ΔI_1, ΔI_2; N is the overall number of measurements.

Numerical characteristics of a two-dimensional law of distribution of two random magnitudes are the covariance K_{I_1, I_2} and the coefficient of correlation r_{I_1, I_2}, that characterizes the correlation between random magnitudes, and likewise mathematical expectations $\bar{I}_1$, $\bar{I}_2$ and central moments. The covariance and the coefficient of correlation are equal respectively to

$$K_{I_1, I_2} = \frac{1}{N-1} \sum_{i=1}^{N} (I_{1,i} - \bar{I}_1)(I_{2,i} - \bar{I}_2), \tag{4.2}$$

$$r_{I_1, I_2} = \frac{K_{I_1, I_2}}{\sigma_{I_1} \sigma_{I_2}}, \tag{4.3}$$

where σ_{I_1}, σ_{I_2} are the mean square deviations of random magnitudes I_1 and I_2.

Mean square deviations and dispersions D_1 are determined from expression

$$\sigma_I^2 = D_I = \frac{1}{N-1} \sum_{i=1}^{N} (I_i - \bar{I})^2. \tag{4.4}$$

Angles of inclination θ_1 and θ_2 of the main axes of dispersion to axes I_1 and I_2 are connected with the covariance by

TABLE 4.1

Spectral interval, microns	Correlation coefficients and angles of inclination of the main axis of dispersion for spectral intervals from 7 to 26 microns												
	7—8	8—9	9—10	10—11	11—12	12—13	13—14	14—15	16—18	18—20	20—22	22—24	24—26
7—8	1,00 45°	0,75 62° 1,00 45°	0.48 71° 0,65 48° 1,00 45°	0,70 71° 0,91 54° 0,65 54° 1.00 45°	0.68 73° 0,87 58° 0,62 60° 0,95 60° 1,00 45°	0,62 74° 0,84 58° 0,60 50° 0,90 48° 0,93 44° 1,00 45°	0,46 75° 0,77 54° 0,56 54° 0,80 44° 0,82 38° 0,88 40° 1,00 45°	0,17 108° 0,39 12° 0,30 8° 0.41 3° 0.37 97° 0.46 8° 0,57 12° 1,00 45°	0,43 77° 0,49 5° 0.33 5° 0,48 6° 0,47 5° 0,46 5° 0.41 5° 0.19 10° 1.00 45°	0.35 18° 0.46 8° 0,30 5° 0,45 6° 0,46 5° 0,49 6° 0,50 7° 0.27 16° 0,62 41° 1.00 45°	0.40 10° 0.53 8° 0,37 5° 0,54 6° 0.53 5° 0.57 5° 0.59 6° 0.34 14° 0,60 40° 0,76 38° 1,00 45°	0.38 7° 0.49 5° 0,34 3° 0.50 4° 0.51 3° 0,54 4° 0,58 5° 0.33 9° 0. 4 27° 0,69 27° 0,82 34° 1.00 45°	0,36 5° 0,46 4° 0,32 2° 0,47 3° 0.40 2° 0,53 3° 0,56 4° 0,32 6° 0,43 16° 0,66 20° 0,75 26° 0,76 36° 1,00 45°
8—9													
9—10													
10—11													
11—12													
12—13													
13—14													
14—15													
16—18													
18—20													
20—22													
22—24													
24—26													

the following dependence:

$$\tan 2\theta = \frac{2K_{I_1, I_2}}{D_{I_1} - D_{I_2}} \Bigg\} \qquad (4.5)$$

Results of calculations of correlation coefficients and of angles of inclination of the main axis of dispersion for all possible combinations of spectral intervals for the whole investigated range of the spectrum from 7 to 26 microns are presented in Table 4.1. In each box of this table in the first line is presented the correlation coefficient, and in the lower is presented the angle of inclination of the main axis of dispersion in degrees. The lower part of the table is not filled, inasmuch as the table is symmetrical relative to the diagonal. One should again note that due to the motion of the satellite during the scanning over the spectrum, a shift of sections of Earth from which radiation is recorded takes place in the field of vision of the spectrophotometer. Consequently, strictly speaking, radiation at different wave lengths is recorded from different sections of the Earth. So, for instance, the time of recording of traces in the range of the spectrum from 7 to 15 microns comprised about 10 seconds; and between moments of recording at wave lengths 11 and 20 microns about 30 seconds. It is not difficult to calculate that during this time the artificial Earth satellite moved respectively about 80 and 240 kilometers. The size of the field of vision of the apparatus on the surface of the Earth comprises about 7 X 10 kilometers. The effect of the given factor leads to some expansion of two-dimensional regions and to attenuation of correlations. It can be expected that with an increase in the determined limits of time between moments of recording radiation at different wave lengths distortion of two-dimensional distributions will increase. In §4.2 of the given chapter an estimate is carried out of distortions of two-dimensional distributions due to the non-simultaneity of measurements, that showed that the effect of the given factor in the case of the conditions considered is insubstantial. Therefore, in spite of the effect of distortions, obtained data on two-dimensional distributions make it possible to analyze correlations between intensities of radiation at different wave lengths.

/80

Analyzing the data of Table 4.1, one can note that the greatest correlation between intensities of radiation is in bands of radiation of one and the same atmospheric gas in the

case of close values of the absorption coefficient. Actually, the correlation coefficient between intensities of radiation has a maximum value in spectral intervals in the window of transparency of the atmosphere 8 to 13 microns (the weakest band of absorption of water vapor with an absorption coefficient that is practically constant along the spectrum). For all combinations of spectral intervals in the given window, the correlation coefficient has a value from 0.84 to 0.91, except the interval of the spectrum 9 to 10 microns. In the latter spectral interval the absorption band of ozone with center at 9.6 microns and in width about 0.5 microns is appreciable. The correlation coefficient of the intensity of radiation in the interval 9 to 10 microns with remaining intervals of the window of transparency 8 to 13 is significantly lower (0.60 to 0.65).

The effect of the ozone band on the correlation of intensities of radiation in the interval 9 to 10 microns with intervals in a window of comparatively weak absorption of water vapors 18 to 26 microns is also appreciable. The coefficient of correlation between intensities of radiation in two windows of transparency 8 to 13 and 18 to 26 microns varies from 0.46 to 0.57, whereas the coefficient of correlation between intensities of radiation in the range 18 to 26 microns with intensity in the interval 9 to 10 microns varies from 0.30 to 0.37 in all. /81

The minimal correlation is between intensities of radiation in absorption bands of various gases (water vapor and carbon dioxide). So, the coefficient of correlation of the intensity of radiation in the interval 14 to 15 microns (absorption band of CO_2) and the remaining intervals (the absorption band of H_2O) is of significance only in the limits from 0.17 to 0.57. Minimal values (0.17 and 0.19) occur when the correlation with the intense absorption band of water vapor (with intervals 7 to 8 and 16 to 18 microns) is considered.

In Figs. 4.1 - 4.4 graphs are presented of two-dimensional differential laws of distribution for some characteristic combinations: 7–8 to 11–12 microns; 7–8 to 14–15 microns; 8–9 to 10–11 microns; 11–12 to 14–15 microns; where the interval of the spectrum 7 to 8 microns corresponds to strong absorption of water vapors, 8 to 9 microns, 10 to 11 microns and 11 to 12 microns correspond to weak absorption of water vapors and 14 to 15 microns correspond to strong absorption of carbon dioxide. /82

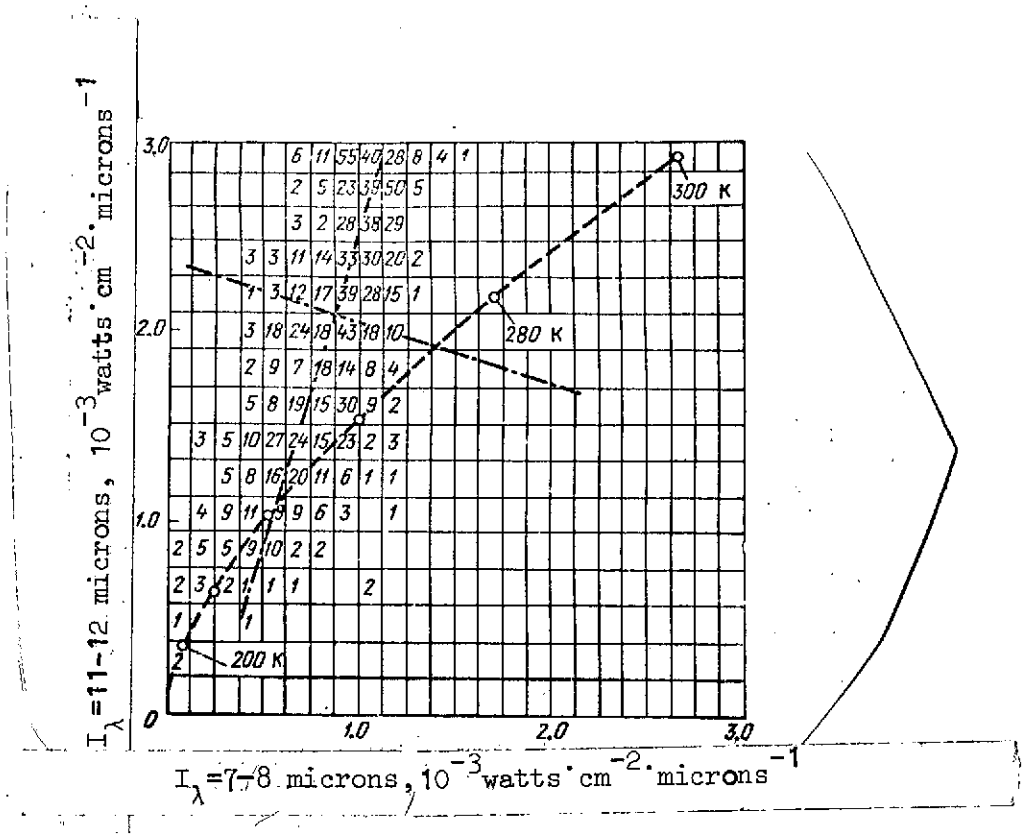

Fig. 4.1. Two-dimensional differential law of distribution of the intensity of radiation for intervals 7 to 8 and 11 to 12 microns.

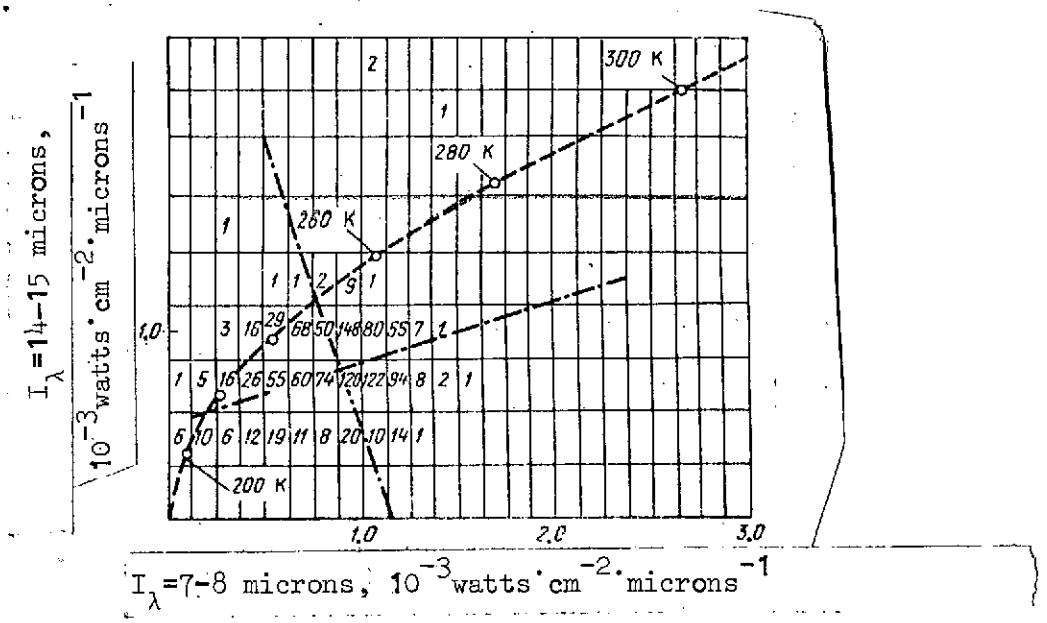

Fig. 4.2. Two-dimensional differential law of the distribution of intensity of radiation for intervals 7 to 8 and 14 to 15 microns.

In the determination of intensities of radiation by spectrograms, in each spectral interval a scale of intensities was marked off for a series of ranks ΔI. In conformity with this in Figs. 4.1 - 4.4 a rectangular grid was drawn with interval ΔI. Inside each rectangle of the given grid the figures signify the number of cases n, when the intensity of radiation in both considered spectral intervals had values that were limited by the corresponding sides of the rectangles. Two-dimensional distributions are plotted as a result of processing N = 1176 spectrograms.

For comparison in Figs. 4.1 - 4.4 thermal dependences of the intensities of radiation of an absolutely black body are drawn at wave lengths that correspond to the centers of the considered spectral intervals. Circles signify intensities of radiation of an absolutely black body with temperatures 200, 220, 240, 260, 280 and 300°K. The main axes of dispersion are shown by dash-dot lines. Coordinates of the center of dispersion are equal to the mathematical expectations along both axes, i.e. $\bar{I}_1$ and $\bar{I}_2$. /83

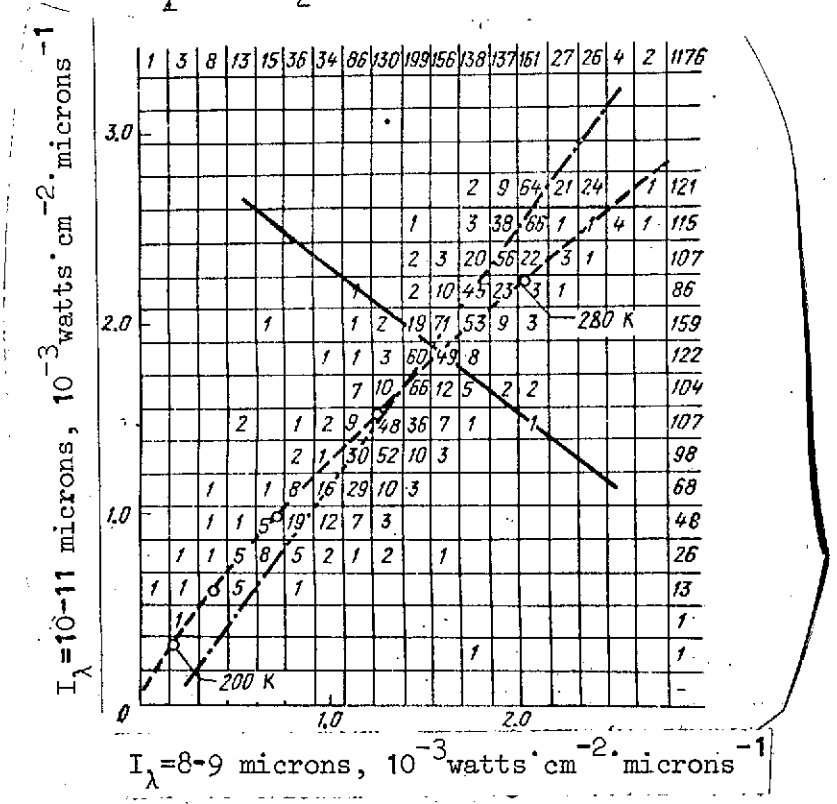

Fig. 4.3. Two-dimensional differential law of the distribution of intensity of radiation for intervals 8 to 9 and 10 to 11 microns.

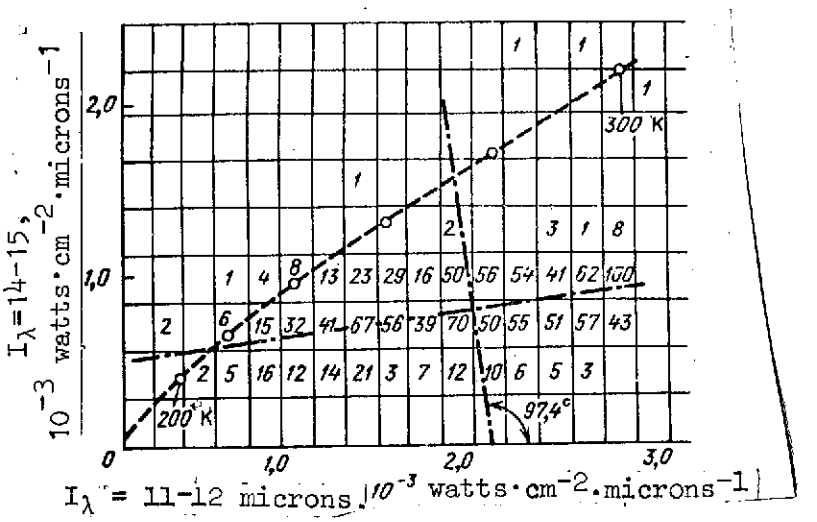

Fig. 4.4. Two-dimensional differential law of distribution of the intensity of radiation for intervals 11 to 12 and 14 to 15 microns.

For two-dimensional laws of distribution of intensities of radiation in the window of transparency 8 to 13 microns, one of the main axes of dispersion lies closer than all of them to the curve that connects intensities of radiation of a black body.

In two-dimensional distributions for a combination of intervals of the spectrum 14 to 15 and 7 to 8 microns the main axes deviate most from the line of intensities of an absolutely black body. This is connected with the fact that in these intervals of the spectrum various layers of the atmosphere radiate that have different temperature, and there is practically no radiation of the surface of the Earth.

The sizes and the angle of inclination of a two-dimensional region of distribution of intensities of radiation depend on the correlation of intensities of radiation in various spectral ranges. As has already been mentioned, partial expansion of two-dimensional regions takes place due to methodological peculiarities of the measurement of spectra. /84

Graphs of two-dimensional differential laws of distribution for remaining combinations of spectral intervals of the range of the spectrum 7 to 26 microns are presented in Figs. P.4.1 - P.4.5 of the appendix.

4.2 Estimation of Readjustments for Non-simultaneity of Measurements to Correlation Dependence Between Spectral Intensities of the Radiation of the Earth.

In accord with results of a large number of measurements of spectral intensities of radiation of the Earth in the infrared range of the spectrum, in the preceding paragraph there were presented calculated correlation dependences between intensities of radiation in spectral intervals. In this case it was noted that due to the great velocity of the artificial Earth satellite during the scanning over the spectrum from 7 to 14 microns the field of vision of the apparatus shifted a distance of up to 80 kilometers. Due to this, intensities of the radiation of the Earth at different wave lengths were recorded from various sections of the surface and there were introduced into calculated correlation dependences both spectral and spatial correlations between intensities of radiation of separate sections of the Earth's surface, that led to some decrease of obtained values of coefficients of correlation. /85

To find more accurate values of coefficients of correlation between intensities of radiation in separate spectral intervals, it is necessary to exclude the effect of spatial variation of the intensity of radiation in the case of passage from one spectral interval to another.

In the case of statistical processing of results of measurements values of mathematical expectations $\overline{I}_\lambda$ and root-mean-square deviations σ_{I_λ} of intensities of radiation I_λ in separate spectral intervals λ were obtained. Inasmuch as their calculation was performed over the whole existing assembly separately for each spectral interval independently of one another, it can be considered that the mathematical expectations and root-mean-square deviations in the case of the shift of the moment of measurement t of magnitude τ do not change, i.e. one can consider that

$$\overline{I}(t) = \overline{I}(t+\tau) = \overline{I} \tag{4.6}$$

and

$$\sigma_I(t) = \sigma_I(t+\tau) = \sigma_I \tag{4.7}$$

Consequently, magnitudes $\bar{I}$ and σ_I are not distorted by the time difference of measurements. The coefficient of correlation in §4.1 is actually calculated by formula

$$r[I_{\lambda_1}(t),\ I_{\lambda_2}(t+\tau)]=\frac{1}{\sigma_{I_{\lambda_1}}\sigma_{I_{\lambda_2}}}\sum_{i=1}^{n}[I_{\lambda_1,i}(t)-\bar{I}_{\lambda_1}][I_{\lambda_2,i}(t+\tau)-\bar{I}_{\lambda_2}]. \qquad (4.8)$$

Having signified by $\Delta I_{\lambda_2}(\tau)$ the increase of the intensity of radiation at wave length λ_2 for time τ due to the shift of the field of vision of the apparatus, one can write the expression of the correlation coefficient in the following manner:

$$r[I_{\lambda_1}(t),\ I_{\lambda_2}(t+\tau)]=\frac{1}{\sigma_{I_{\lambda_1}}\sigma_{I_{\lambda_2}}}\sum_{i=1}^{n}[I_{\lambda_1,i}(t)-\bar{I}_{\lambda_1}]\times$$
$$\times[I_{\lambda_2,i}(t)+\Delta I_{\lambda_2,i}(\tau)-\bar{I}_{\lambda_2}]. \qquad (4.9)$$

The correlation between spectral intensities that interests us is characterized by the correlation coefficient that should be calculated by formula /86

$$r[I_{\lambda_1}(t),\ I_{\lambda_2}(t)]=\frac{1}{\sigma_{\lambda_1}\sigma_{\lambda_2}}\times$$
$$\times\sum_{i=1}^{n}[I_{\lambda_1,i}(t)-\bar{I}_{\lambda_1}][I_{\lambda_2,i}(t)-\bar{I}_{\lambda_2}]. \qquad (4.10)$$

For exclusion in formula (4.9) of the effect of the component of $\Delta I_{\lambda_2}(\tau)$, which supposedly deforms the two-dimensional law of distribution that interests us, a method is presented for modeling deformation of two-dimensional distributions by random increments $\Delta I_{\lambda_2}(\tau)$.

Defining numerical characteristics of undeformed two-dimensional distribution $[\bar{I}_{\lambda_1}, \bar{I}_{\lambda_2}, \sigma_{\lambda_1}, \sigma_{\lambda_2}, r[I_{\lambda_1}, I_{\lambda_2}]]$ and the angle of inclination of the axis of dispersion θ, one can, on a computer with the help of a data unit of random numbers of normal distribution, obtain realization of two-dimensional distribution $(I_{\lambda_1,1}; I_{\lambda_2,1}; \ldots; I_{\lambda_1,n}; I_{\lambda_2,n})$. Giving one of the coordinates of points of the two-dimensional distribution, for instance, coordinate

$I_{\lambda_2,i}$ a random increment $\Delta I_{\lambda_2,i}$ (in the case of given magnitudes $\overline{I}_{\lambda_2}$ and $\sigma_{\Delta I_{\lambda_2}}$), one can obtain deformation similar to that which was the case in experiments. The problem of modeling consists in the selection of such a realization of an undeformed law, as a result of the deformation of which is obtained a two-dimensional distribution with numerical characteristics that agree with experimental characteristics. In case of agreement of characteristics one can consider that characteristics of an undeformed (initial) law are close to characteristics of the desired two-dimensional law, that could be obtained in the case of simultaneous measurements at all wave lengths.

For determination of numerical characteristics of the probable distribution of random increments $\Delta I_\lambda(\tau)$ results of uninterrupted measurements of the intensity of radiation at separate wave lengths (9.5 and 18.5 microns) were used -- the so-called "scans" obtained with the help of the same apparatus.

For estimating the magnitude of the possible variation of intensity of radiation due to shift of the field of vision calculation of increments was performed in 50 processed scans:

$$\Delta I(\tau) = I(t) - I(t+\tau), \tag{4.11}$$

where I(t) is the running value of intensity of radiation, a random function of time t or shift; $I(t+\tau)$ is the running value of the intensity of radiation, shifted in time t with respect to I(t) by magnitude τ. /87

Statistical processing of values $\Delta I(\tau)$, performed at each wave length, showed that the law of distribution of random magnitude $\Delta I(\tau)$ for each value τ is close to normal. In this case the mathematical expectation $\Delta I(\tau)$ for all τ is negligibly small and can be considered equal to zero. The magnitude of the root-mean-square deviation $\sigma[\Delta I(\tau)]$ depends at each wave length only on shift τ. It was found that the ratio $\sigma[\Delta I(\tau)]/\sigma_I$ for considered wave lengths (9.5 and 18.5 microns) agree sufficiently well (maximal divergence of 9% is observed only in the case of the greatest of the considered values of τ). The dependence of the given ratio is

presented in Fig. 4.5 as a function of spectral interval, connected with shift in time of τ by formula:

$$\Delta\lambda = v_p\tau, \tag{4.12}$$

where $v_{scanning}$ is the speed of scanning of the spectrum by the apparatus.

Assuming that the dependence presented in the graph (the average in accord with results of measurements at wave lengths 9.5 and 18.5 microns), is correct for all the other wave lengths, one can determine the root-mean-square deviations of the measurement of intensities of radiation due to spatial shifting for any wave length and any shift $\Delta\lambda$ (up to $\Delta\lambda$ = 5 microns) from the relation

$$\sigma[\Delta I(\tau)] = \frac{\sigma[\Delta I(\tau)]}{\sigma_I}\sigma_{I_\lambda}\text{exp}, \tag{4.13}$$

where $\sigma_{I_\lambda\ \text{exp}}$ is the magnitude of the root-mean-square deviation of intensity of radiation in the spectral interval, determined in accord with results of statistical processing of the totality of spectral measurements for the Earth as a whole. /88

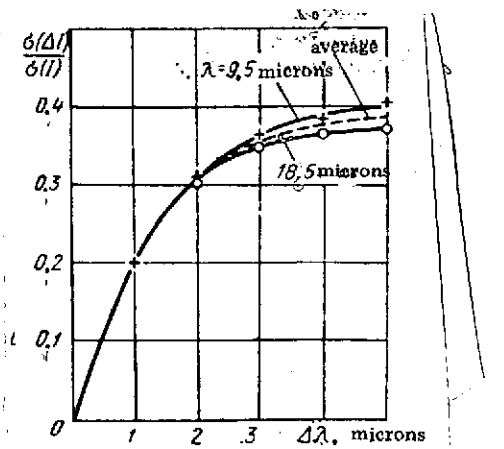

Fig. 4.5. Dependence of the ratio $\sigma[\Delta I(\tau)]/\sigma_I$ on the length of the spectral interval $\Delta\lambda$.

To determine the correlation dependence that interests us between intensities of radiation at wave lengths λ_1 and λ_2, it is necessary to have the values of intensities $I_{\lambda_1}(t)$ and $I_{\lambda_1}(t)$ [sic], measured at the same moment of time.

Actually, the intensities $I_{\lambda_2}(t)$ and $I_{\lambda_2}(t+\tau)$ were measured in the experiment, where τ is the shift in time, determined by the speed of scanning over the spectrum within the limits of wave lengths from λ_1 to λ_2.

Due to this shift, random magnitude I_{λ_2} during τ obtained random increment ΔI_{λ_2}, that is

$$I_{\lambda_2}(t+\tau) = I_{\lambda_2}(t) + \Delta I_{\lambda_2}(\tau). \tag{4.14}$$

As was noted above, in the case of statistical processing of results of measurements, a two-dimensional law of distribution of random magnitudes $I_{\lambda_1}(t)$ and $I_{\lambda_2}(t+\tau)$ was obtained and magnitudes

$$r[I_{\lambda_1}(t),\ I_{\lambda_2}(t+\tau)],$$
$$\theta[I_{\lambda_1}(t),\ I_{\lambda_2}(t+\tau)],$$

were determined, where r and θ are the coefficient of correlation and the angle of inclination of main axes of dispersion, that differ from the desired values $r[I_{\lambda_1}(t),\ I_{\lambda_2}(t)]$ and $\theta[I_{\lambda_1}(t),\ I_{\lambda_2}(t)]$, i.e. a two-dimensional law as if deformed due to non-simultaneity of measurements.

This deformation of a two-dimensional law was simulated on an electronic computer in accord with formula (4.14). It was assumed that the distribution of random magnitudes I_{λ_2} and ΔI_{λ_2} obey a normal law. Magnitude $\sigma[\Delta I_{\lambda_2}]$ was calculated in accord with formula (4.13) and graph Fig. 4.5.

If, as a result of modeling, a two-dimensional law of

distribution was obtained, the characteristics of which agree with characteristics of the experimental two-dimensional law of the distribution of magnitudes $I_{\lambda_1}(t)$ and $I_{\lambda_2}(t+\tau)$, then it was assumed that characteristics of the initial two-dimensional law, subjected to deformation, should correspond to characteristics of the two-dimensional law that could be obtained in the case of simultaneous measurements.

In accord with this proposition, the problem of determining corrections was reduced to the selection of characteristics of the two-dimensional law, as a result of the deformation of which a two-dimensional law is obtained with characteristics close to the characteristics of the law obtained in the case of measurements from an artificial earth satellite.

The modeling of deformation of a random law was carried out on electronic computer BESM-2M. The realization of two-dimensional distribution I_{λ_1}, I_{λ_2} and one-dimensional distribution of magnitude ΔI_{λ_2} was accomplished with the help of a programmed data unit of normal distribution of quasi-random numbers. /89

As initial data for the realization of an undeformed (ud) two-dimensional law of distribution, values $\bar{I}_{\lambda_1}$, $\bar{I}_{\lambda_2}$ and σ_{λ_1} were assigned in accord with results of experiment. Undeformed value σ_{λ_2} was determined according to a formula that is connected with root-mean-square deviations, the coefficient of correlation and the angle of inclination of the axis of dispersal:

$$\sigma_{\lambda_{ud}} = \sigma_{\lambda_1}\left[\sqrt{\left(\frac{r_{ud}}{\tan 2\theta}\right)^2 - 1} - \frac{r_{ud}}{\tan 2\theta}\right] \qquad (4.15)$$

At the beginning of the calculation, values of the correlation coefficient (r_{ud}) and of the angle of inclination (θ_{ud}) of the undeformed two-dimensional law were assigned arbitrarily.

After this, root-mean-square deviations were determined along main axes of dispersal ξ_1 and ξ_2 (Fig. 4.6):

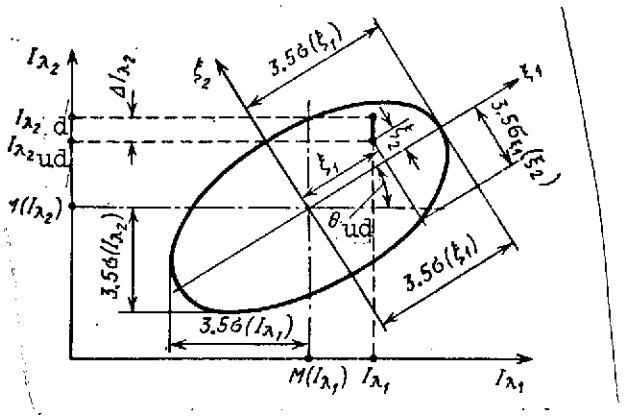

Fig. 4.6. Scheme of "deformation" of the two-dimensional law.

$$\sigma_{\xi_1}^2 = \sigma_{\lambda_1}^2 \cos^2\theta_{ud} + r_{ud}\sigma_{\lambda_1}\sigma_{\lambda_2 ud} \sin 2\theta_{ud} + \sigma_{\lambda_2 ud}^2 \sin^2\theta_{ud} \quad (4.16)$$

$$\sigma_{\xi_2}^2 = \sigma_{\lambda_1}^2 \sin^2\theta_{ud} - r_{ud}\sigma_{\lambda_2 ud}\sigma_{\lambda_1} \sin 2\theta_{ud} + \sigma_{\lambda_2 ud}^2 \cos^2\theta_{ud} \quad (4.17)$$

In accord with calculated value σ_{ξ_1}, with the help of a random number generator, the coordinate was obtained of a random point on axis ξ_1 in accord with formula

$$\xi_1 = \psi_1 \cdot 3.5\,\sigma_{\xi_1} \quad (4.18)$$

where ψ_1 is a random number from the first sequence, used for reproduction of the realization of random coordinate ξ_1. /90

The programmed data unit used in operation achieved the realization of normal distribution of quasi-randon numbers ψ within limits $-1 < \psi < 1$ with root-mean-square deviation

$$\sigma_\psi = \frac{1}{3.5}.$$

For determination of the second coordinate of the random point, the root-mean-square deviation σ_{ξ_2/ξ_1} was calculated as

a function of random magnitude ξ_1 from ellipse equation

$$\sigma^2_{\xi_2/\xi_1} = \sigma^2_{\xi_2}\left[1 - \frac{\xi_1^2}{\sigma^2_{\xi_1}}\right]. \quad (4.19)$$

Coordinate ξ_2 was likewise obtained with the help of a data unit of random numbers in accord with formula

$$\xi_2 = \psi_2 \cdot 3{,}5\sigma_{\xi_2/\xi_1}, \quad (4.20)$$

where ψ_2 is a random number from the second sequence, used for realization ξ_2.

Obtained coordinates of a random point ξ_1 and ξ_2 were listed inversely in the initial system of coordinates I_{λ_1}, I_{λ_2}:

$$I_{\lambda_1} = \overline{I}_{\lambda_1} + \xi_1 \cos\theta_{ud} - \xi_2 \sin\theta_{ud}, \quad (4.21)$$

$$I_{\lambda_2} = \overline{I}_{\lambda_2} + \xi_1 \sin\theta_{ud} + \xi_2 \cos\theta_{ud}. \quad (4.22)$$

With the help of random number ψ_3 (from the third sequence) on the basis of known magnitude $\sigma[\Delta I_{\lambda_2}]$, determined in accord with formula (4.13), the random deviation was found

$$\Delta I_{\lambda_2} = \psi_3 \cdot 3{,}5\sigma[\Delta I_{\lambda_2}], \quad (4.23)$$

and deformation of the two-dimensional distribution along axis I_{λ_2} was produced:

$$I_{\lambda_2 d} = I_{\lambda_2 ud} + \Delta I_{\lambda_2}, \quad (4.24)$$

where $I_{\lambda_2 d}$, $I_{\lambda_2 ud}$ are respectively the deformed and undeformed random coordinates of a point along axis I_{λ_2}.

The obtained coordinates I_{λ_1} and I_{λ_2} are the random realization of a two-dimensional distribution taking account of the fact that random value I_{λ_2} d was shifted in time of measurement with reference to I_{λ_1} to given magnitude τ.

After obtaining of 500 realizations, statistical processing of the two-dimensional distribution was performed and values were calculated of coefficient of correlation r_d and of the angle of inclination of the main axes of dispersal θ_d of the deformed distribution, that were compared with experimental values. /91

Differences $\Delta\theta = \theta_d - \theta_{exp}$ and $\Delta r = r_d - r_{exp}$ were introduced as corrections to the values of given magnitudes θ_{ud} and r_{ud}, and the whole cycle of modelling was repeated until the desired accuracy of agreement of θ_d and r_d with experimental values.

Magnitudes θ_{ud} and r_{ud}, having participated in the last cycle of the iteration process, were assumed to be equal to the initial values of the angle of inclination of the main axes of dispersal and of the coefficient of correlation, that could be obtained in the case of simultaneous measurements at two wave lengths λ_1 and λ_2.

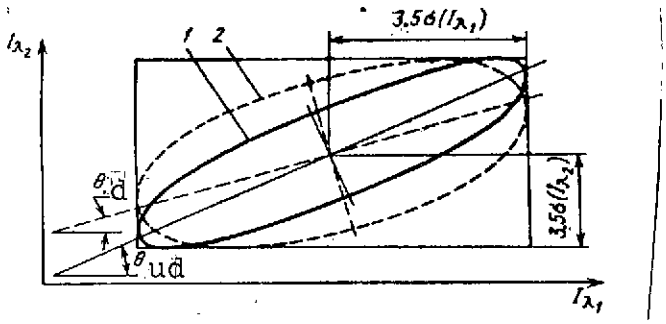

Fig. 4.7. Undeformed 1 and deformed 2 ellipses of dispersal.

In Fig. 4.7 as an explanation are shown undeformed 1 and deformed 2 ellipses of dispersal, where for clearer representation large deformation (r_{ud} = 0.9, r_d = 0.5) is produced.

TABLE 4.2

λ_1, microns	λ_2, microns	r		θ, degrees	
		Without correction	With correction	Without correction	With correction
8–9	11–12	0.870	0.918	58.49	59.39
7–8	11–12	0.684	0.719	73.38	73.62
11–12	14–15	0.372	0.386	97.40	97.44
8–9	10–11	0.909	0.945	53.82	54.66
7–8	14–15	0.171	0.173	107.96	105.75

Results of calculation of coefficients of correlation and of the angle of inclination of the main axes of dispersal for some spectral intervals are presented in Table 4.2. /92

Analyzing results of calculations, one can draw the conclusion that, as one should expect, spatial shifting of the field of vision exerts the greatest influence (correction at 5.5%) on the coefficient of correlation between intensities of radiation inside spectral intervals 8 to 9 and 11 to 12 microns, i.e. in a window of transparency of the atmosphere, where spatial variation of the landscape is more strongly expressed.

The least effect is observed inside spectral interval 7 to 8 and 14 to 15 microns, where the atmosphere does not transmit radiation of the surface of the Earth, and spatial variation of the intensity of radiation is insignificant, due to the high uniformity of radiation atmospheric formations.

4.3 Processing of Traces with the Introduction of Constraints in the Initial Experimental Data.

One can propose another method of processing initial experimental material. The idea of this method consists of selecting from all the experimental material (1176 traces of spectra) for processing only those traces that are obtained in uniform background formations, that have practically not changed their characteristics of radiation for one full cycle of measurement of the spectrum. In this case non-simultaneity of measurement has no significance in the determination of the correlation coefficient, since one can consider that characteristics of radiation of the underlying surface in all spectral intervals do not vary during the time of recording of one spectrum.

Selection of traces, obtained in uniform assemblies, was performed in the following fashion. Three identical cycles of spectra, measured in succession one after the other, were found. Spectra were considered identical in that case, if intensities of radiation in each of 14 spectral intervals differed from spectrum to spectrum no more than 10%. In this case, intensities of radiation for the second spectrum of three identical spectra was written out in a separate blank. Uniform background formations of great extent (clouds, oceans, large forest tracts, deserts, etc.) correspond to this spectrum on the surface of the planet.

In all, 131 of 1176 traces were selected for processing, i.e. 11% of all the experimental material. On the basis of these sample data the correlation matrix presented in table 4.3 is plotted. /95

From 91 correlation coefficients, presented in the normalized matrix (Table 4.3), 75 exceed coefficients of the correlation matrix (see Table 4.1), a fact that attests to sufficient basis of the sample method of processing. There are only sixteen coefficients of correlation in the matrix (Table 4.3) on the average 11% less than coefficients of correlation in the matrix (see Table 4.1), that is explained by the limited number of sample statistics (the small quantity of ranges for a given combination of spectra in the data sample).

On the basis of data, presented in matrices (see Table 4.1) and (Table 4.3), a generalized normalized matrix (Table 4.4) was compiled that contains maximal coefficients of correlation, obtained by both methods of processing.

TABLE 4.3

Correlation matrix for 13 spectral intervals from 7 to 26 microns'													№p/p	λ, microns
1	2	3	4	5	6	7	8	9	10	11	12	13		
1	0.67	0.59	0.62	0.61	0.55	0,35	0,10	0.59	0.53	0,58	0,47	0,44	1	7—8
	1	0,92	0,94	0,92	0,90	0,75	0,37	0,73	0,71	0,76	0,64	0,57	2	8—9
		1	0,93	0,90	0,88	0,76	0,39	0,66	0,66	0,69	0,58	0,53	3	9—10
			1	0,96	0,93	0,78	0,40	0,71	0,73	0,78	0,63	0,59	4	10—11
				1	0,96	0,80	0,40	0,73	0,75	0,80	0,64	0,59	5	11—12
					1	0,87	0,47	0,72	0,77	0,82	0,66	0,61	6	12—13
						1	0,64	0,59	0,71	0,73	0,65	0,63	7	13—14
							1	0,30	0,38	0,43	0,37	0,34	8	14—15
								1	0,66	0,74	0,66	0,54	9	16—18
									1	0,84	0,73	0,79	10	18—20
										1	0,81	0,69	11	20—22
											1	0,73	12	22—24
												1	13	24—26

TABLE 4.4

Generalized normalized correlation matrix for 13 spectral intervals from 7 to 26

1	2	3	4	5	6	7	8	9	10	11	12	13	№p/p	λ, microns
1	0,75	0,59	0.70	0,68	0,62	0,46	0,19	0,59	0,53	0,58	0,47	0,44	1	7—8
	1	0,92	0,94	0,92	0,90	0,75	0,37	0,73	0,71	0,76	0,64	0,57	2	8—9
		1	0,93	0,90	0,88	0,76	0,39	0,66	0,66	0,69	0,58	0,53	3	9—10
			1	0,96	0,93	0,80	0,41	0,71	0,73	0,78	0,68	0,59	4	10—11
				1	0,96	0,82	0,42	0,73	0,75	0,80	0,64	0,59	5	11—12
					1	0,88	0,47	0,72	0,77	0,82	0,66	0,61	6	12—13
						1	0,64	0,59	0,71	0,73	0,65	0,63	7	13—14
							1	0,30	0,38	0,43	0,37	0,34	8	14—15
								1	0,66	0,74	0,66	0,54	9	16—18
									1	0,84	0,73	0,79	10	18—20
										1	0,82	0,75	11	20—22
											1	0,76	12	22—24
												1	13	24—26

Comparison of correlation matrices makes it possible to draw a conclusion about agreement of the overall nature of variation of coefficients of correlation along lines, that confirms the earlier expressed proposition about the dependence of the coefficient of correlation on the coefficient of transmission of the atmosphere.

REFERENCES

1. Abbot, C.G., Fowle, F.E., Annals of the Astroph. Obs. of Smith. Inst., 1908, v. 11.
2. Simpson, G., Met, Roy. Met. Soc. 1929, v. IV, No. 23.
3. Bagrov, N.A., Trudy TsIP, No. 35 (62), 1954.
4. Kondrat'yev, K.Ya., Filipovich, O.P., Vestnik LGU, 1962, No. 6.
5. Houghton, H.C., J. Met., 1954, V. 11, No. 1.
6. London, J., Final Rep., Contr. NAF, 19(122)-165, 1957.
7. Moller F., Zdunkowski W. Met. Inst. Univ. Munich. Contr. A.F. 61(052)-493, 1961.
8. Rakipova, L.R., Kosmicheskiye issledovaniya (Cosmic Investigations), Vol. 3, No. 4, 1965.
9. Elsasser W. M., Harvard, 1962.
10. Berlyand, T.G., "A. I. Voyeykov. Problemy sovremennoy klimatologii", (Problems of Contemporary Climatology), edited by M.I. Budyko, Gidrometeoizdat, 1956.
11. Vinnikov, K.Ya., Trudy GGO, 1965, No. 168.
12. Kondratiev K.J., Nilisk H.Y. "Geofisica pura e Applicata," 1961, V. 49.
13. Raschke E. Goddard Space Flight Center, Greenbelt, Md. NASA, Wash., D. C. July 1968 (TND-4589).
14. Lebedinskiy, A.I., Glovatskiy, D.N., Tulupov, V.I., Khlopov, B.V., Fomichev, A.G., Shuster, G.I. In the collection: "Issledovaniya kosmicheskogo prostranstva" ("Investigations of Cosmic Space"). "Nauka" Press, 1965, page 65.
15. Brounshteyn, A.M., Trudy GGO, 1960, Issue 100, page 93.
16. Yakovlev, E.A., Gerasimov, F.M., Optika i spectroskopiya, 1961, t. 10, page 104.
17. Block, L.C., Zachor A.S. Appl. Opt., 1964, v. 3, p. 209.
18. Lebedinskiy, A.I., Tulupov, V.I., Safronov, Yu.P., Andrianov, Yu.G., Karavayev, I.I., Geomagnetizm i aeronomiya, Vol. 7, page 423. /96
19. Venttsel', E.S., Teoriya veroyatnostey. (Theory of Probability). Fizmatgiz, 1962.

20. Romanovskiy, V.I., Matematicheskaya statistika, (Mathematical Statistics), Book 1, AN Uzb. SSR Press, Tashkent, 1961.

21. "Tiros-II" Radiation Data User's Manual. Washington, U.S. Weather Bureau, NASA, August 15, 1961.

22. "Tiros-III" Radiation Data User's Manual. Washington, U.S. Weather Bureau, NASA, August, 1962.

23. "Tiros-IV" Radiation Data Catalog and User's Manual, Washington, 1963.

24. "Tiros-VII" Radiation Data Catalog and User's Manual, Washington, NASA, 1964.

25. Astling, E.G., Horn, L.H., J. Atm., Sci, 1964, V. 21, No. 1.

26. Astling, E.G., Horn, L.H., Dept. of Meteor. the Univ. Wisconsin Annual Rep., October, 1964.

27. Wark, D.Q., Jamamoto G.J., Lien sch, J.H., J. Atmos. Sci., 1962, V. 19, p. 369.

28. Kondrat'yev, K.Ya., Borisenkov, YE.P., Morozkin, A.M., Prakticheskoe ispol'zovaniye dannykh meteorologicheskikh sputnikov. (Practical Application of Data of Meteorological Satellites.) Gidrometizdat, 1966.

29. Bandeen W.R., Halev M., Strange, J. Goddard Space Flight Center, NASA, X-651-64-218, August, 1964.

30. Bazhulin, P.A., Kartashev, A.V., Markov, M.N., Kosmicheskiye issledovaniya, 1966, Vol. 4, No. 4.

31. Bazhulin, P.A., Kartashev, A.V., Markov, M.N., in the collection: "Issledovaniya kosmicheskogo prostranstva." (Investigations of Outer Space) Izd-vo "Nauka" Press, 1965.

32. Kondrat'yev, K.Ya., Yakushevskaya, K.Yec., v sb. "Iskusstvennye sputniki Zemli" ("Artificial Earth Satellites"), AN SSSR Press, 1962, No. 14, page 13.

33. Kondrat'ev, K.Ya., Yakushevskaya, K.Yec., Trudy GGO, No. 166, Gidrometizdat, 1964, page 75.

34. Yakushevskaya, K.Yec., In the collection: Problemy fiziki atmosfery," ("Problems of Physics of the Atmosphere"), No. 3. Izd. LGU Press, 1965, page 72.

35. McGee, R.A., Appl. Opt., 1962, V. 1, page 649.

36. Hanel, R.A., Bandeen, W.R., Contrath B.J., J. Atmos. Sci., 1963, V. 20, No. 2.

37. Wark, D.Q., Alishouse, J., Jamamoto G., Appl. Opt., 1964, V. 3, page 221.

38. Conrath, B.J., NASA, Technical Note, D-1341, Goddard Space Flight Center, Greenbelt, Md., 1962.

39. Wexler, R., Appl. Opt., 1964, V. 3, page 215.

40. Bandeen, W.R., Conrath, B.J., Hanel, R.A., J. Atmos. Sci., 1963, V. 20, page 609.

41. Lebedinskiy, A.I., Polyakova, T.G., Tulupov, V.I., Geomagnetizm i aeronomiya, 1968, Vol. 8, page 208.

42. Lebedinskiy, A.I., Andrianov, Yu.G., Karavaev, I.I., Safronov, Yu.P., Tulupov, V.I., Geomagnetizm i aeronomiya, 1968, Vol. 8, page 213.

APPENDIX

/97

I. Bar Graphs and One-Dimensional Differential Laws of Distribution of Radiation in Sections $\Delta\lambda$ in the Range of the Spectrum from 7 to 26 Microns.

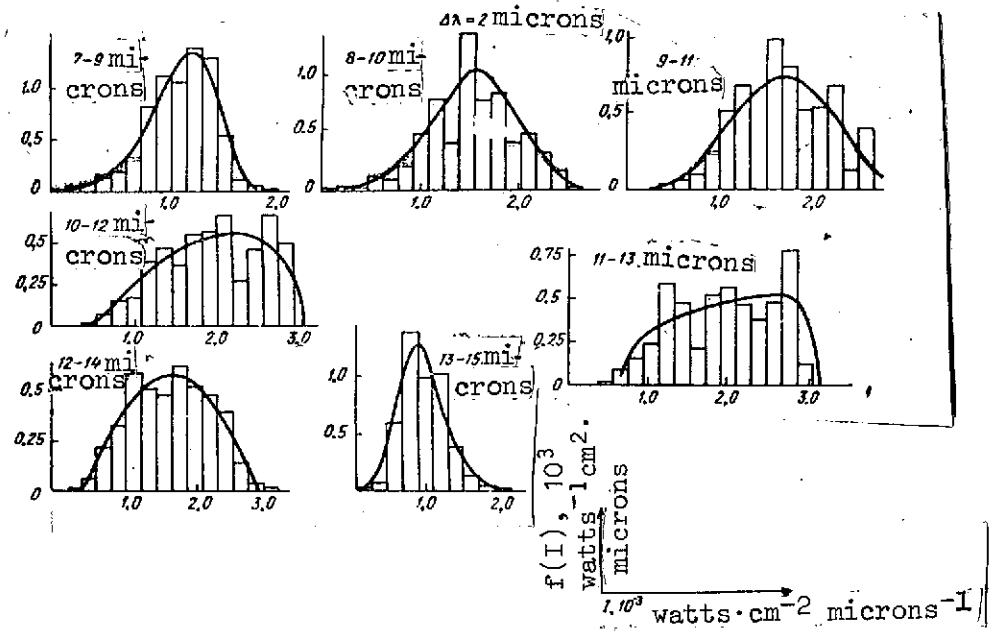

Fig. A.3.1

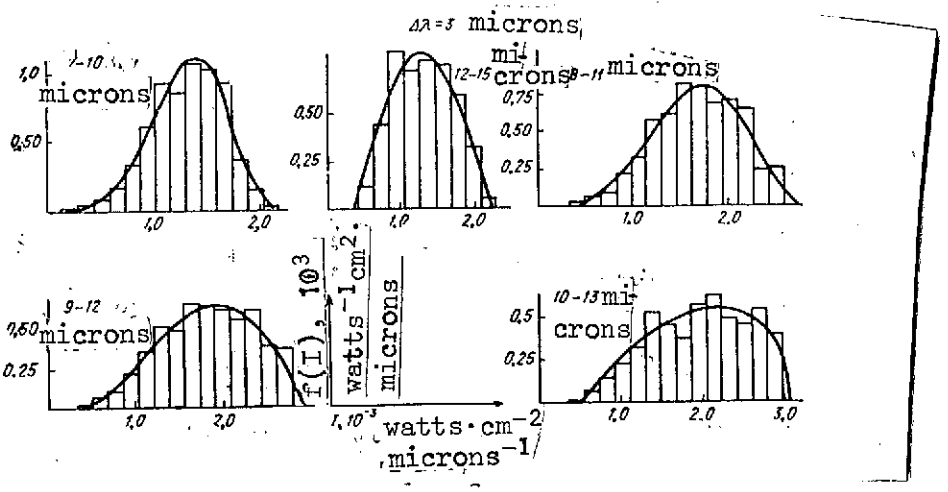

Fig. A.3.2

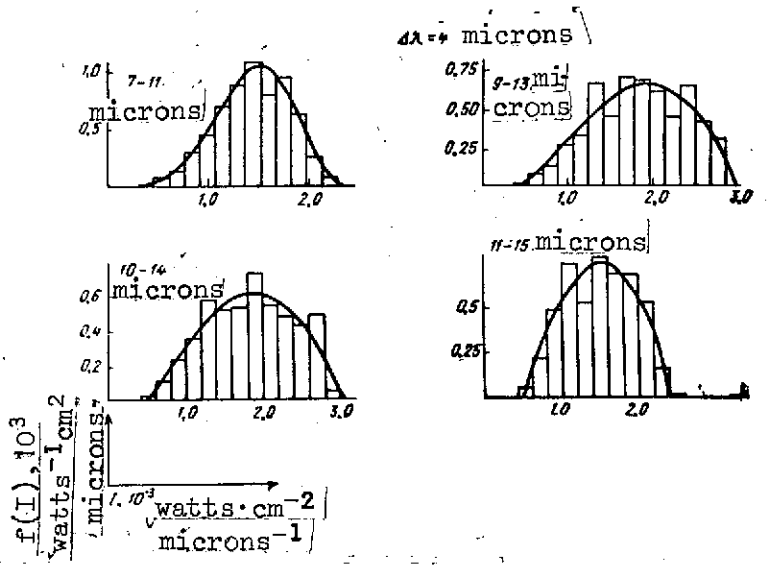

Fig. A.3.3

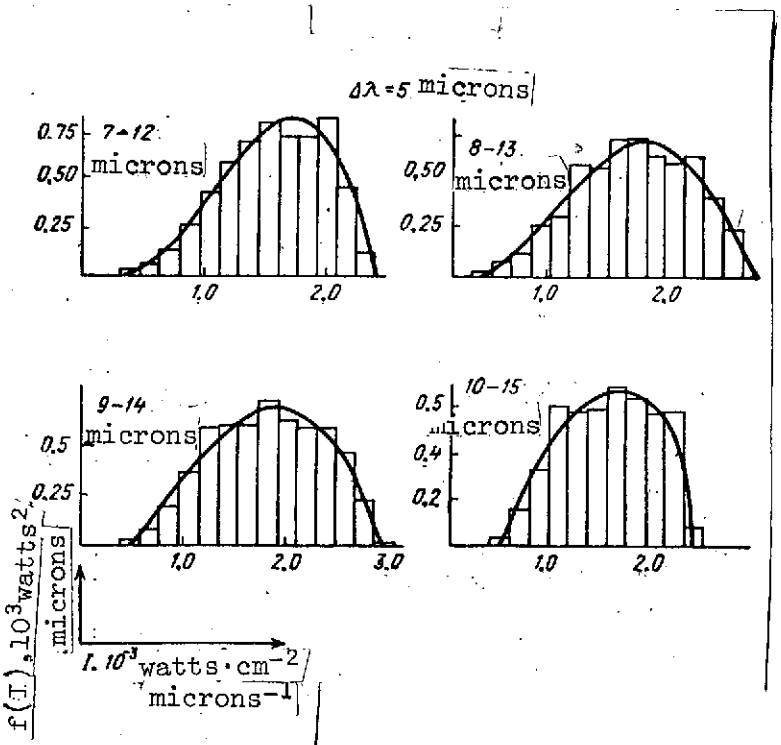

Fig. A.3.4

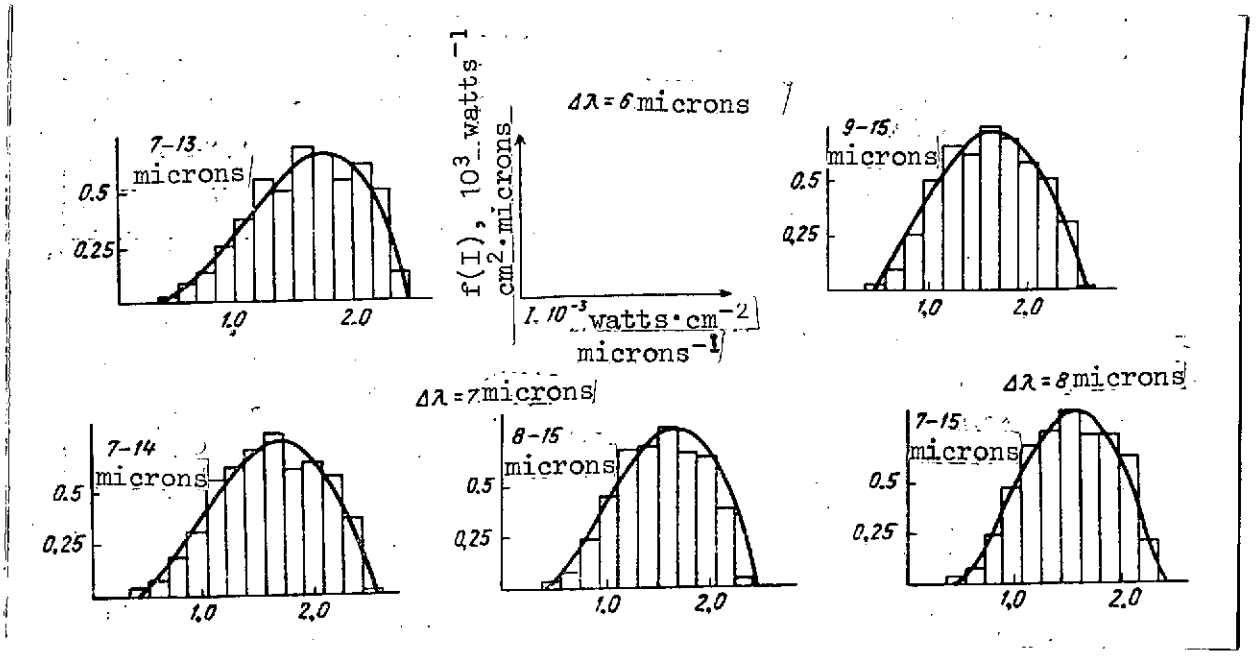
Δλ = 6 microns
f(I), 10^3 watts^-1 cm^2 · microns
I. 10^-3 watts · cm^-2 microns^-1
7-13 microns
9-15 microns
Δλ = 7 microns
7-14 microns
8-15 microns
Δλ = 8 microns
7-15 microns
0.5
0.25
1.0
2.0

Fig. A.3.5

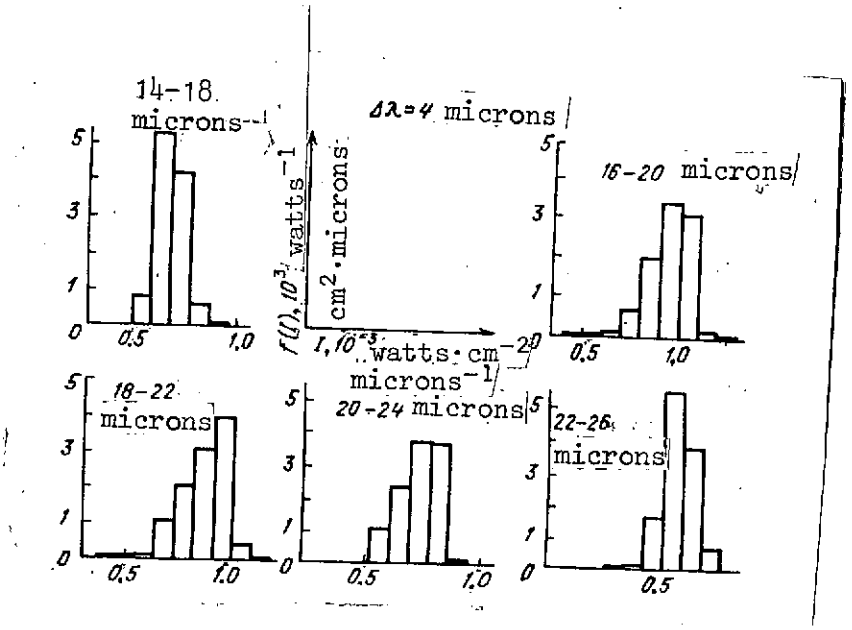

Fig. A.3.6

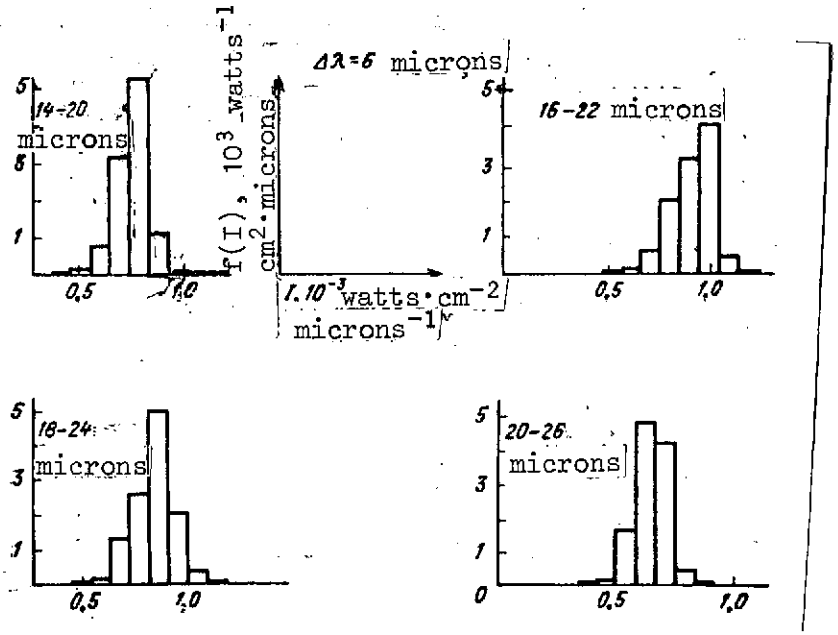

Fig. A.3.7

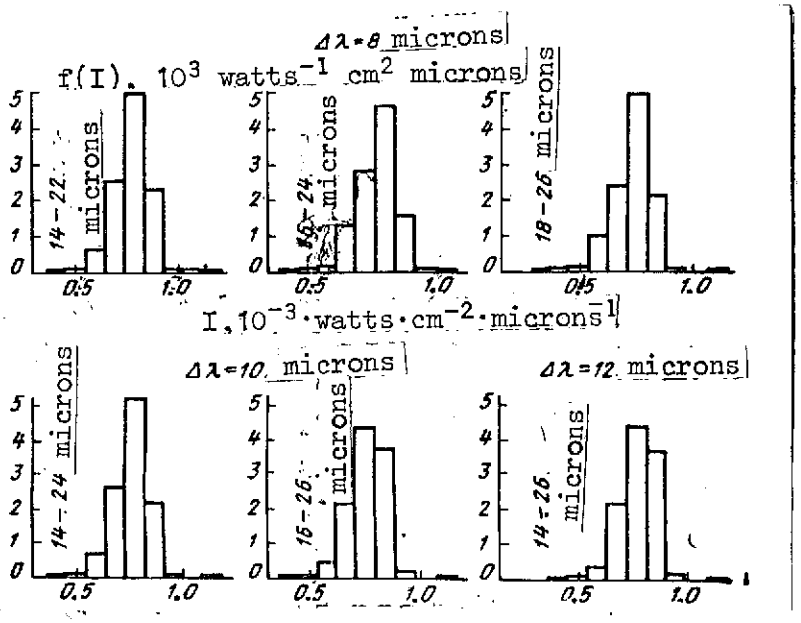

Fig. A.3.8

II. Two-Dimensional Differential Laws of Distribution of Intensity of Radiation for Spectral Intervals from 7 to 15 Microns.

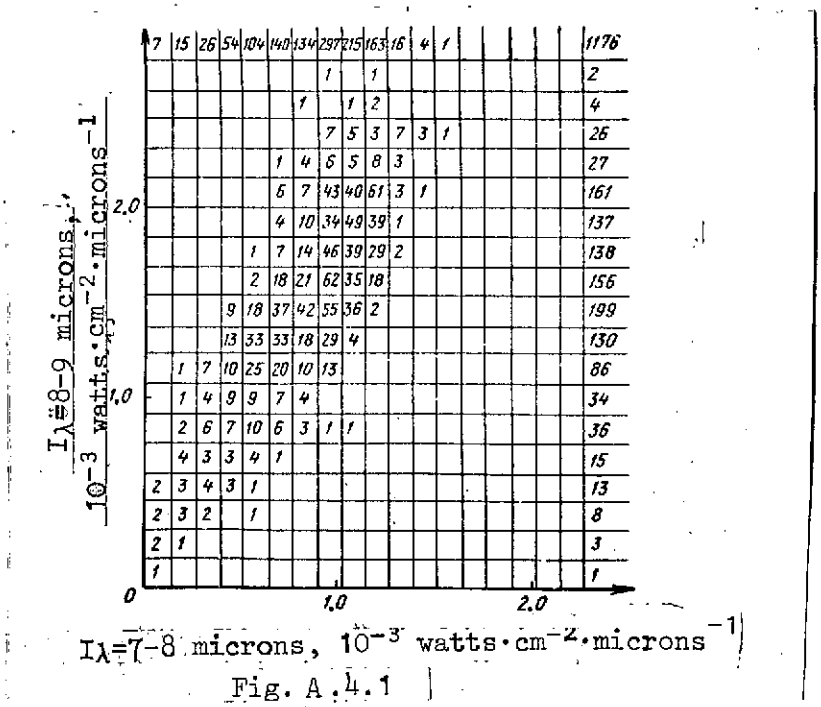

Fig. A.4.1

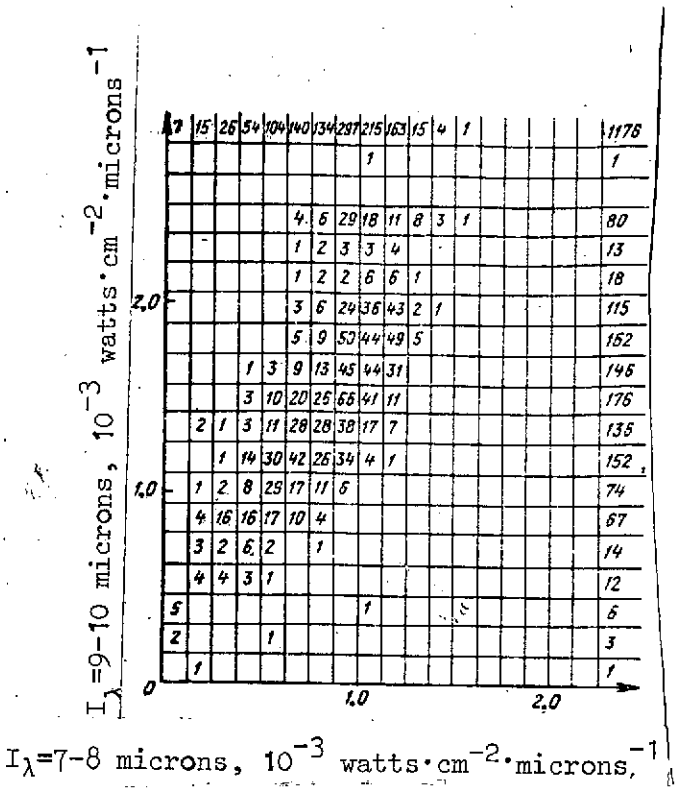

Fig. A.4.2

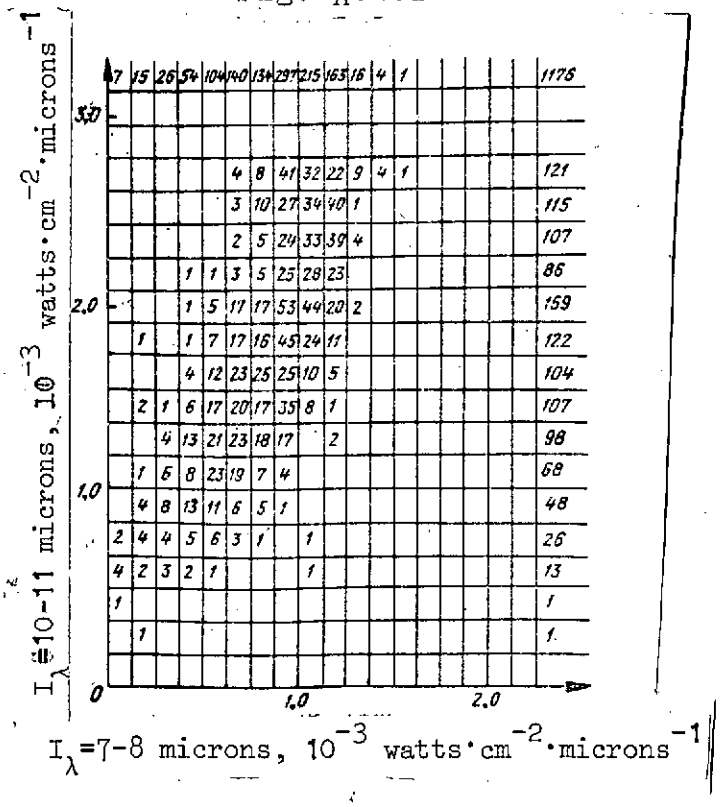

Fig. A.4.3

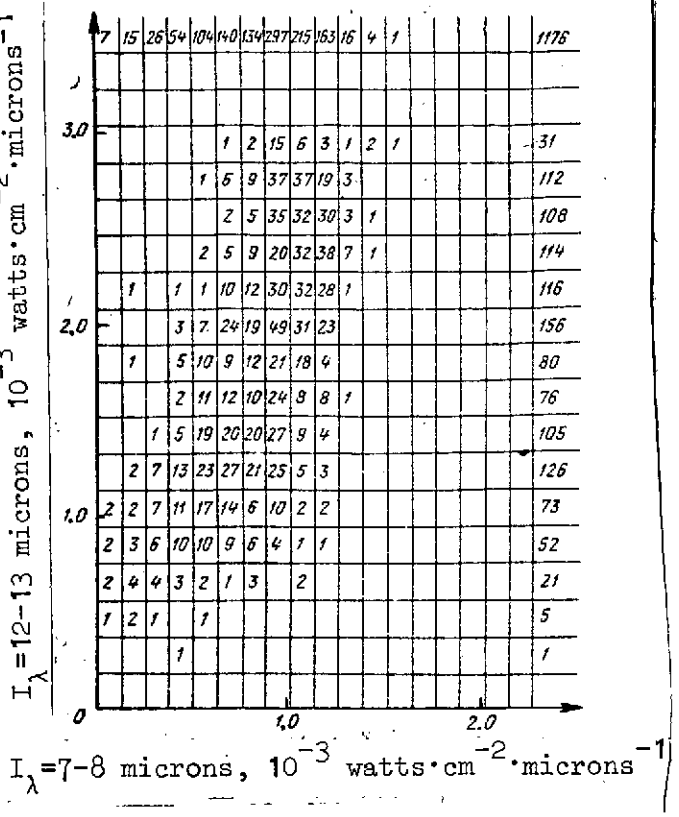

Fig. A.4.4

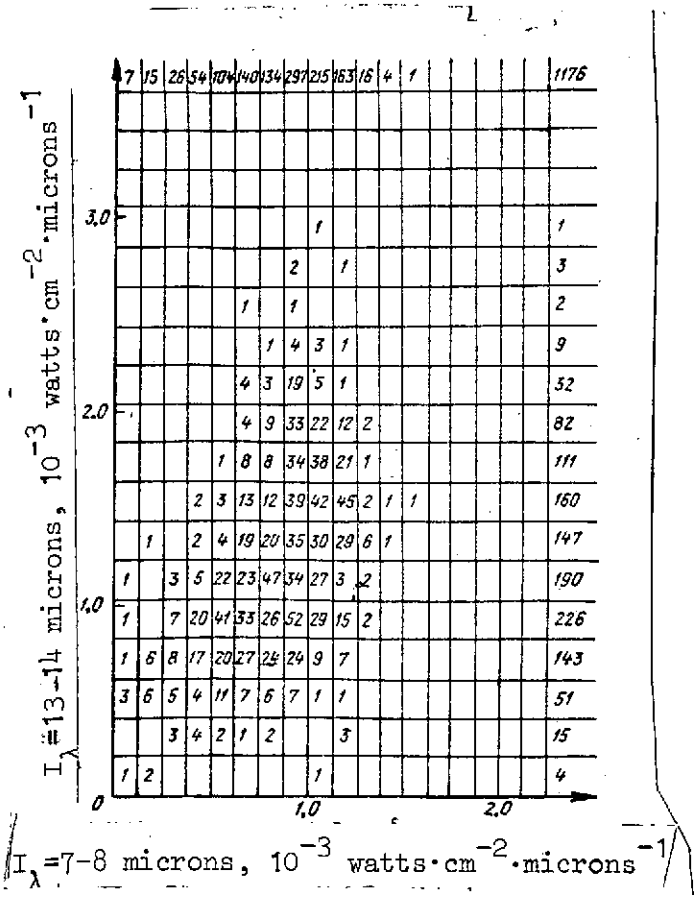

Fig. A.4.5

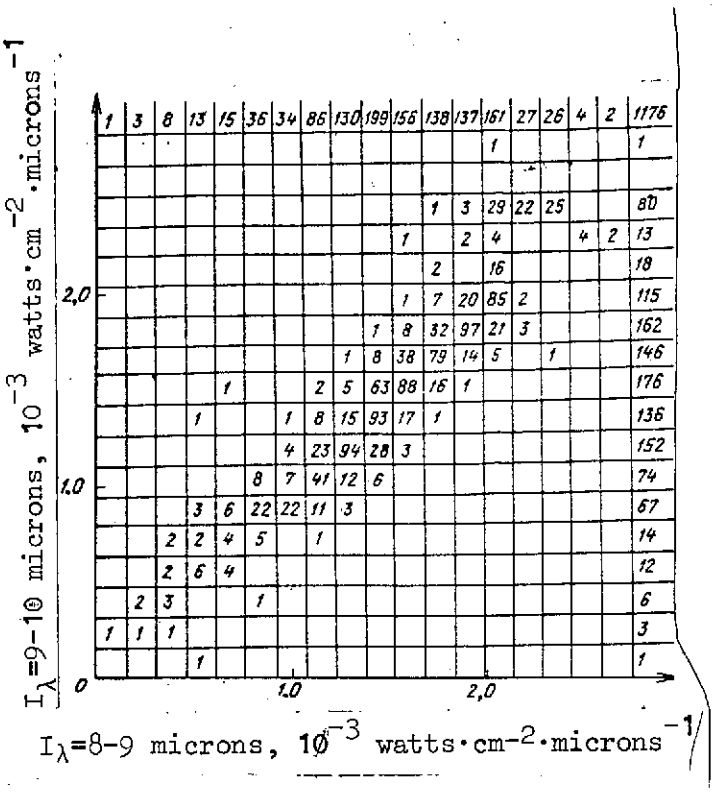

Fig. A.4.6

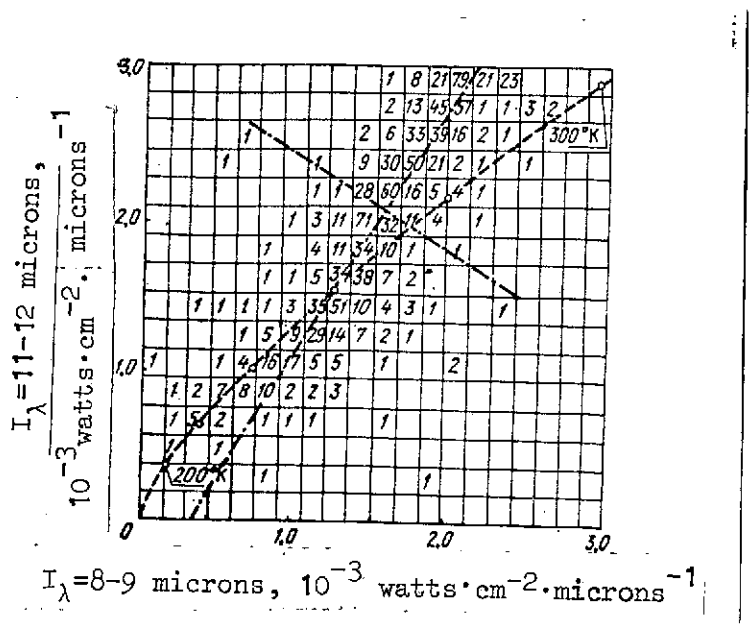

Fig. A.4.7

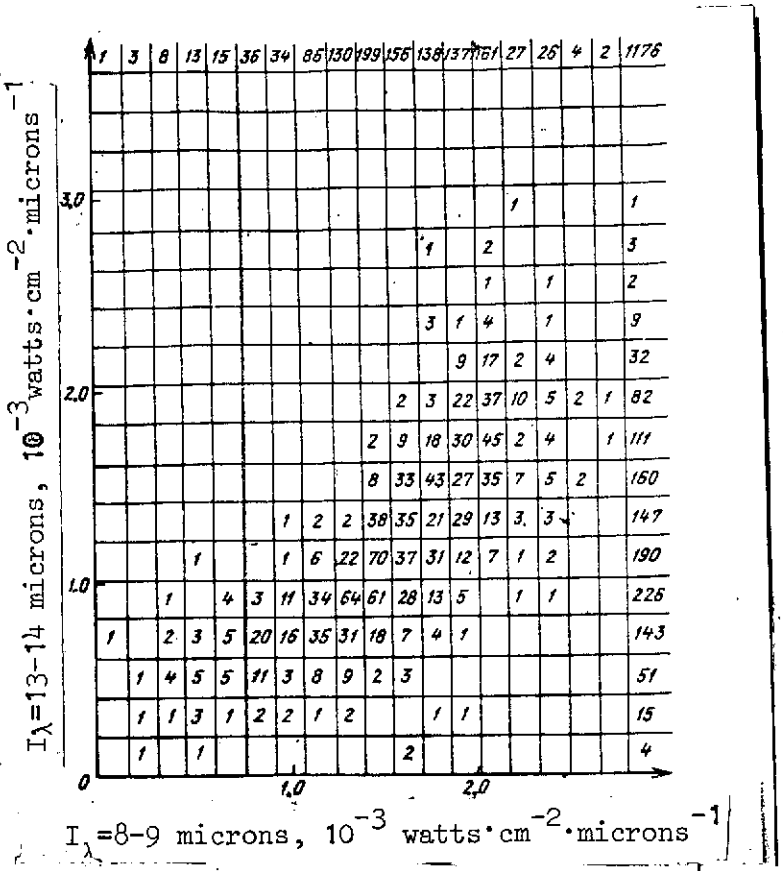

Fig. A.4.8

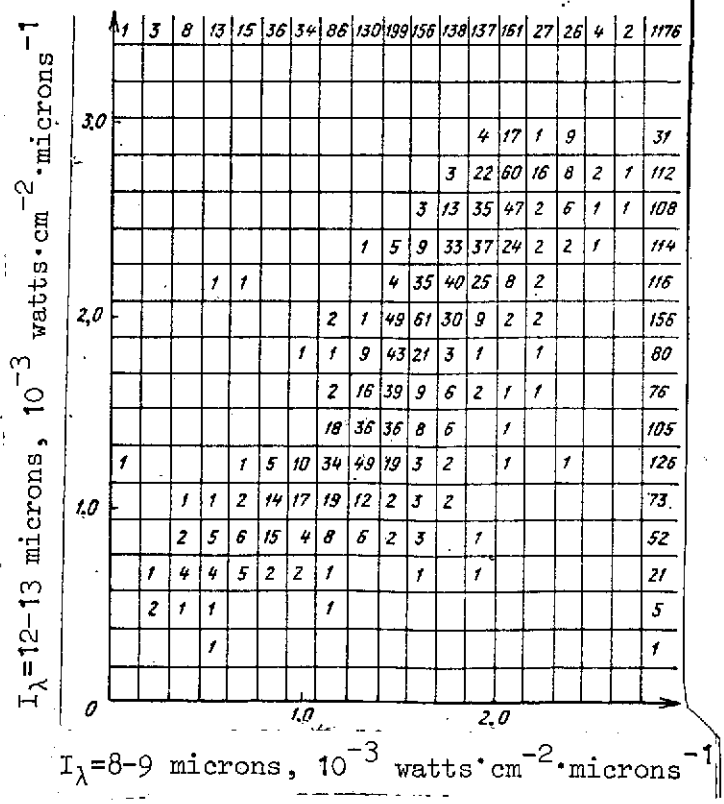

Fig. A.4.9

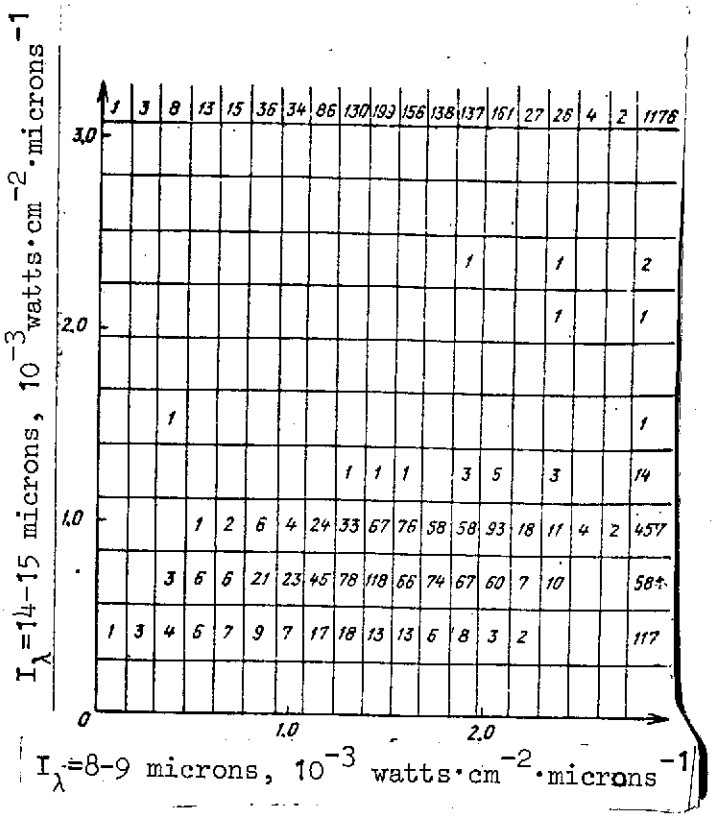

Fig. A.4.10

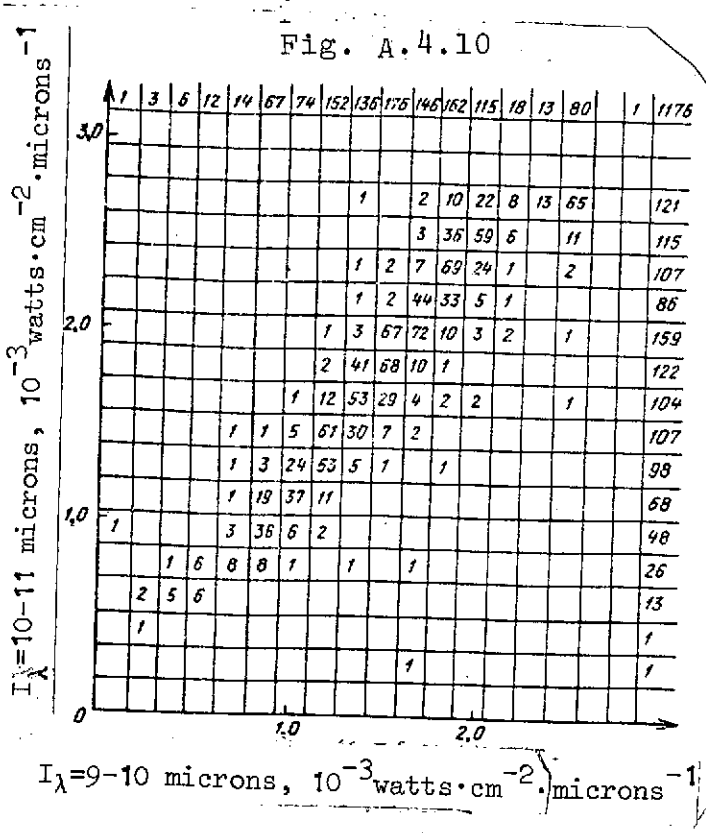

Fig. A.4.11

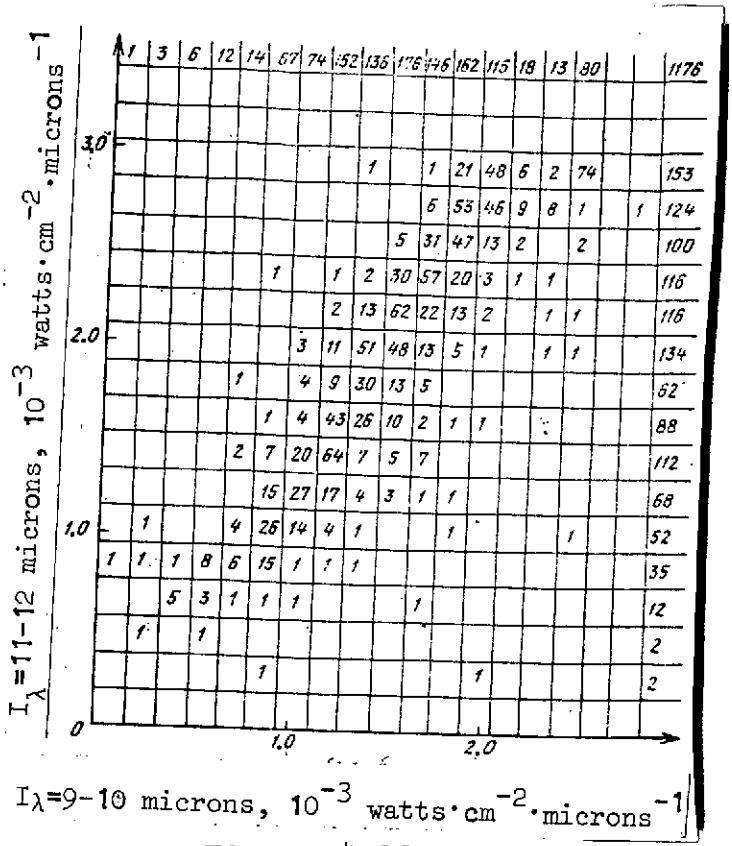

Fig. A.4.12

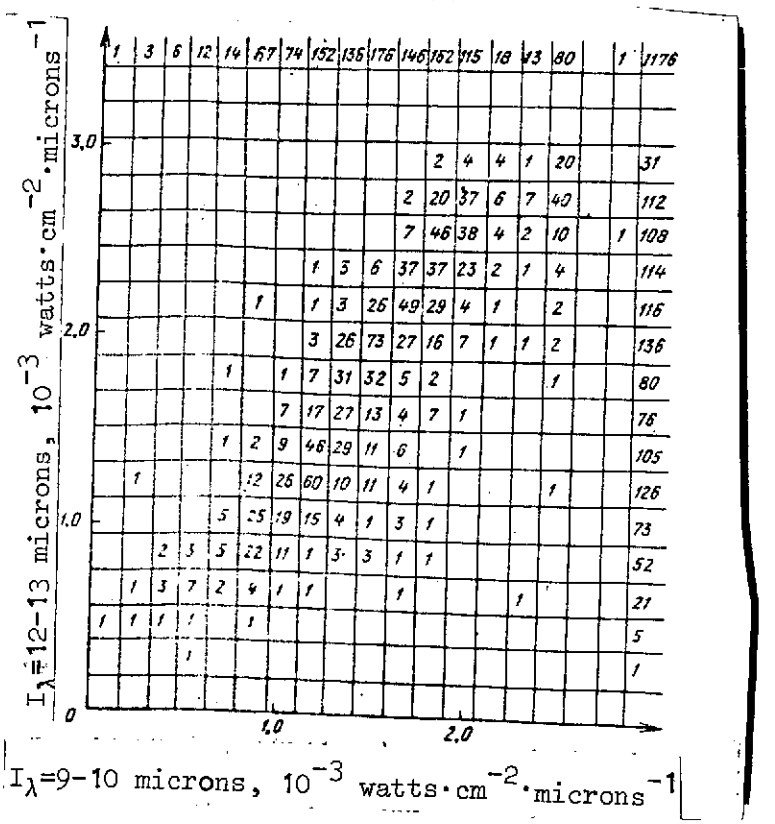

Fig. A.4.13

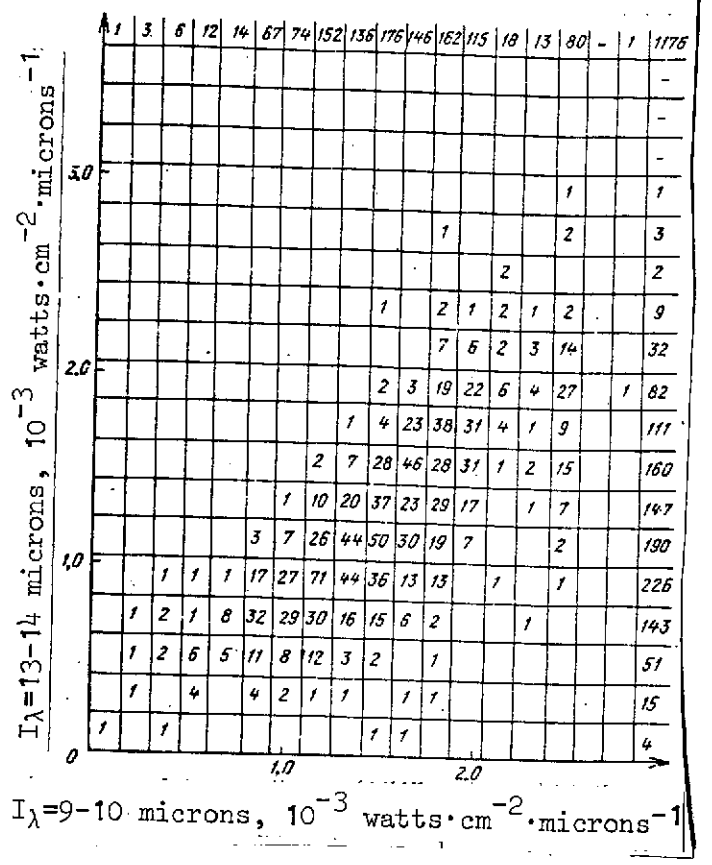

Fig. A.4.14

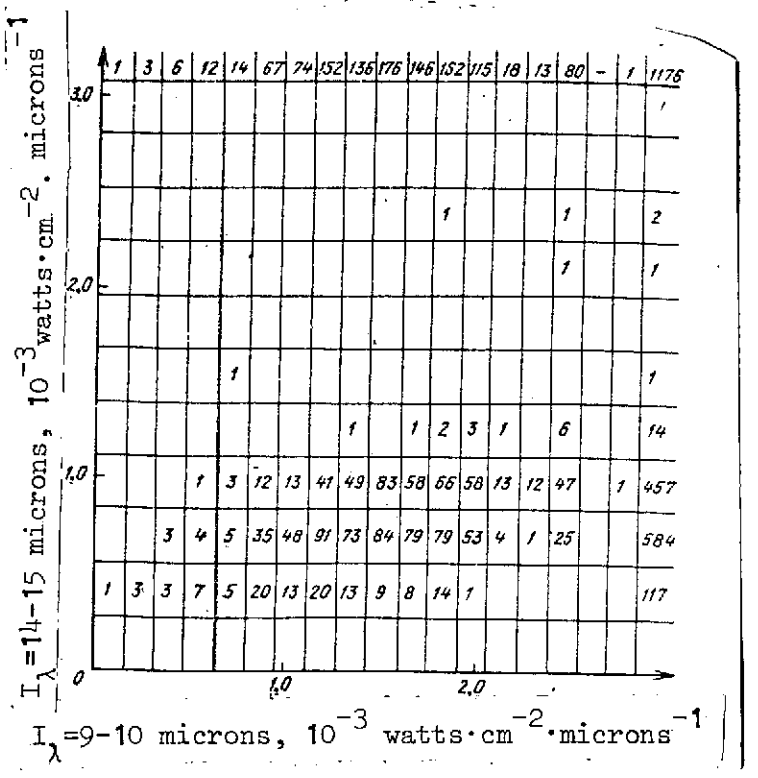

Fig. A.4.15

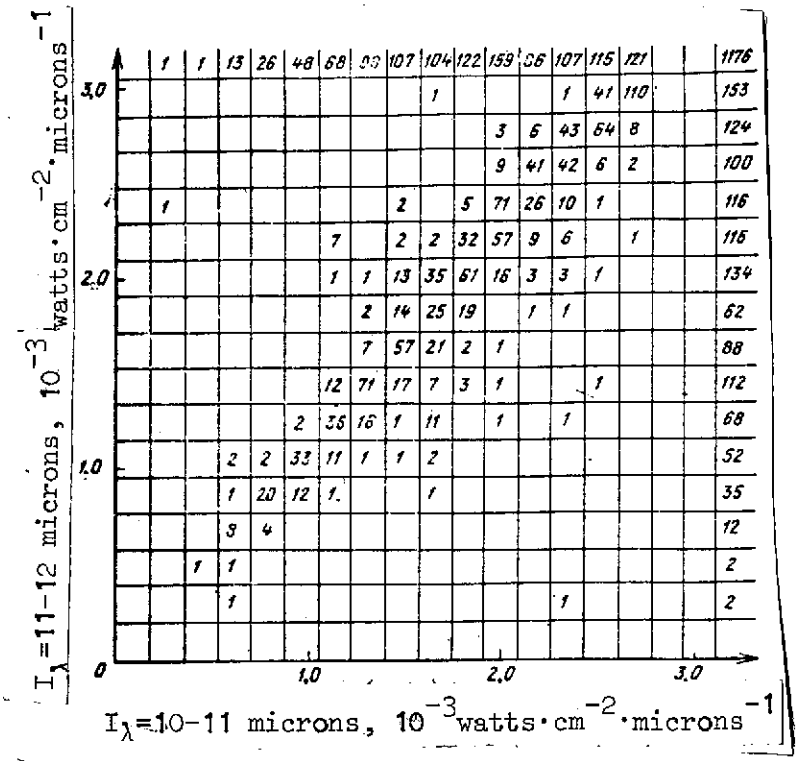

Fig.A.4.16

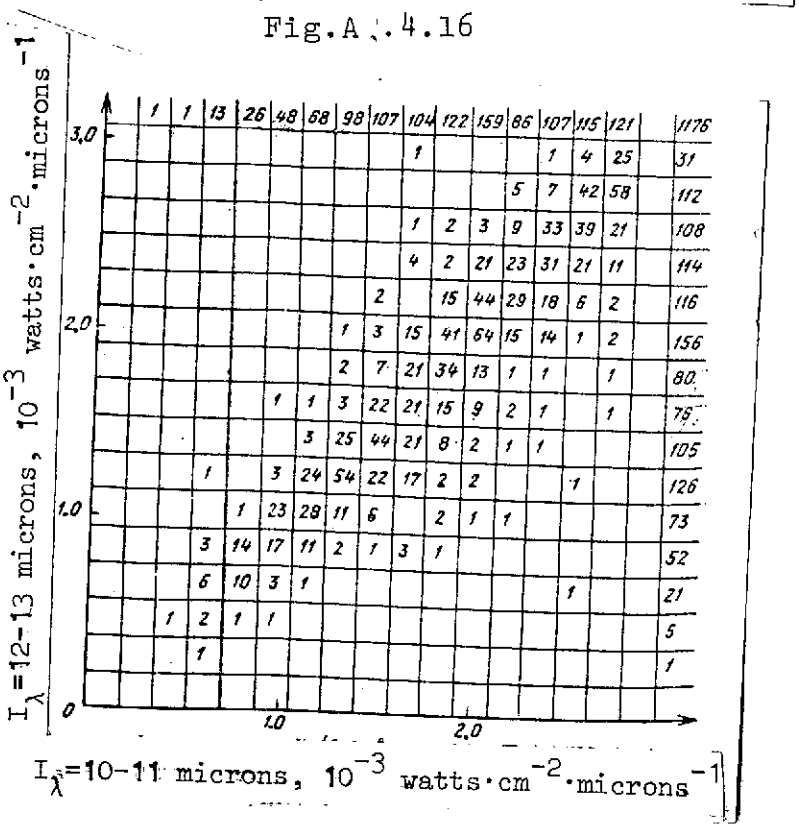

Fig. A.4.17

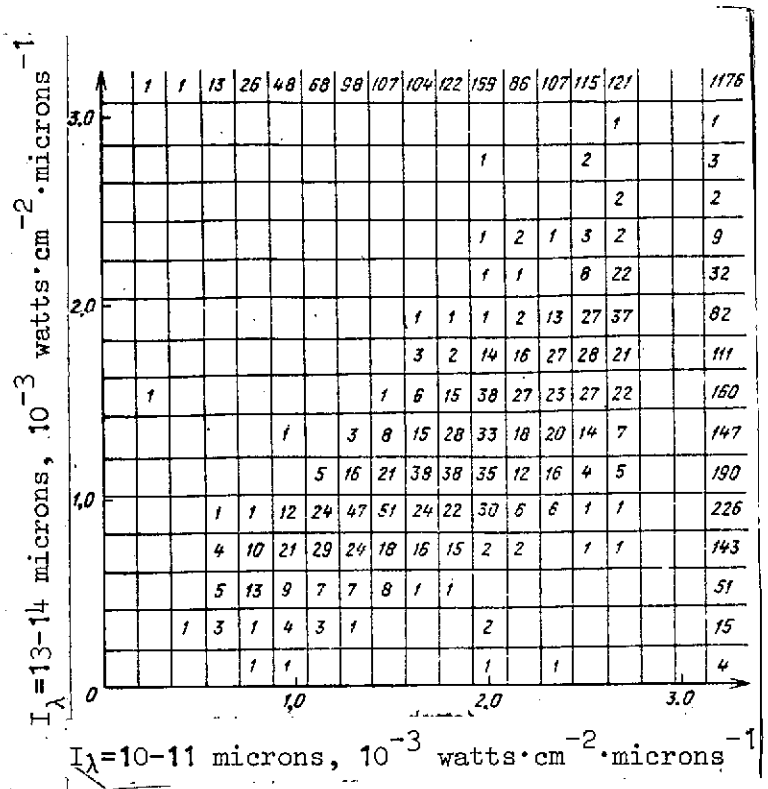

Fig. A.4.18

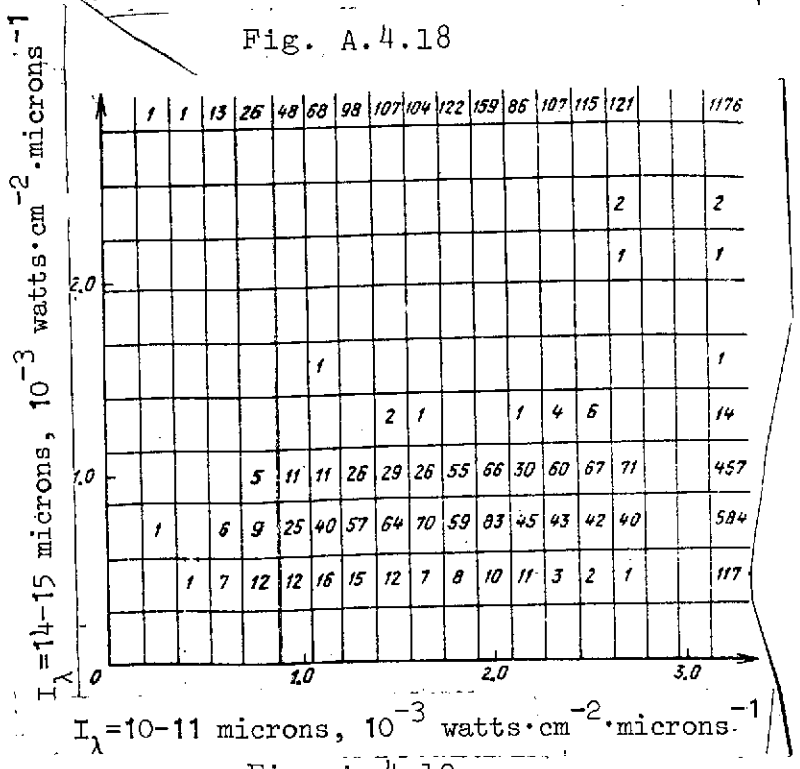

Fig. A.4.19

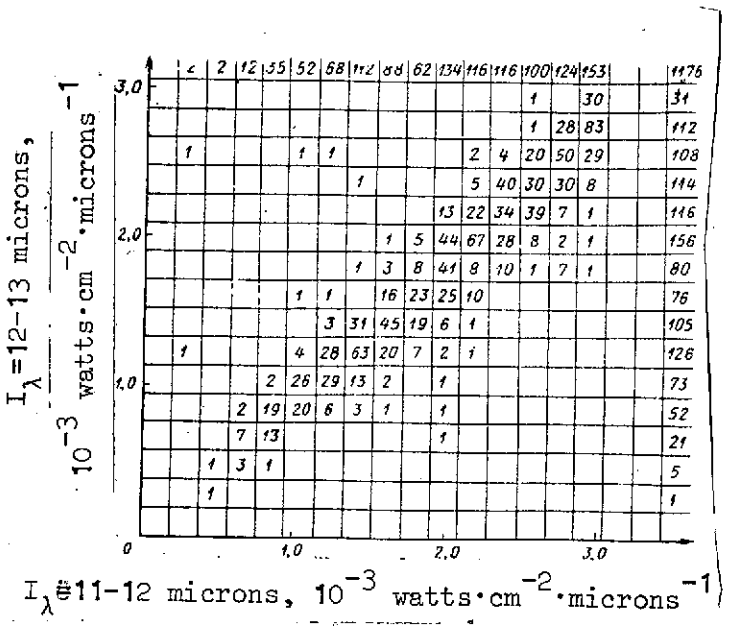

Fig. A.4.20

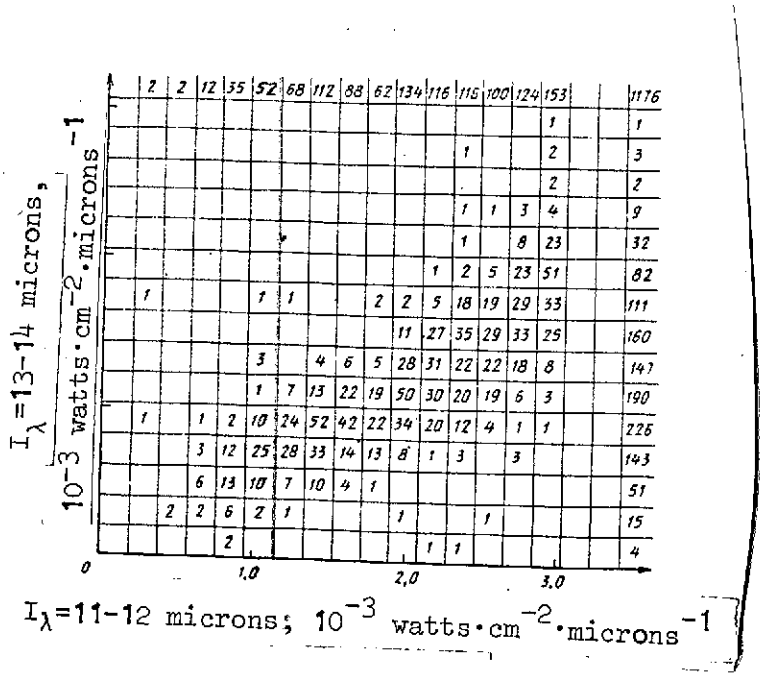

Fig. A.4.21